PHOTONIC CRYSTAL BASED SPECTRAL FILTER DEVICES FOR OPTICAL COMMUNICATION

A Thesis Submitted to
the Graduate School of Engineering and Science of
Izmir Institute of Technology
in Partial Fulfillment of the Requirements for the Degree of

DOCTOR OF PHILOSOPHY

in Electronics and Communication Engineering

by
Özgür Önder KARAKILINÇ

July 2015
İZMİR

We approve the thesis of **Özgür Önder KARAKILINÇ**

Examining Committee Members:

_____
Prof. Dr. M. Salih DİNLEYİCİ
Department of Electrical and Electronics Engineering, Izmir Institute of Technology

_____
Prof. Dr. E. Yeşim ZORAL
Department of Electrical and Electronics Engineering, Dokuz Eylül University

_____
Assoc. Prof. Dr. Alp KUŞTEPELİ
Department of Electrical and Electronics Engineering, Izmir Institute of Technology

_____
Assoc. Prof. Dr. H. Sami SÖZÜER
Department of Physics, Izmir Institute of Technology

_____
Assoc. Prof. Dr. Selçuk HELHEL
Department of Electrical and Electronics Engineering, Akdeniz University

27 July 2015

_____
Prof. Dr. M. Salih DİNLEYİCİ
Supervisor, Department of Electrical and Electronics Engineering
Izmir Institute of Technology

_____
Prof. Dr. M. Salih DİNLEYİCİ
Head of the Department of Electrical
and Electronics Engineering

_____
Prof. Dr. Bilge KARAÇALI
Dean of the Graduate School of
Engineering and Science

ACKNOWLEDGMENTS

I would like to thank my advisor Prof. Dr. M. Salih Dinleyici who has always supported me during this period of time. I appreciate his guidance, knowledge and experience. I am an honor to be his student.

I am grateful to my committee members Assoc. Prof. Dr. Alp Kuştepeli, Assoc. Prof. Dr. H. Sami Sözüer, Prof. Dr. E. Yeşim ZORAL, Assoc. Prof. Dr. Selçuk HELHEL, Assoc. Prof. Dr. Selim BÖREKÇİ, and Assist. Prof. Dr. Ahmet ÖZEK for their valuable contributions. I also wish to thank to my colleagues who supported me during my PhD period.

Finally, I would like to thank my family for their endless support and patience. You deserve the best of everything. I am so lucky to have you.

ABSTRACT

PHOTONIC CRYSTAL BASED SPECTRAL FILTER DEVICES FOR OPTICAL COMMUNICATION

It is already foreseen that future integrated photonic circuits for ultra fast all-optical signal processing will require various types of functional elements that include spectral managements. Consequently, dynamical manipulations of the photonic crystals play an important role in order to route the optical signal between waveguide channels or may be among layers. Hence, in this study, photonic crystal based spectral filters are proposed for all-optical communication applications. Firstly, grating structures composed with Gaussian beam interference equation and stimulated by nonlinearity phenomenon in photonic crystal are studied. The grating structure exhibiting special features on transmission characteristics are shown. After that, idea is expanded with applying a realistic Gaussian beam source, and transient grating in nonlinear photonic crystal structure is considered. At this point, light wave interaction with nonlinear response time plays a significant role on the signal manipulation. So, the behavior of pulse propagation in the medium having the response of instantaneous nonlinearity (Kerr) is summarized. As a second aspect of this work, the optical resonator, which is essential functional block for filtering, modulating, buffering, switching in integrated optical circuits systems, is presented. Photonic crystal microcavity based dual-mode dual-band bandpass filter is designed and its transmission characteristics are investigated for various configurations. Photonic crystal resonator structure is formed by a point defect microcavity that is constituted with a large and three smaller auxiliary perturbation rods. Degenerate modes at each band may also be excited by changing the structure properties of the perturbation. The proposed photonic crystal spectral filters structure can effectively be used for optical communication applications.

ÖZET

OPTİK HABERLEŞME İÇİN FOTONİK KRİSTAL TABANLI SPEKTRAL FİLTRE AYGITLARI

Çok hızlı tamamen optik işaret işleme için gelecek nesil tümleşik fotonik devrelerin spektral yönetimler de dâhil olmak üzere çeşitli tipte işlevsel elemanları gerektireceği öngörülmektedir. Bu nedenle, fotonik kristallerin dinamik işlemesi dalga kılavuzu kanalları arasında ya da katmanlar arasında optik sinyalin yönlendirilmesi için önemli rol oynamaktadır. Dolayısıyla, bu çalışmada, tamamen optik haberleşme uygulamaları için fotonik kristale dayalı spektral filtreler önerilmiştir. İlk olarak, Gauss ışın girişim denklemi ile oluşan ve fotonik kristalin doğrusal olmayan özelliğini ile uyarılan ızgara yapıları incelenmiştir. İletim karakteristiği üzerine kendine özgü özellikler sergileyen ızgara yapısı gösterilmiştir. Daha sonra, gerçeğe uygun Gauss ışın kaynağı uygulayarak fikir genişletilmiş ve doğrusal olmayan fotonik kristal yapısında geçici ızgara ele alınmıştır. Bu noktada, ışık dalgasının doğrusal olmayan cevabı ile etkileşimi sinyal işlemesi üzerinde önemli bir rol oynamaktadır. Bu nedenle, anlık doğrusal olmayan (Kerr) yanıta sahip ortamda darbe yayılma davranışı özetlenmiştir. Daha sonra çalışmanın diğer bir yönü olarak, tümleşik optik devre sistemlerinde filtreleme, modülasyon, belleğe alma ve anahtarlama gibi uygulamalar için temel işlevsel yapı olan optik rezonatör sunulmuştur. Fotonik kristal mikro boşluk tabanlı çift modlu çift bandlı band geçiren filtre tasarlanmış ve iletim karakteristikleri çeşitli konfigürasyonlar için incelenmiştir. Fotonik kristal rezonatör yapısı bir büyük ve daha küçük üç yardımcı pertürbasyon çubuklar ile meydana getirilmiş noktasal kusur mikro boşluk ile oluşturulmaktadır. Her bir banddaki dejenere modlar pertürbasyonun yapı özellikleri değiştirilerek uyarılabilmektedir. Önerilen fotonik kristal spektral filtre yapıları optik haberleşme uygulamaları için etkin bir biçimde kullanılabilir.

Dedicated to my family

TABLE OF CONTENTS

LIST OF FIGURES

Figure **Page**

LIST OF SYMBOLS AND ABBREVIATIONS

PhCs	: Photonic crystals
FDTD	: Finite difference time domain method
PWE	:Plane wave expansion method
CMT	:Coupled mode theory
TMM	:Transfer matrix method
TE	:Transverse electric
TM	:Transverse magnetic
ρ	:Electric charge density
ε	:Permittivity of the medium
ε_0	:Permittivity of the vacuum
μ	:Permeability of the medium
μ_0	:Permeability of the vacuum
χ	:Electric susceptibility of the medium
$\chi^{(3)}$	:Third order nonlinear optical susceptibility
THz	:Terahertz
dB	:Decibel
λ	:Wavelength
f	:Frequency
df	:Frequency width
Q	: Quality factor
c	: Light velocity
a	: Lattice constant

CHAPTER 1

INTRODUCTION

Photonic crystals (PhCs) are artificial materials which include a periodic arrangement of dielectric medium and display photonic band gaps depending on their geometry and refractive index profiles [1]. Because of the unique properties on the light guidance, PhCs have become as indispensable tool for light wave manipulation. It is already foreseen that future integrated photonic circuits for ultra fast all-optical signal processing require various types of functional elements such as switches, memory and logic devices. PhCs will be an enabling technology with the miniaturization and integration of photonic circuits in a broad spectrum of electromagnetic waves. Computationally whole spectrum is the same due to wavelength scaling (λ/a) (Figure 1.1) [2].

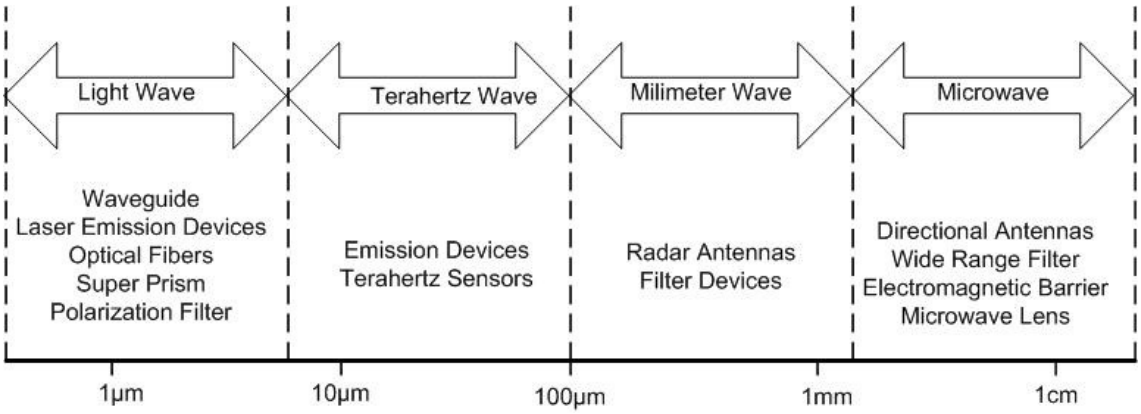

Figure 1.1. Applications of PhCs with the lattice constant dimension [3]

Applications for PhCs may be categorized into two types which are the reflective or transmissive attributes of a photonic crystal [4]. Light can easily be controlled in PhCs on the order of wavelength and it makes bends possible the low loss, large or narrow band and sharp to conventional counterpart [5], [6]. Besides, by

introducing defects into PhCs, one can control and manipulate the light as well as construct integrated optical devices [7]. With adjusting the configuration of defect or resonator structure, several functions for advanced signal processing in all-optical photonic circuits are realized [8], [9] .

Optical light signals can be confined into a narrower region than the conventional optical waveguides by PhCs band gap guiding properties. Therefore PhCs are promising structures exploiting the nonlinearity due to high intensity localization. The latest studies on integrated nonlinear photonic devices has remarkable impact on the all-optical signal processing, ultra low power all-optical switching and quantum photonics [10].

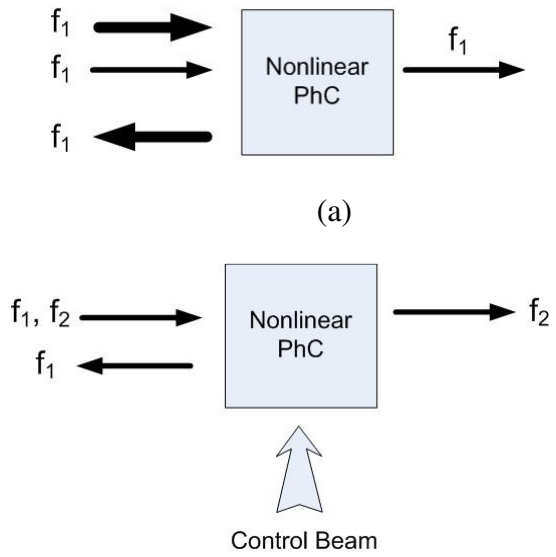

Figure 1.2. Nonlinear switching with (a) self control input signal and (b) control signal in PhC structure

In the PhC composed of Kerr nonlinear optical materials, a strong pump light can induce band gap shift or defect resonant frequency shift due to the refractive index change. Two types of all optical switching with nonlinear PhCs are considered in the literature according to exploiting the nonlinearity (Figure 1.2). One of them is used as a

kind of self switching effects to enhance the nonlinearity of material by adjusting the input signal power. The other one uses control beam signal to trigger the switching of input signal, which is relatively lower power [11], [12]. Searching for nonlinear materials that possess a larger third-order (namely, Kerr) nonlinear susceptibility ($\chi^{(3)}$) and designing more suitable structures that can enhance the inner field at the nonlinear areas are two effective ways to improve the performance of all-optical switching[11]. Because of the very short relaxation time [13] and fast response time [14], Kerr type nonlinearity has been pioneered for the realization of optical fast switching application in the recent years [15], [16].

Along with the progress in THz communication technologies, optical resonator, which is the key elements for filtering, modulating, switching for optical processing, are highly needed in integrated optical communication systems [8], [17]. The aim of this thesis is to investigate novel means of basic building blocks of PhC structures with the potential integration for all-optical communication devices. In this context, resonance structures are investigated for spectral filter application in PhC. Proposed structures in the thesis are verified by using numerical computations. Plane Wave Expansion Method (PWE) and Finite Difference Time-Domain Method (FDTD), which are developed by MIT photonic research group, are used to analyze the device characteristics [18]. MPB is used for band structure and mode analysis and, MEEP is used for time domain simulation and transmission spectra etc. Additionally, MATLAB, MATHCAD are used for data analysis.

At the beginning of the thesis, the fundamentals of PhCs and mathematical background are summarized, and then computational methods used for analyzing the photonic crystal structures are presented. Later, two different spectral filters are proposed in this study.

Firstly, an interference grating structure formed by Gaussian beam interferences in photonic crystal waveguide such that having Kerr type nonlinearity is proposed. The Bragg frequency and the index deviation of the composed grating structure are estimated by transfer matrix methods and its transmission characteristics are investigated. In this study, a chirped grating structure formed by realistic Gaussian beam interference equation is emphasized. Transmission characteristics of these structures have been analyzed for different beam parameters. According to simulation

results, the interference grating has shown that band stop filter characteristics can bring tunability for photonic crystal devices. This can be an effective method for controlling optical signals in the photonic crystal for all optical switching/routing applications as a part of add/drop multiplexing.

Later, PhCs dual-mode dual-band resonator structure is designed and its transmission characteristics are investigated for various configurations. PhC resonator structure is formed by a point defect microcavity equipped with one large and three smaller auxiliary perturbation rods. Degenerate modes at each band may also be excited by changing the structural properties of the perturbation rods and mode splitting is observed. Proposed dual-band dual-mode photonic crystal filter structure can effectively be used for terahertz (THz) communication applications.

Because the nonlinearity phenomenon has been widely used for all optical switching in photonic crystal, another direction that can be taken in this study is to examine the light matter interaction and light propagation in nonlinear and dispersive medium. Most of the studied material is assumed as instantaneous Kerr nonlinearity. However index deviation in transient grating is affected by the pulse duration and nonlinear relaxation time. Transient grating strongly depends on the nonlinear material response time. As a result, pulse propagation in linear and/or nonlinear dispersive media is investigated and its impact on the transmission dynamics is explored.

CHAPTER 2

WAVE PROPAGATION IN PHOTONIC CRYSTALS

Propagation of light in any medium is well defined by the Maxwell equations with the medium characteristics. Generally, the photonic crystal structures are assumed to be lossless, isotropic and nonmagnetic, nonlinear and dispersive properties of medium are also considered in this study. Hence, fundamentals of theoretical foundations are given for linear, nonlinear and dispersive mediums in this chapter.

2.1 Electromagnetic Waves in Linear Periodic Dielectric Materials

Since light is an electromagnetic wave, it follows Maxwell's equations. Time dependent Maxwell's equations in dielectric media can be written as [1]

$$\nabla \times \vec{E} + \frac{\partial \vec{B}}{\partial t} = 0 \tag{2.1}$$

$$\nabla \times \vec{H} - \frac{\partial \vec{D}}{\partial t} = J \tag{2.2}$$

$$\nabla \cdot \vec{D} = \rho \tag{2.3}$$

$$\nabla \cdot \vec{B} = 0 \tag{2.4}$$

where $\vec{E}$ is the electric field vector, $\vec{H}$ is the magnetic field vector, $\vec{D}$ is the electric displacement vector, $\vec{B}$ is the magnetic induction vector, $\vec{J}$ is the electric current density vector, and ρ is the electric charge density. $\vec{D}$ and $\vec{B}$ represent the effect of the electromagnetic field on matter [19].

The set of Equations (2.1) to (2.4) can describe the propagation of electromagnetic waves in a vacuum, as well as in any other media, if we add the relations that show the effect of the electromagnetic fields on the medium through which they propagate. These equations are also known as material equations and written as

$$\vec{D}(\vec{r}) = \varepsilon(\vec{r})\vec{E}(\vec{r}) = \varepsilon_0(\vec{r})E(\vec{r}) + \vec{P}(\vec{r}) \tag{2.5}$$

$$\vec{B}(\vec{r}) = \mu(\vec{r})\vec{H}(\vec{r}) = \mu_0(\vec{r})\left(\vec{H}(\vec{r}) + \vec{M}(\vec{r})\right) \tag{2.6}$$

where ε_0 and ε are, respectively, the permittivity tensors in the vacuum and in the medium; μ_0 and μ are, respectively, the permeability tensors in vacuum and in the medium; and $\vec{P}$ and $\vec{M}$ are, respectively, the electric and magnetic polarizations.

The tensors are of rank 2, and they become scalars if the medium is isotropic. ε and μ will be considered to be independent of E and H, (i.e., a linear regime). For the solution of Maxwell's equations, following conditions are assumed. Lossless (ε is purely real), non-magnetic (μ = 1), dielectric materials without free charges or currents (ρ = 0; J = 0). Then the Equations (2.1)-(2.4) can be reduced to:

$$\nabla \times \vec{E}(\vec{r},t) + \frac{\partial \vec{H}(\vec{r},t)}{\partial t} = 0 \tag{2.7}$$

$$\nabla \times \vec{H}(\vec{r},t) - \varepsilon(\vec{r})\frac{\partial \vec{E}(\vec{r},t)}{\partial t} = 0 \tag{2.8}$$

$$\nabla \cdot \varepsilon(\vec{r})\vec{E}(\vec{r},t) = 0 \tag{2.9}$$

$$\nabla \cdot \vec{H}(\vec{r},t) = 0 \tag{2.10}$$

Equations (2.7)-(2.10) are all linear; therefore, the electric and magnetic fields can be expressed as a set of harmonic modes:

$$\vec{E}(\vec{r},t) = \vec{E}(\vec{r})e^{-i\omega t} \tag{2.11}$$

$$\vec{H}(\vec{r},t) = \vec{H}(\vec{r})e^{-i\omega t} \tag{2.12}$$

Substituting Equations (2.11) and (2.12) into (2.7) and (2.8) yields:

$$\nabla \times \vec{E}(\vec{r}) - i\omega\mu_0 \vec{H}(\vec{r}) = 0 \tag{2.13}$$

$$\nabla \times \vec{H}(\vec{r}) + i\omega\varepsilon_0 \varepsilon(\vec{r})\vec{E}(\vec{r}) = 0 \tag{2.14}$$

This system can be decoupled by dividing Equation (2.14) by ε(r), taking the curl of the result and then substituting the expression for $\vec{E}(\vec{r})$ from Equation (2.13). The end result is a single equation for $\vec{H}(\vec{r})$:

$$\nabla \times \left(\frac{1}{\varepsilon(r)} \nabla \times \vec{H}(\vec{r}) \right) = \left(\frac{\omega}{c} \right)^2 \vec{H}(\vec{r}) \tag{2.15}$$

This equation completely determines all $\vec{H}(\vec{r})$ modes. In order to find the electric field distribution, $\vec{H}(\vec{r})$ must be substituted into:

$$\vec{E}(\vec{r}) = \left(\frac{i}{\omega \varepsilon_0 \varepsilon(\vec{r})} \right) \nabla \times \vec{H}(\vec{r}) \tag{2.16}$$

By this way, the $\vec{E}(\vec{r})$ and $\vec{H}(\vec{r})$ modes for a given frequency and a given ε(r) can be determined. In general, an equation similar to (2.15) can first be derived for $\vec{E}(\vec{r})$, then substituted for $\vec{H}(\vec{r})$, but the transversality of the waves defined by Equations (2.9) and (2.10), will be lost, along with the Hermiticity of the operator $\nabla \times \left(\frac{1}{\varepsilon(\vec{r})} \nabla \times \right)$. By working with operators that are Hermitian, real eigenvalues and orthogonal modes for different frequencies are guaranteed [1].

2.2 Electromagnetic Waves in Nonlinear Periodic Dielectric Materials

Linearity and nonlinearity is a property of the medium through which light travels, rather than a property of the light itself but depends on the light intensity. Nonlinear behavior is not exhibited when light travels in free space due to the weak nonlinearity. Light interacts with light via the medium. The presence of an optical field modifies the properties of the medium which, modify another optical field or even the original field itself.

Properties of a dielectric medium through which an electromagnetic wave propagates are completely described by the relation between the polarization density vector P(**r**,t) and the electric field vector $\vec{E}(\vec{r},t)$. It was suggested that $\vec{P}(\vec{r},t)$ could be regarded as the output of a system whose input was $\vec{E}(\vec{r},t)$. The mathematical relation between the vector function $\vec{P}(\vec{r},t)$ and $\vec{E}(\vec{r},t)$ defines the system and is governed by the characteristic of the medium. The medium is said to be nonlinear if this relation is nonlinear [20].

A linear dielectric medium is characterized by linear relation between the polarization density and the electric field, $\vec{P} = \varepsilon_0 \chi \vec{E}$, where ε_0 is the permittivity of free space and χ is the electric susceptibility of the medium. In nonlinear media, polarization is described by the relationship as

$$\vec{P} = \epsilon_0 \chi(E)\vec{E} = \epsilon_0 \chi^{(1)} E + \epsilon_0 \chi^{(2)} E^2 + \epsilon_0 \chi^{(3)} E^3 + \cdots + \epsilon_0 \chi^{(n)} E^n + \cdots \tag{2.17}$$

The quantities $\chi^{(n)}$ are known as the nonlinear optical susceptibilities of nth order where $\chi^{(1)}$ is the linear susceptibility.

The propagation of light in a nonlinear medium is governed by the following wave equation, which was derived from Maxwell's equation for an arbitrary homogeneous dielectric medium.

$$\nabla^2 \vec{E} - \frac{1}{c_0^{\,2}} \frac{\partial^2 \vec{E}}{\partial t^2} = \mu_0 \frac{\partial^2 \vec{P}}{\partial t^2} \tag{2.18}$$

It is convenient to write P as a sum of linear and nonlinear parts,

$$\vec{P} = \varepsilon_0 \chi \vec{E} + \vec{P}_{NL} \tag{2.19}$$

Using the relations $n^2 = 1 + \chi$, $c_0 = 1/(\mu_0 \varepsilon_0)^{1/2}$ and $c = c_0 / n$, Equation (2.18) may be written

$$\nabla^2 \vec{E} - \frac{1}{c^2} \frac{\partial^2 \vec{E}}{\partial t^2} = -\mu_0 \frac{\partial^2 \vec{P}_{NL}}{\partial t^2} \tag{2.20}$$

Right side of Equation (2.20) behaves as a source term with regards to Born approximation [20]. This is the essential equation that defines the theory of nonlinear optics.

Instantaneous response is characterized by non-dispersive material properties. Non resonant medium where light and matter interacted, the light frequency is far away from optical resonances where strong absorption occurs. Therefore, if the signal with low intensity is applied, a medium with a nonresonant nonlinearity becomes entirely transparent. If the signal with high intensity is applied, material properties are changed by the incident field. Respond is assumed instantaneously to the electric field and it does not have a memory. Although the most of the interactions are represented by instantaneous response even if the pulse duration is order of the 10^{-14} s, memory effects are arise because of the some motion of atomic molecules and nuclei on a fs time scale. If the nonlinear material does not respond instantaneously to the optical field, polarization must be defined as the form of the convolution integrals in Equation (2.21) [21].

$$\vec{P}^{(n)}(t) = \epsilon_0 \iint \dots \int \chi^{(n)}(t_1, t_2, \dots, t_n)\vec{E}(t - t_1)\vec{E}(t - t_1 - t_2) \dots \times \vec{E}(t - t_1 - \cdots - t_n)dt_1 dt_2 \dots dt_n \quad (2.21)$$

Contributions of the Third-Order Nonlinear Polarization:

If the material cannot polarize instantaneously in response to an applied field, polarization is formulized as a function of time. Third-order nonlinear polarization is given by the time convolution between the third-order susceptibility function $\chi^{(3)}(t_1, t_2, t_3)$ and the electric field for the different time scales. It can be modeled by Born-Oppenheimer approximation for simplicity [22], [23].

$$P^{NL}(t) = \varepsilon_0 \chi_0^{(3)} \vec{E}(t) \int_{-\infty}^{\infty} g(t - t')E^2(t')dt' \quad (2.22)$$

where $\chi_0^{(3)}$is the weight of the third-order nonlinearity. The causal response function g(t) is normalized as

$$\int_{-\infty}^{\infty} g(t)dt = 1 \tag{2.23}$$

For modeling the nonresonant and the resonant transitions, g(t) is divided into two parts as

$$g(t) = \alpha\delta(t) + (1-\alpha)g_{Raman}(t) \tag{2.24}$$

where δ(t) is Dirac delta function and first term models the Kerr nonlinearity on the order of 1fs or less. The second term in the Equation (2.24) express the transient Raman nonlinearity by $g_{raman}(t)$ [22]

$$g_{Raman}(t) = \left(\frac{\tau_1^2 + \tau_2^2}{\tau_1\tau_2^2}\right) e^{-t/\tau_2} \sin(1/\tau_1)\, U(t) \tag{2.25}$$

where $\tau_1$and τ_2 are characteristic parameters of the material. This model is characterized by single Lorentzian line centered on the optical phonon frequency $1/\tau_1$and having a bandwidth of $1/\tau_2$ the reciprocal phonon lifetime.

Here, α is a real-valued constant in the range $0 \leq \alpha \leq 1$ which equilibrates the relative strengths of the Kerr and Raman interactions.

Raman Nonlinear Polarization:

If the α is taken 0, Raman nonlinear polarization can be expressed as convolution form of Equation (2.22) [22]

$$\vec{P}_{Raman}(t) = \varepsilon_0 \vec{E}(t)\left[\chi^{(3)}_{Raman}(t) * E^2(t)\right] \tag{2.26}$$

where

$$\chi^{(3)}_{Raman}(t) = (1-\alpha)\chi^{(3)}_0 g_{Raman}(t) \tag{2.27}$$

Instantaneous Kerr Nonlinear Polarization:

If the α is taken 1, instantaneous Kerr nonlinear polarization is given by [22]

$$\begin{aligned}\vec{P}_{Kerr}(t) &= \varepsilon_0 \chi^{(3)}_0 \vec{E}(t) \int_{-\infty}^{\infty} \alpha\delta(t-t')E^2(t')dt' \\ &= \alpha\varepsilon_0\chi^{(3)}_0 E^3(t)\end{aligned} \tag{2.28}$$

and material is called Kerr medium. Kerr media respond to optical fields by generating third harmonics and sums and differences of triplet of frequency.

The response of nonlinear medium to a monochromatic optical field $\vec{E}(t) = Re\{\vec{E}(\omega)\exp(j\omega t)\}$ is a nonlinear polarization $P_{NL}(t)$ containing a component at frequency ω and another at frequency 3ω,

$$\vec{P}_{NL}(\omega) = 3\chi^{(3)}\left|E(\omega)\right|^2 E(\omega) \tag{2.29}$$

$$\vec{P}_{NL}(3\omega) = \chi^{(3)}E^3(\omega) \tag{2.30}$$

The polarization component at frequency ω in Equation (2.29) corresponds to an incremental change of the optical susceptibility Δχ at frequency ω given by

$$\varepsilon_0\Delta\chi = \frac{P_{NL}(\omega)}{E(\omega)} = 3\chi^{(3)}\left|\vec{E}(\omega)\right|^2 = 6\chi^{(3)}\eta I \tag{2.31}$$

where $I = |E(\omega)|^2 / 2\eta$ is optical intensity of the initial wave and η is impedance of the medium. Since $n^2 = 1 + \chi$, this is equivalent to incremental refractive index $\Delta n = (\partial n / \partial \chi)\Delta\chi = \Delta\chi / 2n$, so that

$$\Delta n = \frac{3\eta}{\varepsilon_0 n} \chi^{(3)} I = n_2 I \tag{2.32}$$

Thus the change in the refractive index is proportional to the optical intensity. The overall refractive index is therefore a linear function of the optical intensity I,

$$n(I) = n + n_2 I \tag{2.33}$$

where

$$n_2 = \frac{3\eta_0}{n^2 \varepsilon_0} \chi^{(3)} \tag{2.34}$$

This effect is known as the optical Kerr effect. The optical Kerr effect is a self-induced effect in which the phase velocity of the wave depends on the wave's own intensity. The order of magnitude of the coefficient n_2 is 10^{-16} to 10^{-14} in glasses, 10^{-14} to 10^{-7} in doped glasses, 10^{-10} to 10^{-8} in organic materials and 10^{-10} to 10^{-2} in semiconductors [20]. It is sensitive to the operating wavelength and depends on the polarization. The elevation of the electromagnetic field inside the PhC allows strong nonlinear effects to occur without the need for extremely high-power lasers. Materials, that Kerr effect is stronger, are good nonlinear candidates as their relaxation time scales can be very short allowing fast switching applications [13]

2.3 Electromagnetic Waves in Dispersive Dielectric Materials

Generally in many problems, assuming constant of material parameters like permittivity and/or permeability is acceptable. However, a medium whose permittivity and/or permeability depend on the frequency of the wave is called dispersive and this phenomenon is known dispersion. Linear dispersion is divided to three common types like the Debye relaxation, the Lorentzian resonance, and the Drude model of metals and characterized by a complex-valued, frequency-domain susceptibility function χ (ω) [22].

2.3.1 Debye Media

Frequency domain susceptibility function χ(ω) has one or more real poles at separate frequencies in Debye media. Assuming a single-pole in Debye medium, susceptibility function is described by Equation (2.35).

$$\chi_p(\omega) = \frac{\varepsilon_{s,p} - \varepsilon_{\infty,p}}{1 + j\omega\tau_p} \equiv \frac{\Delta\varepsilon_p}{1 + j\omega\tau_p} \tag{2.35}$$

Where $\varepsilon_{s,p}$ is the static or zero-frequency relative permittivity, $\varepsilon_{\infty,p}$ at infinite frequency, $\Delta\varepsilon_p$ is the change in relative permittivity due to the Debye pole, and τ_p is the pole relaxation time [22]. Taking the inverse Fourier transformation of $\chi_p(\omega)$, real valued time-domain susceptibility function $\chi(t)$ is obtained such that

$$\chi_p(t) = \frac{\Delta\varepsilon_p}{\tau_p} e^{-t/\tau_p} U(t) \tag{2.36}$$

where U(t) is the unit step. Relative permittivity for a P poles is written as

$$\varepsilon(\omega) = \varepsilon_\infty + \sum_{p=1}^{p} \frac{\Delta\varepsilon_p}{1 + j\omega\tau_p} \tag{2.37}$$

2.3.2 Lorentz Media

Differently from Debye medium, frequency domain susceptibility function $\chi(\omega)$ has one or more pairs of complex-conjugate poles in Lorentz medium. Let's taking a single pole pair,

$$\chi_p(\omega) = \frac{\Delta\varepsilon_p \omega_p^2}{\omega_p^2 + 2j\omega\delta_p - \omega^2} \tag{2.38}$$

where $\Delta\varepsilon_p = \varepsilon_{s,p} - \varepsilon_{\infty,p}$ is the change in relative permittivity due to the Lorentz pole pair, ω_p is the frequency of the pole pair (the undamped resonant frequency of the medium), and δ_p is the damping coefficient [22].

Taking the inverse Fourier transformation of $\chi_p(\omega)$, real valued time-domain susceptibility function $\chi(t)$ is obtained such that

$$\chi_p(\omega) = \frac{\Delta\varepsilon_p \omega_p^2}{\sqrt{\omega_p^2 - \delta_p^2}} e^{-\delta_p t} \sin\left(\sqrt{\omega_p^2 - \delta_p^2}\, t\right) U(t) \tag{2.39}$$

Relative permittivity for a P pole pairs is written as

$$\varepsilon(\omega) = \varepsilon_\infty + \sum_{p=1}^{p} \frac{\Delta\varepsilon_p \omega_p^2}{\omega_p^2 + 2j\omega\delta_p - \omega^2} \tag{2.40}$$

2.3.3 Drude Media

Apart from the other dispersive models, Drude model can be used to handle optical wave interaction with dispersive metals. If the Drude medium has single pole, frequency domain susceptibility function is described by

$$\chi_p(\omega) = -\frac{\omega_p^2}{\omega^2 - j\omega\gamma_p} \tag{2.41}$$

where ω_p is the Drude pole frequency and γ_p is the inverse of the pole relaxation time [22]. Taking the inverse Fourier transformation of $\chi_p(\omega)$, real valued time-domain susceptibility function $\chi(t)$ is obtained such that

$$\chi_p(\omega) = \frac{\omega_p^2}{\gamma_p}(1 - e^{-\gamma_p t})U(t) \tag{2.42}$$

Relative permittivity for P poles is given as

$$\varepsilon(\omega) = \varepsilon_\infty - \sum_{p=1}^{p} \frac{\omega_p^2}{\omega^2 - j\omega\gamma_p} \tag{2.43}$$

When the wave interactions with material are studied, foregoing characteristics are should be deliberated.

CHAPTER 3

NUMERICAL METHODS FOR PHOTONIC CRYSTAL ANALYSIS

3.1 Computational Methods of Photonic Crystal

Numerical methods are employed to analyze and design of photonic structures because of the difficulty in analytical approaches. Therefore, various computational EM methods have been used for this purpose [22], [24]–[26], including the plane wave method (PWM) [27], [28] the transfer-matrix method (TMM) [29], the FDTD [22] method. These methods can be divided into two groups as frequency domain and time domain calculations. While the frequency domain method (PWE) is preferably for calculation of band structure, time domain method (FDTD) is most suitable for calculation of wave propagation and transmission, resonance modes and decays time etc.

3.1.1 Plane Wave Expansion Method (PWE)

As the summarized in the following, in this method, frequencies are found by solving the eigenvalue problem basically than the field changes are obtained with the corresponding eigenvectors. Once Maxwell's equations are solved for the constant $\varepsilon(r)$, it is possible to investigate the case when an electromagnetic wave is propagating through a dielectric media with a periodically changing dielectric constant.

It was also assumed that the materials are nonmagnetic. Thus their optical properties are fully described by $\varepsilon(r)$ alone. The most specific structural property of a photonic crystal is that it possesses discrete translational symmetry, which can be written as:

$$\varepsilon(\vec{r}) = \varepsilon(\vec{r} + \vec{a}_i), \text{ i= 1,2,3} \tag{3.1}$$

where $\{a_i\}$ are the real lattice vectors of the photonic crystal.

Due to the $\varepsilon(r)$ is periodic in PhC, $1/\varepsilon(r)$ is also periodic in Equation (2.15) and then expansion in terms of Fourier series as,

$$\frac{1}{\varepsilon(r)} = \sum_{G} \varepsilon_G e^{j\vec{G}\vec{r}} \tag{3.2}$$

where ε_G is

$$\varepsilon_G = \frac{1}{V_{cell}} \iiint_{cell} \frac{1}{\varepsilon(r)} e^{j\vec{G}\vec{r}} dv \tag{3.3}$$

V_{cell} and G in Equation (3.3) are volume of primitive unit cell and primitive vectors of the reciprocal lattice respectively.

According to the Bloch theorem, which states that in a periodic medium, the electric and the magnetic field modes can be presented as plane waves modulated with a periodic function with a period equal to the periodicity of the medium[30]. Thus,

$$\vec{E}(\vec{r}) = \vec{E}_k(\vec{r}) e^{i\vec{k}\cdot\vec{r}} \tag{3.4}$$

$$\vec{H}(\vec{r}) = \vec{H}_k(\vec{r}) e^{i\vec{k}\cdot\vec{r}} \tag{3.5}$$

where $E_k(r)$ and $H_k(r)$ are periodic functions described by:

$$\vec{E}_k(\vec{r}) = \vec{E}_k(\vec{r} + \vec{a}_i) \qquad \vec{H}_k(\vec{r}) = \vec{H}_k(\vec{r} + \vec{a}_i) \tag{3.6}$$

and expansion in terms of Fourier series as

$$\vec{H}(\vec{r}) = \sum_G H_{G,k} e^{[i(\vec{k}+\vec{G})\vec{r}]} \tag{3.7}$$

$$\vec{E}(\vec{r}) = \sum_G E_{G,k} e^{[i(\vec{k}+\vec{G})\vec{r}]} \tag{3.8}$$

Since both functions ε(r) and H(r) are periodic, they can be expanded into a Fourier series, the expansions substituted back into Equation (2.15), and the resulting Hermitian eigenvalue equations in (3.19) and (3.20) are solved

$$-\sum_G \varepsilon_G(\vec{G} - \vec{G}')(\vec{k} + \vec{G}') \times \left[(\vec{k} + \vec{G}') \times \vec{E}_{n,k}(\vec{G}')\right] = \frac{\omega_{n,k}^2}{c^2} \vec{E}_{n,k}(\vec{G}) \tag{3.9}$$

$$-\sum_G \varepsilon_G(\vec{G} - \vec{G}')(\vec{k} + \vec{G}') \times \left[(\vec{k} + \vec{G}') \times \vec{H}_{n,k}(\vec{G}')\right] = \frac{\omega_{n,k}^2}{c^2} \vec{H}_{n,k}(\vec{G}) \tag{3.10}$$

The analysis is carried out for all wavevectors within the irreducible Brillouin zone. In this manner, the frequencies ω for a given k-vector can be calculated, and this dependence plotted, resulting in the so-called "photonic band structure" or "photonic band diagram". This approach for resolving the band structure of a photonic crystal is called the "plane wave expansion method," due to the Fourier expansion of the

electromagnetic field and the dielectric function [31]. For example, Figure 3.1 shows the TE and TM photonic band diagram of a 2D photonic crystal with a triangular lattice comprised of air holes surrounded by dielectric material with epsilon 13 and r = 0.48*a* where transverse electric (transverse magnetic) means that the electric (magnetic) field vector E (B) lies in the plane of the periodicity. Such a gap can be achieved by carefully tailoring the parameters of the crystal, such as geometry, period, features size and materials used to make the photonic crystal.

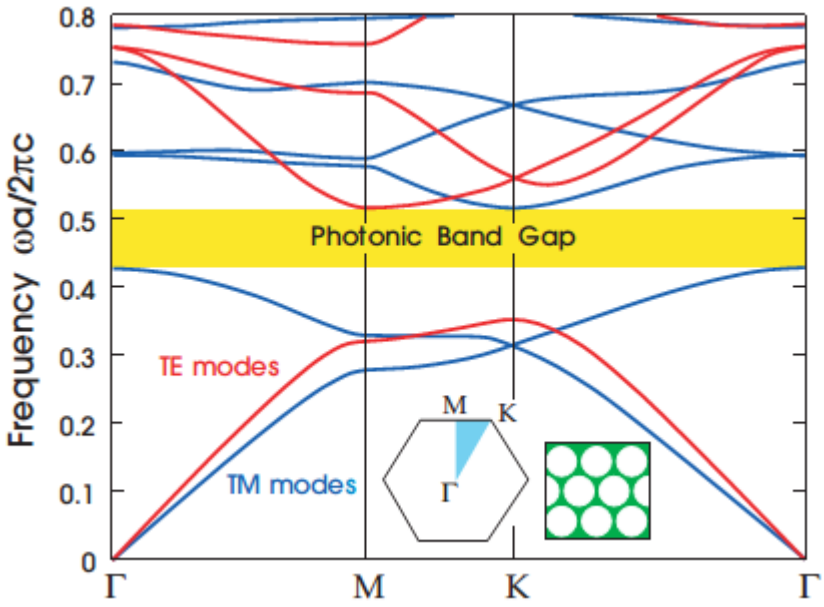

Figure 3.1. TE and TM band diagram of PhC [1]

3.1.2 Finite Difference Time Domain Method (FDTD)

Finite Difference Time Domain Method (FDTD) proposed by Yee at al.[32] is widely used methods for time domain analysis of PhC structures, because of the directly solution of Maxwell's curl equations. In this method, structure is composed to grid which is discretized in space and time as shown in Figure 3.2. Derivatives of the Maxwell's equations are defined in terms of finite differences on the grid points. By solving the difference equations, update equations which are used for determining the

unknown future field values in terms of the past field are obtained. Then the field distribution and interaction with structure are revealed [33].

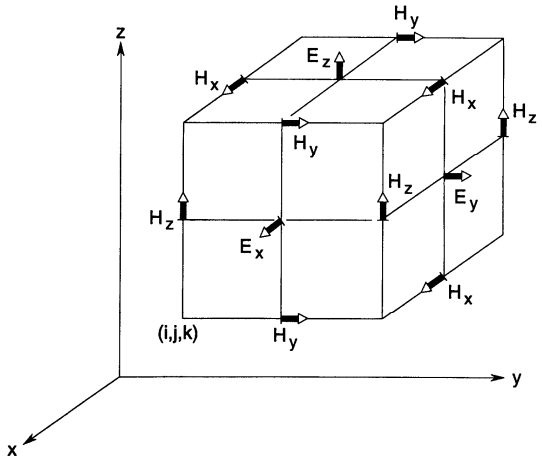

Figure 3.2. Discretization space and time in the unit cell of Yee lattice [32]

When $\delta=\delta x=\delta y=\delta z$ and δt are indicated to increase of space and time respectively, finite difference derivatives can be written as [22], [34]

$$\frac{\partial F^n(i,j,k)}{\partial} = \frac{F^n(i+\frac{1}{2},j,k) - F^n(i-\frac{1}{2},j,k)}{\delta} + O(\delta^2) \tag{3.11}$$

$$\frac{\partial F^n(i,j,k)}{\partial t} = \frac{F^{n+1/2}(i,j,k) - F^{n-1/2}(i,j,k)}{\delta t} + O(\delta t^2) \tag{3.12}$$

Here, the statement shown in brackets with O is the amount of error in this method. If the distance between two points taken derivative is small enough that all the terms represented by O are negligible.

TM and TE modes components are taken as (E_z, H_x, H_y) and (H_z, E_x, E_y) for two dimensional structure respectively. Applying the difference Equations (3.11) and (3.12) to maxwell's equation, following equations are obtained for TM mode.

$$E_z^{n+1/2}(i,j) = E_z^{n-1/2}(i,j) + \frac{c\delta t}{\varepsilon(i,j)\delta x}\left[H_y^n\left(i+\frac{1}{2},j\right) - H_y^n\left(i-\frac{1}{2},j\right)\right] - \frac{c\delta t}{\varepsilon(i,j)\delta y}\left[H_x^n\left(i,j+\frac{1}{2}\right) - H_x^n\left(i,j-\frac{1}{2}\right)\right] \tag{3.13}$$

$$H_x^{n+1}\left(i,j+\frac{1}{2}\right) = H_x^n\left(i,j+\frac{1}{2}\right) + \frac{c\delta t}{\mu\left(i,j+\frac{1}{2}\right)\delta y}\left[E_z^{n+\frac{1}{2}}(i,j) - E_z^{n+\frac{1}{2}}(i,j+1)\right] \tag{3.14}$$

$$H_y^{n+1}\left(i+\frac{1}{2},j\right) = H_y^n\left(i+\frac{1}{2},j\right) + \frac{c\delta t}{\mu\left(i+\frac{1}{2},j\right)\delta x}\left[E_z^{n+\frac{1}{2}}(i+1,j) - E_z^{n+\frac{1}{2}}(i,j)\right] \tag{3.15}$$

Solving the Equations (3.13), (3.14) and (3.15) numerically for each lattice point with beginning from initial values to the next point, time domain analysis of PhC can be performed. To keep the stability, following Courant condition must be satisfied for time and space.

$$v_{max}\delta t \leq \left(\frac{1}{\delta x^2} + \frac{1}{\delta y^2} + \frac{1}{\delta z^2}\right)^{-1/2} \tag{3.16}$$

Besides, to prevent the reflection from structure side, perfectly matched layer (PML) should be placed around the structure [35].

3.1.2.1 Nonlinear and Dispersive Medium

In nonlinear dispersive medium, material's permittivity and/or permeability varies with the sinusoidal frequency as well as the intensity of the wave [22]. Although the frequency dependence of time harmonic form of field is simple in frequency domain, FDTD technique use time domain. Hence, update equation should be written in time domain. Auxiliary differential equation (ADE) method is applicable with FDTD for simulation of the materials which have linear dispersion and a third-order Kerr and Raman dispersive nonlinearity [22]. Electric displacement D is related to the polarization density P by constitutive equations as

$$\vec{D} = \varepsilon_0 \varepsilon_\infty \vec{E} + \vec{P}^L + \vec{P}^{NL} \tag{3.17}$$

where the dielectric polarization is divided into two parts: a linear part P^L and a nonlinear part P^{NL}. Linear polarization P^L has two dispersion parts which are P_{Debye} and $P_{Lorentz}$ and nonlinear polarization is also two parts which are P_{Kerr} and P_{Raman}.

Linear Part:

Contribution of the Linear Debye polarization:

Frequency domain susceptibility for a single-pole Debye medium is written as

$$\chi_p(\omega) = \frac{\varepsilon_{s,p} - \varepsilon_{\infty,p}}{1 + j\omega\tau_p} \equiv \frac{\Delta\varepsilon_p}{1 + j\omega\tau_p} \tag{3.18}$$

The electric polarization is then given by

$$\check{P}_{Debye} = \frac{\Delta\varepsilon_p}{1 + j\omega\tau_p}\check{E} \tag{3.19}$$

Assuming the single field component E for simplicity and representing the equation (3.19) in time domain, auxiliary differential equation is obtained.

$$P_{Debye} + \tau_p \frac{\partial P_{Debye}}{\partial t} = \varepsilon_0 \Delta\varepsilon_p E \tag{3.20}$$

Expressing the Equation (3.20) in finite difference form, update equation of P_{Debye} centered at time-step n +1/2 is

$$P_{Debye}^{n+1} = \left[\frac{2\tau_p - \Delta t}{2\tau_p + \Delta t}\right] P_{Debye}^{n} + \left[\frac{\varepsilon_p \Delta\varepsilon_p \Delta t}{2\tau_p + \Delta t}\right] (E^{n+1} + E^{n}) \tag{3.21}$$

where Δt is the time-step [22].

Contribution of the Linear Lorentz polarization:

Frequency domain susceptibility for a single-pole-pair Lorentz medium is written as

$$\chi_p(\omega) = \frac{\Delta\varepsilon_p \omega_p^2}{\omega_p^2 + 2j\omega\delta_p - \omega^2} \tag{3.22}$$

The electric polarization is then given by

$$\check{P}_{Lorentz} = \frac{\varepsilon_0 \Delta \varepsilon_p \omega_p^2}{\omega_p^2 + 2j\omega\delta_p - \omega^2} \check{E} \tag{3.23}$$

Transforming Equation (3.23) to the time domain, following auxiliary differential equation is obtained [22].

$$\omega_p^2 P_{Lorentz} + 2\delta_p \frac{\partial P_{Lorentz}}{\partial t} + \frac{\partial {P_{Lorentz}}^2}{\partial t^2} = \varepsilon_0 \Delta \varepsilon_p \omega_p^2 E \tag{3.24}$$

Expressing the Equation (3.24) in finite difference form, update equation of $P_{Lorentz}$ centered at time-step n is

$$\begin{aligned} P_{Lorentz}^{n+1} = &\left[\frac{2 - \omega_p^2 \Delta t^2}{\delta_p \Delta t + 1}\right] P_{Lorentz}^{n} + \left[\frac{\delta_p \Delta t - 1}{\delta_p \Delta t + 1}\right] P_{Lorentz}^{n-1} \\ &+ \left[\frac{\varepsilon_p \Delta \varepsilon_p \omega_p^2 \Delta t}{\delta_p \Delta t + 1}\right] E^n \end{aligned} \tag{3.25}$$

Nonlinear Part:

Instantaneous Kerr Nonlinear Polarization:

The polarization contributed by the instantaneous Kerr nonlinearity is given by [22]

$$\begin{aligned} P_{Kerr}(t) &= \varepsilon_0 \chi_0^{(3)} E(t) \int_{-\infty}^{\infty} \alpha \delta(t - t') E^2(t') dt' \\ &= \alpha \varepsilon_0 \chi_0^{(3)} E^3(t) \end{aligned} \tag{3.26}$$

Update equation can be written as

$$P_{Kerr}(t) = \alpha\varepsilon_0\chi_0^{(3)}(E^{n+1})^3 \tag{3.27}$$

Third Order Raman Nonlinear Polarization:

From Equation (2.22), the polarization contributed by the Raman effects can be expressed as the convolution

$$P_{Raman}(t) = \varepsilon_0 E(t)\left[\chi_{Raman}^{(3)}(t) * E^2(t)\right] \tag{3.28}$$

where

$$\chi_{Raman}^{(3)}(t) = (1-\alpha)\chi_0^{(3)} g_{Raman}(t) \tag{3.29}$$

Introducing an auxiliary variable for the convolution

$$S(t) = \chi_{Raman}^{(3)}(t) * E^2(t) \tag{3.30}$$

The Fourier transform of (3.30) is expressed as

$$S(\omega) = \chi_{Raman}^{(3)}(\omega) \cdot \mathcal{F}[E^2(t)] \tag{3.31}$$

where $\mathcal{F}$ symbolize the Fourier transform, and the frequency-domain response function is given by

$$\chi_{Raman}^{(3)}(\omega) = \frac{(1-\alpha)\chi_0^{(3)}\omega_{\mathrm{Raman}}^2}{\omega_{\mathrm{Raman}}^2 + 2\mathrm{j}\omega\delta_{\mathrm{Raman}} - \omega^2} \tag{3.32}$$

where $\omega_{Raman} = \sqrt{\frac{\tau_1^2+\tau_2^2}{\tau_1\tau_2^2}}$ and $\delta_{Raman} = 1/\tau_2$. Auxiliary variable in Equation (3.31) is rewritten as

$$S(\omega) = \frac{(1-\alpha)\chi_0^{(3)}\omega_{\mathrm{Raman}}^2}{\omega_{\mathrm{Raman}}^2 + 2\mathrm{j}\omega\delta_{\mathrm{Raman}} - \omega^2}\mathcal{F}[E^2(t)] \tag{3.33}$$

Transforming to the time domain by taking inverse Fourier transformation, following auxiliary differential equation is yield.

$$\omega_{Raman}^2 S + 2\delta_{Raman}\frac{\partial S}{\partial t} + \frac{\partial^2 S}{\partial t^2} = (1-\alpha)\chi_0^{(3)}\omega_{\mathrm{Raman}}^2\mathrm{E}^2 \tag{3.34}$$

Expressing in finite-difference form of Equation (3.34) centered at time-step n, the following update for S is obtained.

$$\begin{aligned} S^{n+1} = &\left[\frac{2-\omega_{\mathrm{Raman}}^2(\Delta\mathrm{t})^2}{\delta_{Raman}\Delta t + 1}\right]S^n + \left[\frac{\delta_{Raman}\Delta t - 1}{\delta_{Raman}\Delta t + 1}\right]S^{n-1} \\ &+ \left[\frac{(1-\alpha)\chi_0^{(3)}\omega_{\mathrm{Raman}}^2(\Delta\mathrm{t})^2}{\delta_{Raman}\Delta t + 1}\right](E^n)^2 \end{aligned} \tag{3.35}$$

Since from (3.28) and (3.30) we have

$$P_{Raman}(t) = \varepsilon_0 E(t)S(t) \tag{3.36}$$

The update equation for the Raman polarization is

$$P_{Raman}^{n+1}(t) = \varepsilon_0 E^{n+1} S^{n+1} \tag{3.37}$$

where S^{n+1} is given by (3.35) [22]. For finalizing the linear and nonlinear polarization contributions, equations (3.21), (3.25), (3.27) and (3.37) are substituted into (3.17), and expanded form of time-stepping is

$$D^{n+1} = \varepsilon_0 \varepsilon_\infty E^{n+1} + P_{Debye}^{n+1} + P_{Lorentz}^{n+1} + P_{Kerr}^{n+1} + P_{Raman}^{n+1} \tag{3.38}$$

Separating the E^{n+1} term, electric field update is obtained.

$$E^{n+1} = \left(D^{n+1} - P_{Debye}^{n+1} - P_{Lorentz}^{n+1} - P_{Kerr}^{n+1} - P_{Raman}^{n+1}\right)/\varepsilon_0 \varepsilon_\infty \tag{3.39}$$

Meep supports instantaneous isotropic (or diagonal anisotropic) nonlinear effects of the form [18]:

$$D_i - P_i = \varepsilon^{(1)} E_i + \chi_i^{(2)} {E_i}^2 + \chi_i^{(3)} |\mathbf{E}|^2 E_i \tag{3.40}$$

where $\varepsilon^{(1)}$ represents the nondispersive terms and P_i is a dispersive polarization $P = \chi_{dispersive}^{(1)}(\omega)\mathbf{E}$ from dispersive materials. Meep solves this equation with **D** is updated from $\nabla \times \mathbf{H}$ before updating **E** from **D**. Padé approximant is used for approximate solution of Equation (3.40) in Meep as the following

$$E_i = \left[\frac{1 + \left(\frac{\chi^{(2)}}{\left[\varepsilon^{(1)}\right]^2} \tilde{D}_i \right) + 2\left(\frac{\chi^{(3)}}{\left[\varepsilon^{(1)}\right]^3} \left\|\tilde{\mathbf{D}}\right\|^2 \right)}{1 + 2\left(\frac{\chi^{(2)}}{\left[\varepsilon^{(1)}\right]^2} \tilde{D}_i \right) + 3\left(\frac{\chi^{(3)}}{\left[\varepsilon^{(1)}\right]^3} \left\|\tilde{\mathbf{D}}\right\|^2 \right)} \right] \left[\varepsilon^{(1)}\right]^{-1} \tilde{D}_i \tag{3.41}$$

where $\tilde{D}_i = D_i - P_i$. Meep supports material dispersion with the following form of a sum of harmonic resonances;

$$\varepsilon(\omega, x) = \varepsilon_\infty(x) + \sum_n \frac{\sigma_n(x) \cdot \omega_2^2 \Delta\varepsilon_n}{\omega_n^2 - \omega^2 - i\omega\gamma_n} \tag{3.42}$$

Where ω_n , γ_n and $\Delta\varepsilon_n$ are constants and $\sigma_n(x)$ is function of position. Related polarization equation is written as

$$\frac{d^2 P_n}{dt^2} + \gamma_n \frac{dP_n}{dt} + \omega_n^2 P_n = \sigma_n(x)\omega_n^2 \Delta\varepsilon_n E \tag{3.43}$$

This equation is easily transformed to the Drude model by taken ω_n=0 which is generally used for metals [18].

3.2 Computational Methods of Bragg Gratings

Estimation of Bragg frequency is important to save the time. Since the simulation time is quite long, simulation is focused especially around the Bragg frequency region. Bragg frequency is estimated from expected index profile along the grating x-axis. There are several methods used for simulating the Bragg grating in the literature. [36]–[39]. In this study we prefer widely used transfer matrix method which is based on discretization the grating structure in subsections. Each subsection is described as a matrix transforming the fields on one side to the fields its other side.

Definition of matrix formation is another variation in the literature. Transfer matrix of thin layer approach and transfer matrix solution of coupled mode equations are used in this chapter.

3.2.1 Thin Layer Matrix Method (TMM)

In this method, multilayered medium is divided into N sub-section and it is assumed as thin and its refractive index is constant from one side to the other side of section. The transmission matrix M is depicted in Figure 3.3 and it is defined as Equation (3.44). Transmitted and reflected amplitudes in all medium are defined in single matrix which is matrix product in Equation (3.45) [20].

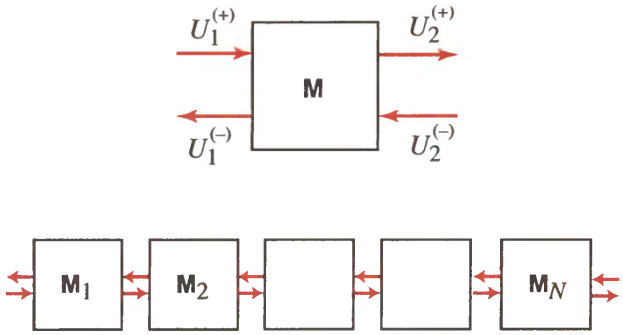

Figure 3.3. Matrix formation of periodic structure [20]

$$\begin{bmatrix} U_2^{(+)} \\ U_1^{(-)} \end{bmatrix} = \begin{bmatrix} A & B \\ C & D \end{bmatrix} \begin{bmatrix} U_2^{(+)} \\ U_1^{(-)} \end{bmatrix} \tag{3.44}$$

$$M = M_N \dots M_2 M_1 \tag{3.45}$$

Reflection r and transmission t at the interface of adjacent section is defined by the Fresnel equation as

$$r_p = \frac{n_{p-1} - n_p}{n_{p-1} + n_p} \tag{3.46}$$

$$t_p = \frac{2n_p}{n_{p-1} + n_p} \tag{3.47}$$

$$\acute{r}_p = -\acute{r}_p \tag{3.48}$$

$$t_p t'_p = 1 - r_p^2 \tag{3.49}$$

where n_p , and n_{p-1} are the refractive index values of two connected grating sections.

Indicating the forward and backward travelling waves as before the intersection A, B and after the intersection fields A', B' , we can write the following relation that

$$\acute{A} = tA + r'B' \tag{3.50}$$

$$B = rA + t'B' \tag{3.51}$$

or

$$A = \left(\frac{1}{t}\right)\acute{A} + \left(\frac{r}{t}\right)B' \tag{3.52}$$

$$B = \left(\frac{r}{t}\right)\acute{A} + \left(\frac{1}{t}\right)B' \tag{3.53}$$

We can write this expression in matrix form,

$$\begin{pmatrix} A_{p-1} \\ B_{p-1} \end{pmatrix} = \frac{1}{2n_p} \begin{pmatrix} n_{p-1}+n_p & n_{p-1}-n_p \\ n_{p-1}-n_p & n_{p-1}+n_p \end{pmatrix} \begin{pmatrix} \acute{A}_p \\ \acute{B}_p \end{pmatrix} \tag{3.54}$$

In order to obtain accurately model, propagation distance though the section must be introduced in to the matrix form. Phase term is defined as

$$\delta\phi_p = \frac{2\pi}{\lambda} n_p l \tag{3.55}$$

Where λ is vacuum wavelength and l is length of the section. So, field at each side of grating section is related with the following matrix form,

$$\begin{pmatrix} A_{p-1} \\ B_{p-1} \end{pmatrix} = \frac{1}{2n_p} \begin{pmatrix} n_{p-1}+n_p & n_{p-1}-n_p \\ n_{p-1}-n_p & n_{p-1}+n_p \end{pmatrix} \begin{pmatrix} e^{-i\frac{2\pi}{\lambda}n_p l} & 0 \\ 0 & e^{i\frac{2\pi}{\lambda}n_p l} \end{pmatrix} \begin{pmatrix} A_p \\ B_p \end{pmatrix} \tag{3.56}$$

or

$$\begin{pmatrix} A_{p-1} \\ B_{p-1} \end{pmatrix} = \frac{1}{2n_p} M_p T_p \begin{pmatrix} A_p \\ B_p \end{pmatrix} \tag{3.57}$$

where $\mathbf{M}_p$ and $\mathbf{T}_p$ are intersection and propagation matrices respectively. Total transfer matrix of grating expressed by N section is

$$\begin{pmatrix} A_0 \\ B_0 \end{pmatrix} = \prod_{p=1}^{N} \frac{1}{2n_p} M_p T_p \begin{pmatrix} A_N \\ 0 \end{pmatrix} \tag{3.58}$$

Note that there is no light of incident at the end of grating face, B_N=0. Defining the transfer matrix

$$\begin{pmatrix} I_{11} & I_{12} \\ I_{21} & I_{22} \end{pmatrix} = \prod_{p=1}^{N} \frac{1}{2n_p} M_p T_p \tag{3.59}$$

then reflection and transmission coefficients are obtained as,

$$r(\lambda) = \frac{B_0}{A_0} = \frac{I_{21}}{I_{11}} \tag{3.60}$$

$$t(\lambda) = \frac{A_N}{A_0} = \frac{1}{I_{11}} \tag{3.61}$$

3.2.2 Transfer Matrix Solution of Coupled Mode Equation

Transverse component of electric field can be written as a superposition of modes as

$$\vec{E}_t(x,y,z,t) = \sum_j \left[A_j(z)e^{i\beta_j z} + B_j(z)e^{-i\beta_j z}\right]\vec{e}_{jt}(x,y)e^{-i\omega t} \tag{3.62}$$

where A_j(z) and B_j(z) are slowly varying amplitudes of the *j*th mode travelling in the +z and –z directions, respectively[40]. Coupling relation of modes is given as following equations [41];

$$\begin{aligned} \frac{dA_j}{dz} = i \sum_k A_k \left(K_{kj}^t + K_{kj}^z\right) exp\left[i(\beta_k - \beta_j)z\right] \\ + i \sum_k B_k \left(K_{kj}^t - K_{kj}^z\right) exp\left[-i(\beta_k + \beta_j)z\right] \end{aligned} \tag{3.63}$$

$$\frac{dB_j}{dz} = -i\sum_k A_k\left(K_{kj}^t - K_{kj}^z\right)exp\left[i(\beta_k + \beta_j)z\right] - i\sum_k B_k\left(K_{kj}^t + K_{kj}^z\right)exp\left[-i(\beta_k - \beta_j)z\right] \tag{3.64}$$

Under the counter-propagation mode coupling approach, coupling equations are simplified as

$$\frac{dR}{dz} = i\hat{\sigma}R(z) + i\kappa S(z) \tag{3.65}$$

$$\frac{dS}{dz} = -i\hat{\sigma}S(z) - i\kappa^* R(z) \tag{3.66}$$

where R and S are the amplitudes defined as $R(z) = A(z)\exp(i\delta z - \phi/2)$ and $S(z) = B(z)\exp(-i\delta z + \phi/2)$ and κ and $\hat{\sigma}$ is AC and DC coupling coefficient. DC (sef-coupling) coefficient $\hat{\sigma}$ is defined as

$$\hat{\sigma} = \delta + \sigma - \frac{1}{2}\frac{d\phi}{dz} \tag{3.67}$$

Detuning parameter δ is independent from *z* for all gratings and defined as

$$\delta = \beta - \frac{\pi}{\Lambda} = \beta - \beta_B = 2\pi n_{eff}\left(\frac{1}{\lambda} - \frac{1}{\lambda_D}\right) \tag{3.68}$$

where $\lambda_D = 2n_{eff}\Lambda$ is the design wavelength for Bragg scattering by weak grating. If the δ=0, we can find Bragg condition predicted by qualitative grating picture.

For single mode Bragg reflection grating, simple relation of coupling coefficient is written as

$$\sigma = \frac{2\pi}{\lambda}\overline{\delta n}_{eff} \tag{3.69}$$

$$\kappa = \frac{\pi}{\lambda}\nu\overline{\delta n}_{eff} \tag{3.70}$$

According to the transfer matrix method, we can divide the grating M uniform short section and define R_i and S_i for each section. Propagation through each section *i* is described by $\mathbf{F}_i$ as

$$\begin{bmatrix} R_i \\ S_i \end{bmatrix} = \mathbf{F}_i \begin{bmatrix} R_{i-1} \\ S_{i-1} \end{bmatrix} \tag{3.71}$$

For each section of grating, $\mathbf{F}_i$ is given by [42]

$$\mathbf{F}_i = \begin{bmatrix} \cosh(\gamma_B \Delta z) - i\frac{\hat{\sigma}}{\gamma_B}\sinh(\gamma_B \Delta z) & -i\frac{\kappa}{\gamma_B}\sinh(\gamma_B \Delta z) \\ i\frac{\kappa}{\gamma_B}\sinh(\gamma_B \Delta z) & \cosh(\gamma_B \Delta z) + i\frac{\hat{\sigma}}{\gamma_B}\sinh(\gamma_B \Delta z) \end{bmatrix} \tag{3.72}$$

where the coupling coefficient κ and $\hat{\sigma}$ are the local value of the section *i* and Δz is the section length and γ_B is defined by

$$\gamma_B = \sqrt{\kappa^2 - \hat{\sigma}^2} \tag{3.73}$$

Although these parameters are z-dependent for apodized grating, they might be evaluated constant at the center of each section according to piecewise-uniform approach. **F** matrix elements are given as

$$\mathbf{F} = \begin{pmatrix} T_{11} & T_{12} \\ T_{21} & T_{22} \end{pmatrix} \tag{3.74}$$

$$T_{11}^{*} = T_{22} \tag{3.75}$$

$$T_{12}^{*} = T_{21} \tag{3.76}$$

where (*) denotes the complex conjugation. For single section,

$$\begin{pmatrix} A(l)e^{-i\beta\Delta z} \\ B(l)e^{i\beta\Delta z} \end{pmatrix} = \begin{pmatrix} T_{11} & T_{12} \\ T_{21} & T_{22} \end{pmatrix} \begin{pmatrix} A_0 \\ B_0 \end{pmatrix} \tag{3.77}$$

and solving the equation for field at the front face with

$$\begin{pmatrix} A_0 \\ B_0 \end{pmatrix} = \begin{pmatrix} T_{22} & -T_{21} \\ -T_{12} & T_{11} \end{pmatrix} \begin{pmatrix} A(l)e^{-i\beta\Delta z} \\ B(l)e^{-i\beta\Delta z} \end{pmatrix} \tag{3.78}$$

If a matrix of all each section is known, we can find amplitudes by transfer matrix of whole grating of length *L* from

$$\begin{pmatrix} A_0 \\ B_0 \end{pmatrix} = \begin{pmatrix} I_{11} & I_{12} \\ I_{21} & I_{22} \end{pmatrix} \begin{pmatrix} A(l)e^{-i\beta\Delta z} \\ 0 \end{pmatrix} \tag{3.79}$$

where

$$\begin{pmatrix} I_{11} & I_{12} \\ I_{21} & I_{22} \end{pmatrix} = \prod_{p=1}^{N} \begin{pmatrix} T_{22} & -T_{12} \\ -T_{21} & T_{11} \end{pmatrix} \tag{3.80}$$

Reflection and transmission coefficients are calculated from

$$r(\lambda) = \frac{B_0}{A_0} = \frac{I_{21}}{I_{11}} \tag{3.81}$$

$$t(\lambda) = \frac{1}{I_{11}} \tag{3.82}$$

For phase-shifted and sampled gratings, phase shift matrix $\mathbf{F}_{pi}$ must be included between $\mathbf{F}_i$ and $\mathbf{F}_{i+1}$ like

$$\mathbf{F}_{pi}^{B} = \begin{bmatrix} e^{-i\frac{\phi_i}{2}} & 0 \\ 0 & e^{i\frac{\phi_i}{2}} \end{bmatrix} \tag{3.83}$$

TMM can be used for the unraveling of transmission, reflection and absorption spectra for multilayer systems including PhCs. [43].

CHAPTER 4

INTERFERENCE GRATING FILTERS IN PHOTONIC CRYSTALS

4.1 Multiple Wave Interference Patterns

The intensity distribution of a superposition of two or more coherent plane-waves will have a spatial structure that is non-uniform, a phenomenon known as interference. When two or more coherent optical waves are present simultaneously in the region, the waves interfere and produce a periodic intensity distribution [44]. While two wave interferences result in one-dimensional periodic structures, three waves are required for two-dimensional periodic structures, as depicted in Figure 4.1.

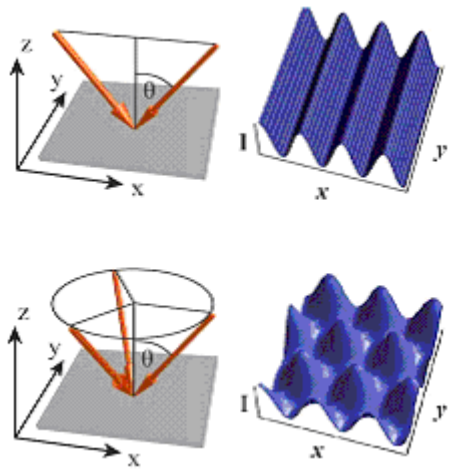

Figure 4.1. Interferences wave vectors [44]

Light intensity is the important quantity in a lithographic exposure, and can be formulated in terms of the electric field as

$$I = \frac{c}{4\pi}\sqrt{\frac{\varepsilon}{\mu}}\left\langle \vec{E}(\vec{r},t)^2 \right\rangle \tag{4.1}$$

In the above equation, c is the speed of light and the pointy brackets represent a time average. Averaging over a time interval that is large compared to the temporal periodicity of the wave, the spatial variations of the intensity distribution are proportional to the squared phasor field. The proportionality constants are dropped for simplicity.

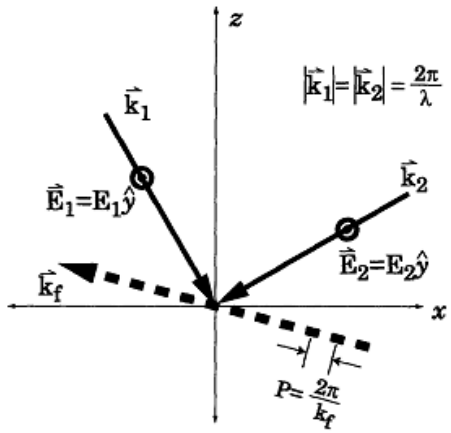

Figure 4.2. The periodicity of fringes formed by the interference of two plane waves is inversely proportional to the magnitude of the fringe vector $\vec{k}_f$ [45]

For two overlapping plane-waves $\mathbf{E}_1$ and $\mathbf{E}_2$, the intensity $\mathbf{I}_{12}$ at a given spatial point **r** can also be described by Equation (4.2), except that the sum electric field of the two waves is substituted for the field of a single wave

$$I \approx \vec{E}(\vec{r}) \cdot \vec{E}(\vec{r})^* \tag{4.2}$$

The phasor descriptions of two plane-waves are given below in Equations (4.3) and (4.4). An arbitrary phase difference $\Delta\phi$ between the two waves is included in the description of $\mathbf{E}_2$

$$\vec{E}_1(\vec{r}) = \vec{E}_1 e^{i\vec{k}_1 \cdot \vec{r}} \tag{4.3}$$

$$\vec{E}_2(\vec{r}) = \vec{E}_2 e^{i\vec{k}_{21} \cdot \vec{r} + i\Delta\phi} \tag{4.4}$$

The intensity distribution of the superposition of the two waves is equal to the square magnitude of the sum electric field.

$$I_{12} = \left|\vec{E}_1(\vec{r}) + \vec{E}_2(\vec{r})\right|^2 \tag{4.5}$$

$$I_{12} = I_1 + I_2 + \left[\left(\vec{E}_1(\vec{r}) \cdot \vec{E}_2{}^*(\vec{r})\right) + \left(\vec{E}_1{}^*(\vec{r}) \cdot \vec{E}_2(\vec{r})\right)\right] \tag{4.6}$$

The intensity of the two waves together is seen to be more complex than simply the sum of intensities for the two waves. The bracketed term above is known as the interference term, which modulates the sum intensity of the two waves. Solving the interference term, we see two important features; the spatial dependence is sinusoidal and depends on the orientation of the two electric fields.

$$I_{12} = I_1 + I_2 + 2\left(\vec{E}_1 \vec{E}_2\right)\cos\left[\left(\vec{k}_1 - \vec{k}_2\right) \cdot \vec{r} + \Delta\phi\right] \tag{4.7}$$

In practical terms, it is easier to write the above equation using only the intensity, which is measurable, rather than the electric field, which is not. Writing the

electric fields in terms of their magnitude ($\sqrt{I_1}$ and $\sqrt{I_2}$) and direction ($\hat{e}_1$ and $\hat{e}_2$) the general description of the intensity distribution is given in Equation (4.8). This is known as the interference pattern.

$$I_{12} = I_1 + I_2 + 2\sqrt{I_1 I_2}(\hat{e}_1 \cdot \hat{e}_2)\cos\left[(\vec{k}_1 - \vec{k}_2)\cdot \vec{r} + \Delta\phi\right] \tag{4.8}$$

The intensity distribution of the N interference field can be described by a Fourier superposition:

$$I = \sum_{i=1}^{N}\left|\vec{E}_i\right|^2 + \sum_{i\neq j}^{N}\vec{E}_i^{\,*}\cdot\vec{E}_j \exp\left[i\left\{(\vec{k}_j - \vec{k}_i)\cdot\vec{r} + (\phi_j - \phi_i)\right\}\right] \tag{4.9}$$

where $\vec{r}$ is the position vector, $\vec{E}_i$, $\vec{k}_i$ and ϕ_i are the complex amplitude, wave vector, and phase of the *i*th wave, respectively [46]. The complex amplitude vector of the *i*th wave can be written as

$$\vec{E}_i = E_i \exp\left(i\vec{k}_i \cdot \vec{r} + \phi_j\right)e_i \tag{4.10}$$

where E_i, and e_i are the *i*th wave's real amplitude and polarization vector, respectively. The difference between two of the wave vectors $(\vec{k}_i - \vec{k}_j)$, where *i,j* = 1,2,…N and *i*<*j* determines the spatial periodicity, or transformational symmetry of the interference pattern [46]–[48].

The contrast of the interference pattern is controlled by the real amplitude, polarization and phase of each wave as shown in Figure 4.3 [46], [49], [50]. It should be noted, though, that the planewave is an idealized, non-physical entity. Furthermore,

application of Fourier techniques allows an arbitrary wavefront to be described as a sum of plane-wave components.

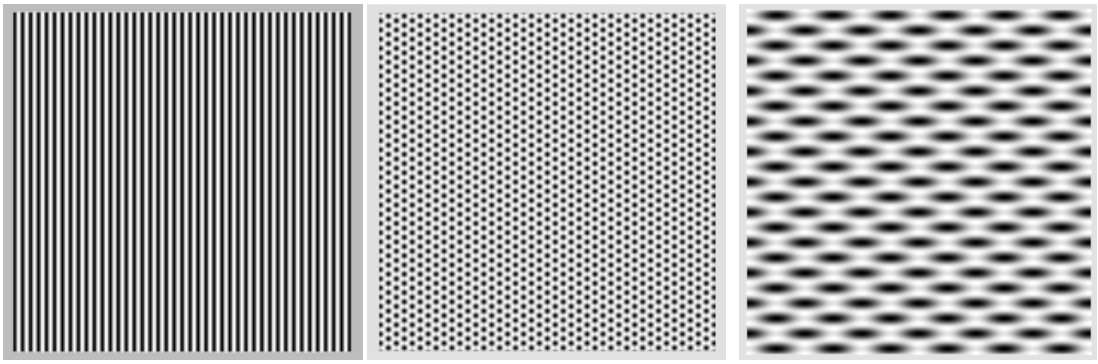

a) b) c)

Figure 4.3. Two and three wave interference patterns obtained by MEEP for a) $\theta_1= \theta_2=\pi/3$, $\phi_1= 2\pi/3$ $\phi_2=4\pi/3$ b) $\theta_1= \theta_2= \theta_3= \pi/3$, $\phi_1= 2\pi/3$ $\phi_2= 4\pi/3$, $\phi_3= 6\pi/3$ c) $\theta_1= \theta_2= \theta_3=29\pi/180$, $\phi_1=34\pi/180$, $\phi_2=90\pi/180$, $\phi_3=146\pi/180$

4.2 Proposed Interference Grating in Photonic Crystal

For two or more coherent beams (instead of waves) the intensity distribution will be spatially quasi-periodic and non-uniform [51]. In this work, two-dimensional Gaussian beams interference geometry (two beams are in the same plane) has been considered for simplicity and one dimensional interference grating geometry is depicted in the Figure 4.4. Here, interference waves are realistic Gaussian beams rather than plane waves.

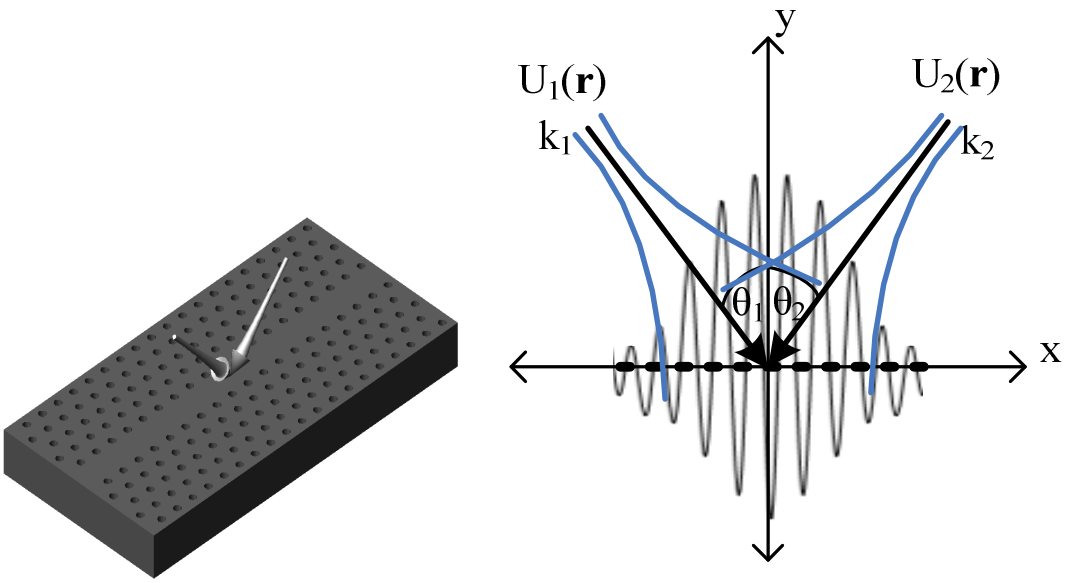

Figure 4.4.Gaussian beam interference geometry in PhC

After the coordinate transformation and the first order approximation, complex Gaussian beam equation can be written as follows;

$$U(x)=\frac{A}{\left(L+y\cdot\cos(\theta)-x\cdot\sin(\theta)+i\cdot z_0\right)}\times\exp\left[-ik\left(L+y\cdot\cos(\theta)-x\cdot\sin(\theta)\right)\right]$$
$$\times\exp\left[\frac{-1}{2\left[L+y\cdot\cos(\theta)-x\cdot\sin(\theta+i\cdot z_0\right)]}\cdot ik\left[\left(x\cdot\cos(\theta)+y\cdot\sin(\theta)\right)^2\right]\right] \quad (4.11)$$

Where z_0 is Rayleigh range, θ is incidence angle, L is the axial distance from minimum waist of beam to interference plane and A is constant.

Interference equation will be in the following equation.

$$I(\mathbf{r},t)=\left|U_1(\mathbf{r},t)+U_2(\mathbf{r},t)\right|^2 \quad (4.12)$$

The period of the uniform grating Λ is given as

$$\Lambda = \frac{\lambda_{beam}}{2\sin\theta} \tag{4.13}$$

where λ_{beam} is the wavelength of the Gaussian beam and θ is the incident angle of beam. Bragg wavelength which corresponds to input signal reflected back in a uniform grating structure is given as,

$$\lambda_B = 2\Lambda\bar{n} \tag{4.14}$$

where $\bar{n}$ the effective average refractive index as defined in [20].

In general, an interference grating structure can be generated in a third order (Kerr type) nonlinear waveguide by exposing the intensity distribution of the interference as shown in Figure 4.5. The nonlinear Kerr medium will be modified according to refractive index profile of the intensity distribution (Figure 4.7), because the Kerr type nonlinearity is a linear function of the optical intensity *I* in the following equations,

$$n(I) = n + n_2 I \tag{5}$$

and n_2 is given as

$$n_2 = \frac{3\eta_0}{n^2\varepsilon_0}\chi^{(3)} \tag{6}$$

where n is refractive index , $\Delta n = n_2 I$ is nonlinear index change, η_0 is impedance of free space, and $\chi^{(3)}$ is Kerr coefficient [20].

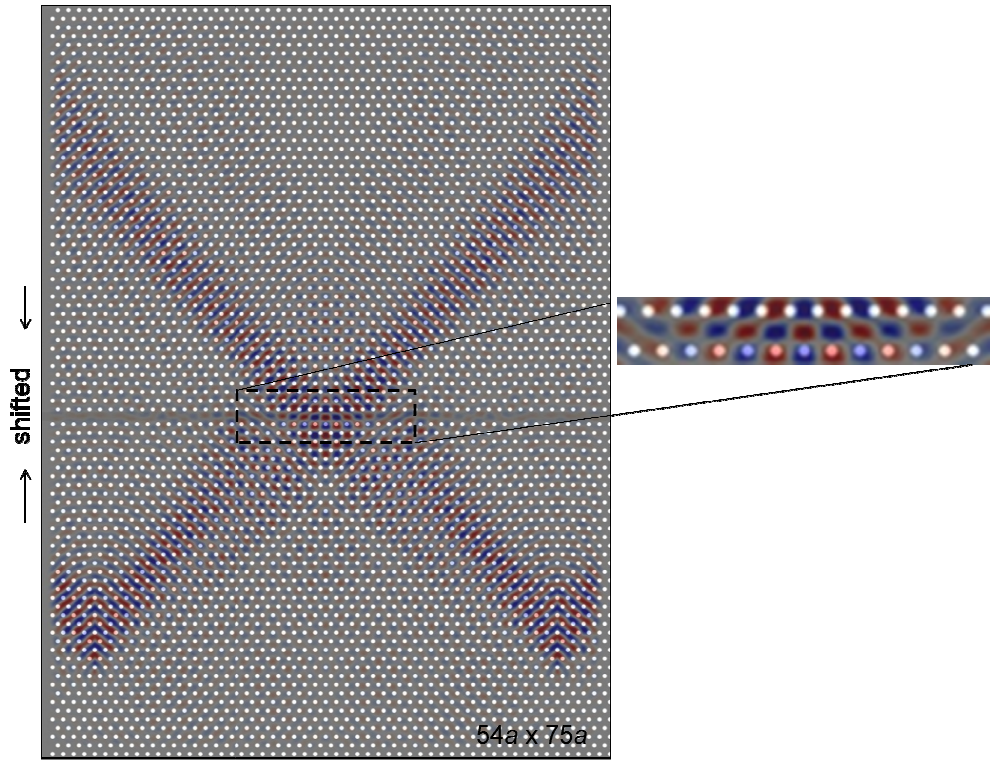

Figure 4.5. Gaussian beams (H_z polarized) interference pattern in PhC structure ($54a$ x $75a$), (U_1, U_2 are identical and incident angle is taken θ=45º)

When the beams interference occurs at the y=0 plane, a stationary grating pattern is created. The grating period, along the x-direction, depends on the interference beam angle, the writing beam wavelength, and the interference plane (y).

According to the interference equation (4.12), there are two terms that make the refractive index profile different than the uniform grating. The first term is an amplitude modulation (envelope) that diminishes exponentially and the second term is a pitch modulation that modifies the grating period. The grating length is bounded with the envelope function of the interference equation [52].

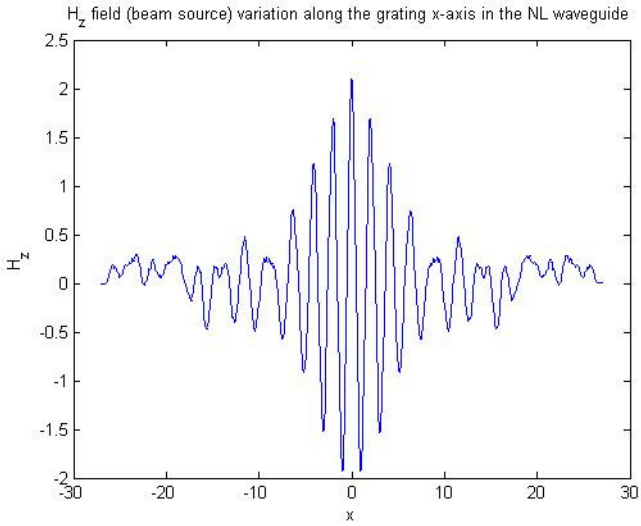

Figure 4.6. Electric field variation along the grating axis in PhC nonlinear simulation.

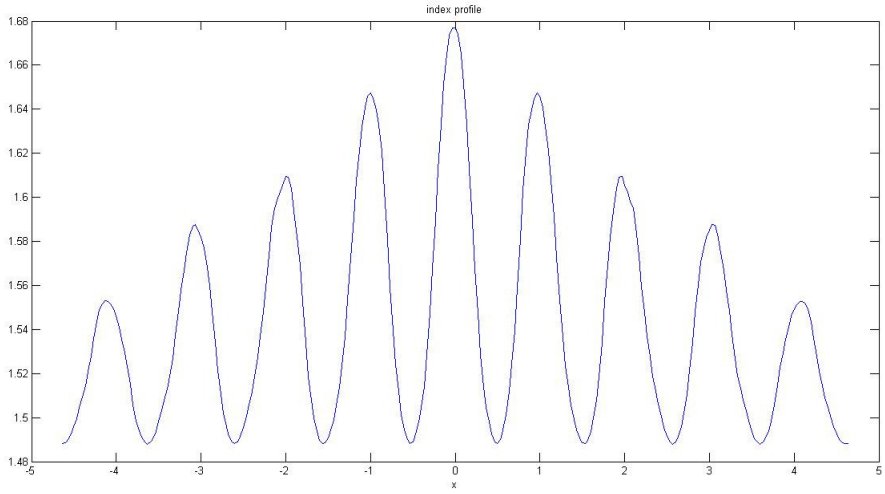

Figure 4.7. Expected index profile along the grating *x*-axis

Estimation of Bragg Frequency:

Corresponded Bragg frequency is calculated by TMM from expected index profile in Figure 4.7. Index profile is divided into subsections and each part should be smaller than grating pitch to obtain correctly resulting as shown in Figure 4.8 where red parts indicate the each cell of transfer matrix. Transfer matrix is defined for each part and Bragg frequency is obtained as 0.33 c/a and matched with the calculated from Equation (4.14) with the parameters of $\bar{n} = 1.543$ and $\Lambda = 0.96\mu m$.

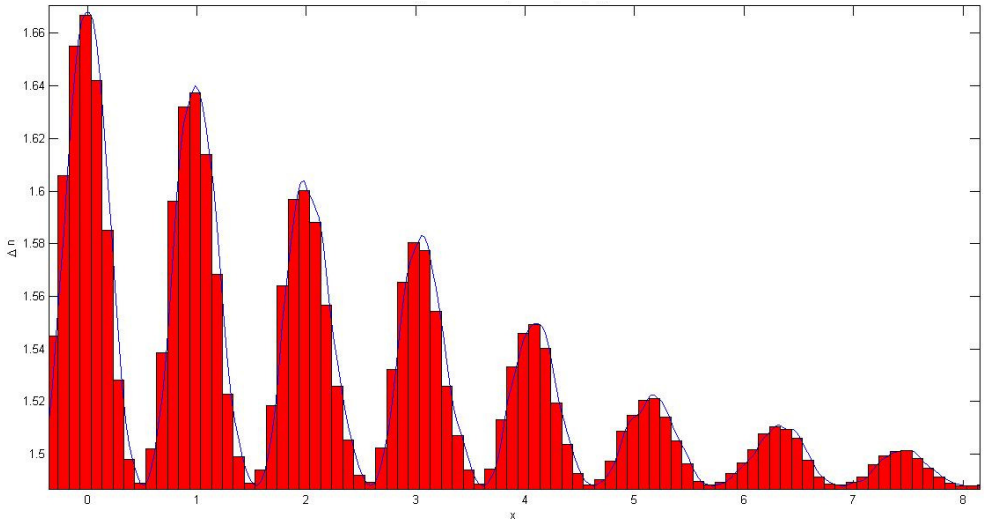

Figure 4.8. Segmentation of grating index profile

Mode Excitation:

Mode excitation is another important point to guarantee the maximum power transmits to the waveguide. If more than one mode excited and source is not well guided (Figure 4.11b), and some faulty occur in the flux graphs. Every mode has a unique wave number and field profile which is orthogonal to propagation direction. Hence, to excite the mode, mode profile obtained from band structure should be used for source amplitude function as shown in Figure 4.9-Figure 4.10. Especially, detailed band structure is obtained around the estimated Bragg frequency and modes are distinguished and verified by visualization.

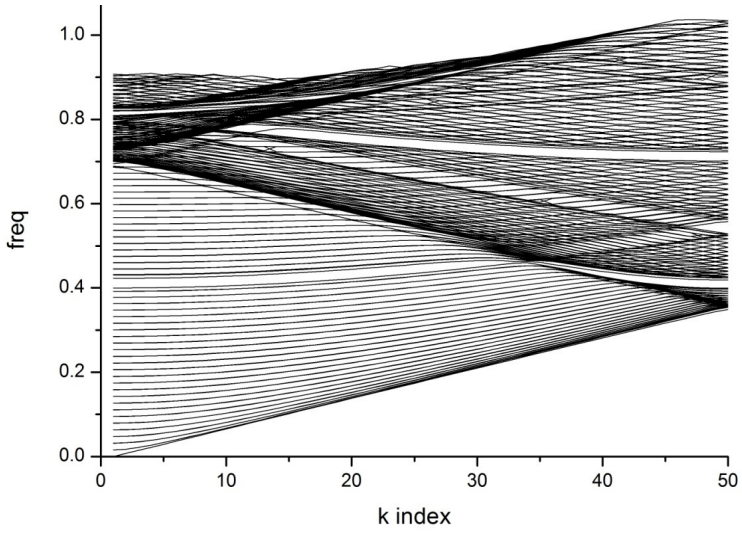

Figure 4.9. TM band structure of the PhC with line defect waveguide.

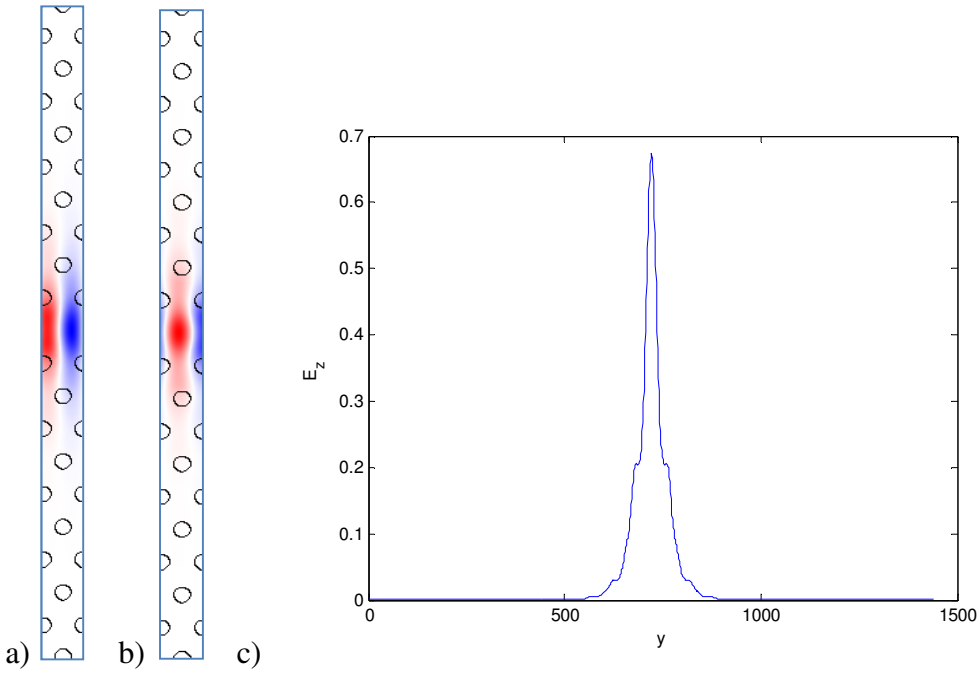

Figure 4.10. Defect mode profile at frequency 0.524605 c/*a* a) imaginer part b) real part c) Ez field (TM) mode profile along the *y*-axis

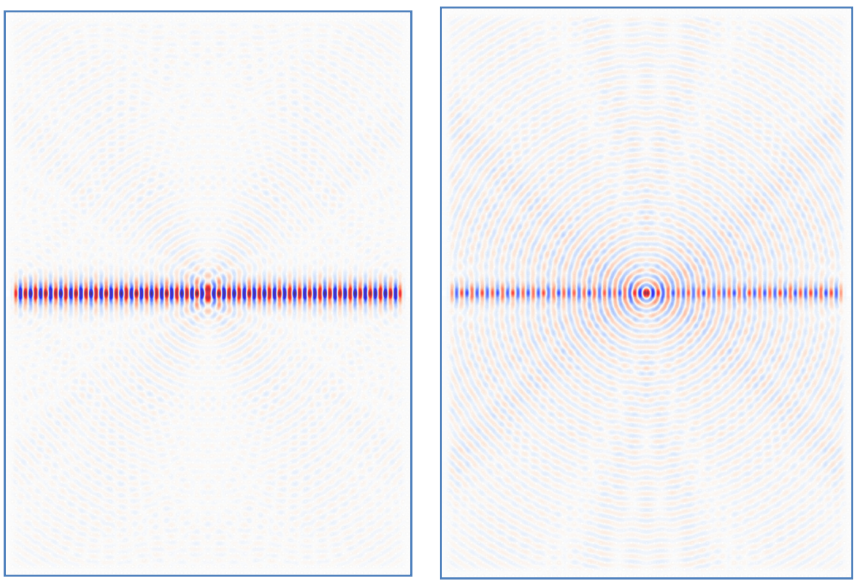

a) b)

Figure 4.11. Wave propagation with (a) and without (b) mode excitation at frequency 0.524605 c/*a*

4.2.1 The Model Used For The Simulation

For the simulation, U_1 and U_2 Gaussian beams in interference equation are taken identical and applied to Kerr type nonlinear waveguide in PhC simultaneously. The way to deliver the interfering beams into the nonlinear waveguide is through the bulk of PhC. Propagation modes are obtained from bulk PhC band structure graphs thus the possible interference angles of the beam are delimited. Propagated beam frequency 0.949 *c*/*a* is chosen from the bulk PhC band structure as shown in the Figure 4.12. Thereby, propagation of interfering beams through bulk PhC is guaranteed.

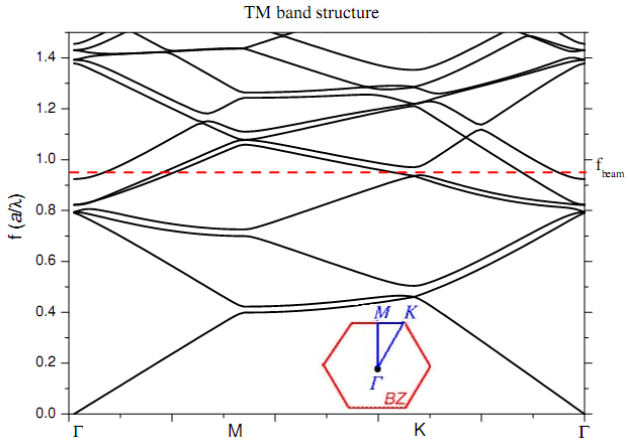

(a)

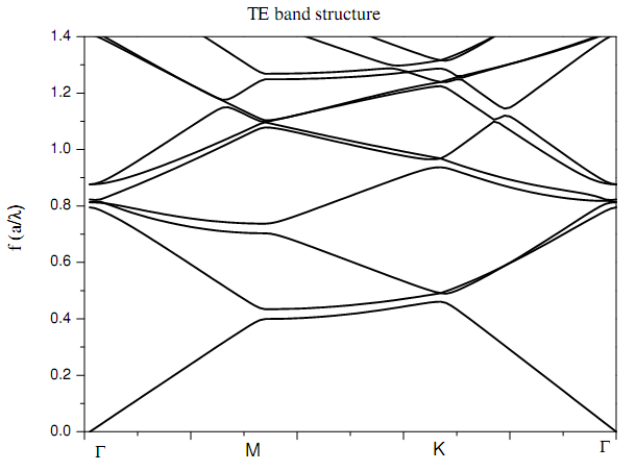

(b)

Figure 4.12. (a) TM and (b) TE band structures

Interference of beams and corresponding electric field profile in interference region versus the different incident angle are pictured in the following simulation graphics (Figure 4.13, Figure 4.14).

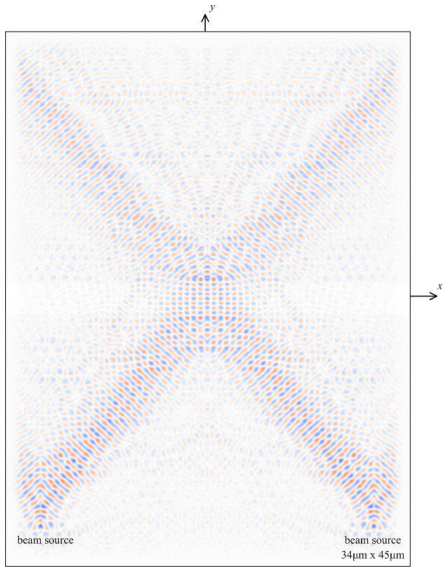

(a)

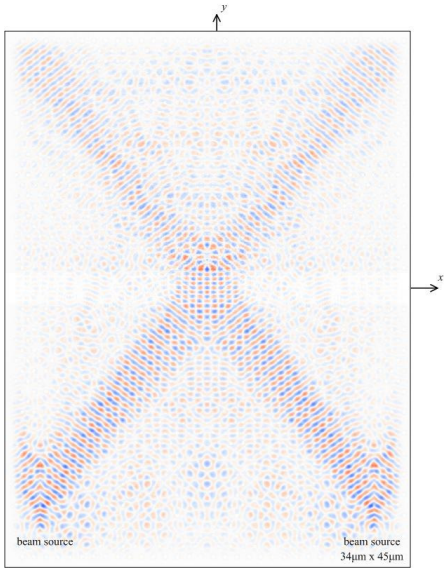

(b)

Figure 4.13. Gaussian beams interference pattern in PhC structure (U_1, U_2 are identical and incident angle is taken (a) θ=45º (b) θ=50º)

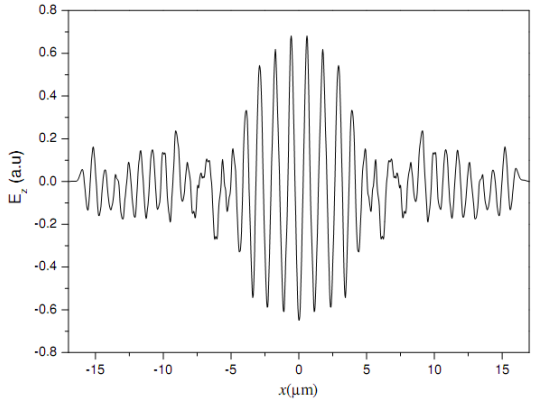

Figure 4.14. Electric field variation along the grating axis in PhC nonlinear waveguide belong to Figure 4.12a

It is expected to incremental refractive index change of the medium in accordance with interference equation depending on optical property of the material. As simulation geometry depicted in Figure 4.15, there is a hexagonal photonic crystal structure with air holes into linear polymer substrate with nonlinear Kerr type line defect waveguide that placed at the center part. The waveguide embedded into the PhC is a nonlinear polymer channel waveguide. Nonlinear interaction in surrounding materials is weak and can be neglected. The radius of the rods is chosen 0.2*a* and the refractive index of background Silicon Dioxide (SiO2) and the nonlinear material, Methyl Red (MR) doped Polyvinyl Alcohol (PVA) are 1.46 and 1.488 respectively. The lattice constant '*a*' is in unit of μm and all the values in the simulation are normalized with μm. Also, frequency is normalized to a/λ. When the lattice constant *a* is taken 1 μm, the normalized frequency 0.65 is wavelength of 1.54 μm which is in the communication window. Also, for the given geometry, the waveguide width $3a\sqrt{3}/2$ becomes 2.59 μm if *a* is taken 1μm, therefore this correspondence to single mode waveguide for the given frequency range.

Methyl Red (MR) doped Polyvinyl Alcohol (PVA) is chosen as nonlinear waveguide material because of the high nonlinear coefficient, high chemical stability and suitability for the sub micron scale fabrication process. The nonlinearity considered in this study is instantaneous nonlinearity and third order nonlinear coefficient of doped PVA can be taken as $2\text{x}10^{-9}$ cm^2/W compatible with the literature [53], [54].

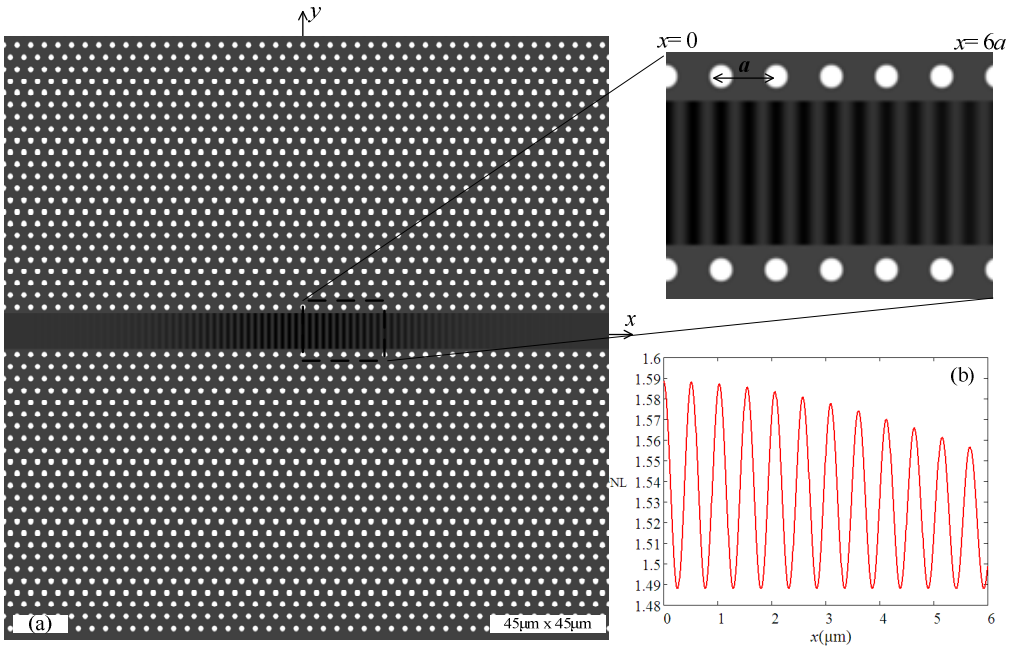

(a) (b)

Figure 4.15. (a) Realistic index grating profile embedded into PhC

4.3 Simulation Results: Band Stop Filter Characteristics

Transmission characteristics and relation with some beam parameters have been investigated and presented in this section. Input signal source is defined in the waveguide as a carrier signal. Propagated beam frequency 0.949 c/*a* is chosen from the bulk PhC band structure as shown in the Figure 4.12. Throughout the simulations, all beams are TE polarized (TM, according to MEEP). Transmission coefficient of the interference grating is defined as the ratio of the output flux at the end of the waveguide to the output flux measured after the interference grating applied. Transmission characteristics of nonlinear waveguide versus to beam parameters like θ (incident angle), λ (control beam wavelength), P_0 (beam power) are given in the following subsections.

FDTD algorithm is not accurate for very low frequencies and misses high frequencies in pulse propagation. Some spurious peaks are produces in the spectrum. Although the spurious results can be improved by increasing the resolution, simulation

time increase extensively. Increment of resolution does not make significant improvement in the results. Hence, grid resolution in FDTD algorithm is chosen as optimum for the representation of studied wavelength range.

4.3.1 Transmission characteristics versus control beam angle (θº)

The transmission coefficients are obtained for the interference beam angle of incidence 45º and 50º. Corresponded beam frequency is 0.949 c/*a* and chosen from dispersion diagram in Figure 4.12. The interfering beam wavelength and the power, consequently nonlinear index deviation, are held constant as 1.053 μm and P_0 respectively. The power (P_0) required to make necessary refractive index change of 0.1 is about 0.5 W/μm^2.

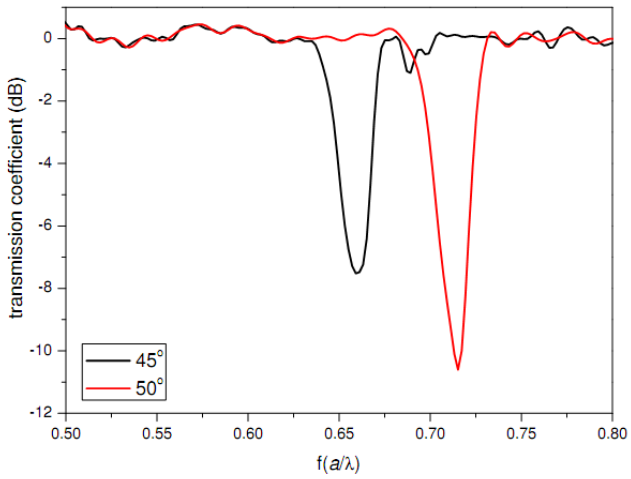

Figure 4.16. Transmission coefficient for two different θ values ($P=P_0$ and λ=1.053μm)

As the results shown in the Figure 4.16, when interference angle of incidence is increased, the stop frequency shifted to the higher frequency region and the bandwidth (3dB bandwidth) also increases. The bandwidth is about 0.022c/*a* at 45º which is about 6.6 THz if the lattice constant is taken 1μm. This kind of characteristic is predicted and confirmed by the Bragg law given in the equations (3) and (4). When the angle of

incidence is increased, the grating period (Λ) decreases; corresponding Bragg wavelength (λ_B) decreases too. On the other hand, grating length increases for the larger incidence angle. Hence, the contrast ratio reaches 10 dB at the higher frequencies rather than 8 dB at the lower part of the spectrum with the change of incidence angle.

4.3.2 Transmission characteristics versus control beam power (P_0)

The effect of beams power on the stop frequency is presented in the following Figure 4.17 and Figure 4.18. Power density still remains under the threshold damage power level of MR PVA polymer [54]. Actually, this power is belong to two beam interferences in the center of grating region. Power of one beam is 0.125 W/μm^2 for P_0.

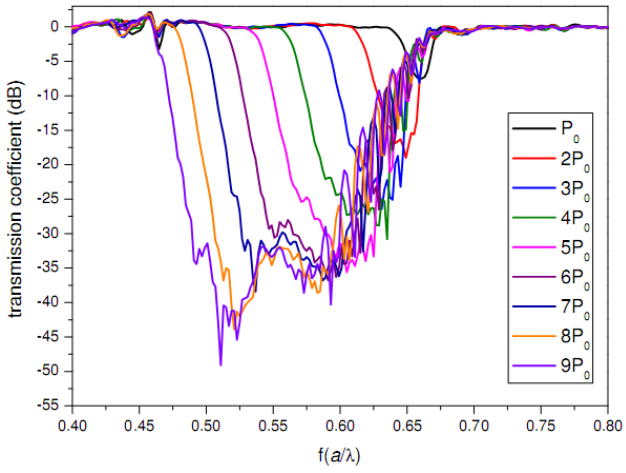

Figure 4.17. Transmission coefficient for power variation (θ=45° and λ=1.053μm)

When the beam power is increased and then the refractive index is modified accordingly. Hence, the bandwidth is broadened and the stop frequency is shifted to lower frequency part of the spectrum. That can be explained with an increase in the effective average refractive index; therefore, the Bragg wavelength (λ_B) shifts according to the Bragg law in equation (4.14).

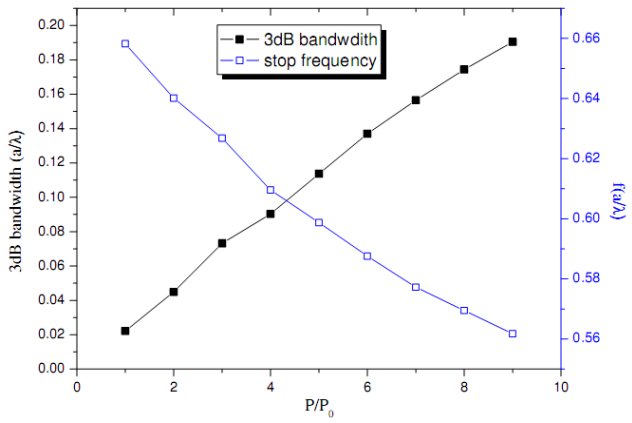

Figure 4.18. Shifting of stop frequency and 3dB bandwidth for various beam power

Noticeably, the contrast ratio enhances from 8dB to 45 dB with the increased P_0. The calculated crosstalk between adjacent frequencies is significantly low with the increased power change above $2P_0$ where P_0 is the power requirements for $\Delta n \sim 0.1$. Interestingly, the beam power change dominantly affects the bandwidth as shown in the Figure 4.18, in which the bandwidth broadens to 0.190c/a (57 Thz for a is 1 μm) Therefore, that feature can be used in applications that require ultra-wide-band width; since it can easily be tuned with the beam power.

4.3.3 Transmission characteristics versus beam wavelength (λ_{beam})

The effect of interfering beam frequency on the transmission characteristic is considered for two wavelengths λ_1 = 1 μm, λ_2 = 1.053 μm. The beam angle of incidence and the amplitude are held constant. According to the equations (4.13) and (4.14), when the beam wavelength is increased, Bragg period (Λ), corresponding Bragg wavelength (λ_B) and grating length are increased. When the wavelength is decreased, the stop frequency shifts toward to higher frequency region of the spectrum. For these wavelengths, the calculated crosstalk is -8 dB.

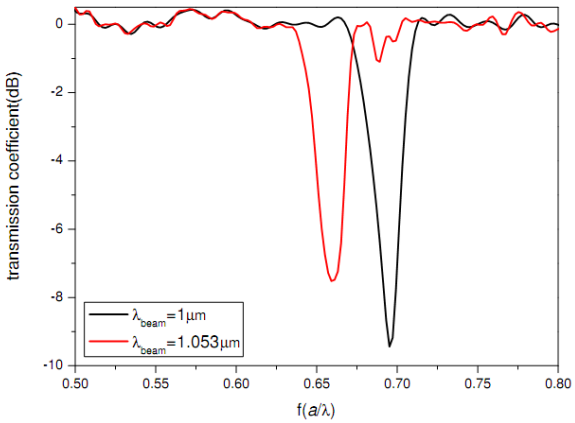

Figure 4.19. Transmission coefficient for beam wavelength (θ=45° and $P=P_0$)

At the end of the study, Figure 4.19 is confirmed with the FDTD simulation. As we can see in Figure 4.19, there is a stop frequency at 0.65 c/*a* for the control beam of 1.053μm. In order to demonstrate the stop mechanism, continuous wave input signal source is chosen 0.65 c/*a* and launched into the waveguide as carrier signal. In the Figure 4.20, the propagation of input signal is shown with/without the grating. Under the grating condition, the input signal is literally stopped as in agreement with the simulation in Figure 4.19. The transmission is down to -8 dB.

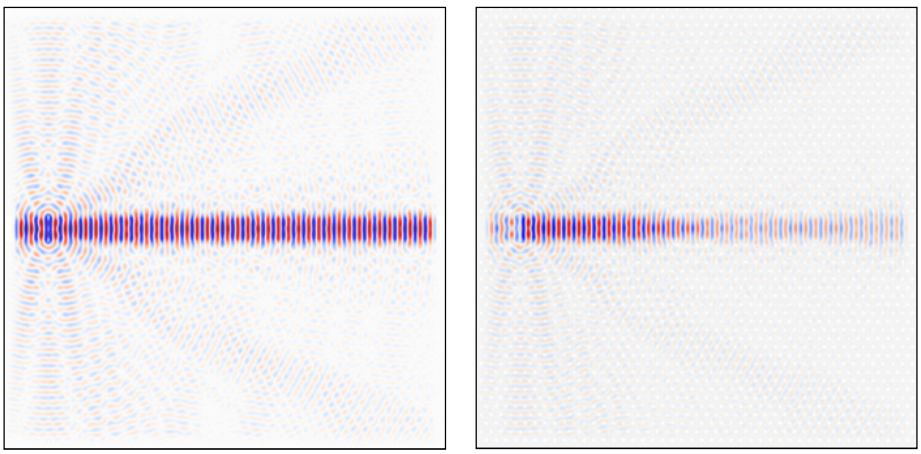

(a) (b)

Figure 4.20. Input signal propagation (a) without grating (f_{input}=0.65) (b) with grating (f_{input}=0.65, λ=1.053 μm, θ=45° and $P=P_0$)

As a conclusion, the concept of interference grating structures formed by interference of Gaussian beams in a nonlinear PhC waveguide medium as a control signal is proposed and investigated in this section. These gratings have profiles that chirped and apodized. An embedded Kerr type nonlinear waveguide in the PhCs has been considered as the beam interference grating medium for manipulating the optical signals. Finite-Difference Time-Domain (FDTD) Method is used to analyze these type photonic structures for the transmission characteristics. Since the interference grating structures are slightly chirped and apodized, in the transmission characteristics stop frequency with various bandwidths has been observed in the Figure 4.16, Figure 4.17 and Figure 4.19. In the Figure 4.16 and Figure 4.17 the contrast ratio is in the range of 8 to 45 dB and becomes lower in the long wavelength region of the spectrum. Importantly, the stop frequency can be detuned with the interference angle about 0.05c/*a* (15 THz if *a* is 1μm) when the angle is inclined 5º. Similarly, the stop frequency can also be detuned about 0.015c/*a* (4.5 THz if *a* is 1μm) when the beam power is P~P_0. On the other hand, the bandwidth is also affected, starting from 0.02 to 0.19c/*a* with the frequencies ranging from 0.66 to 0.56c/*a* for the power detuning. The power (P_0) required to make necessary refractive index change of 0.1 is about 0.5W/μm^2. Although, that power intensity might be achievable, the interfering beams can be confined into the narrower region by designing novel PhCs structures which accommodate the desired angle of incidence. Finally, at two beam wavelengths, 1 and 1.053μm, the transmission characteristics have the stop at the frequencies 0.65 and 0.69c/a, with the crosstalk about −8dB. The results suggest that the interference gratings can be employed in the PhC circuits that require tunability for the complex photonics functions of DWDM switching/routing devices.

4.4 Dynamic Grating Properties

The gratings are composed of the spatial modulation of n, ε or χ. Permanent gratings are used in the most of the studies so far. Differently from the permanent grating, the grating is occurred as long as the light source is applied. Then, it has disappeared when the induced light is switched off in the transient or dynamic gratings.

Besides, common transient grating structure can be assumed quasi-stationary because of the maxima and minima nodes are neither oscillate nor propagate. The grating does not change during the propagation of probe signal. The grating amplitude decays without oscillation when the light source is switched off [55]. Additionally, non-instantaneous case is called different phenomena in the literature and cannot be easily described as a modification of refractive index. Its effect is called Raman, and is not considered to be a part of the Kerr effect. Such grating system is a time variant system and must be modeled as Raman [21], [55], [56].

The interaction between pump and probe is widely investigated in linear and nonlinear steady grating structures [57], [58]. Previous studies have focused on the detecting diffracted waves from grating by applying a third probe or self diffraction of inducing light wave especially the stationary grating [59]. Different from these studies, reflection and transmission properties have been observed with a third probe beam propagation through the grating in this study part. Moreover, light propagation in grating with finite response time and temporal and spectral characteristics are considered.

On the other hand, the simulation platform Meep supports only instantaneous Kerr nonlinearity case. Meep supports dispersion media like Lorentz and Drude separately. To observe the dispersion and nonlinear effect on the pulse propagation and grating, the following cases are applied.

4.4.1 Input Signal Variation in Instantaneous Kerr Nonlinear Grating

Input signal (probe signal) propagation and variation in waveguide grating which is formed by different pump (control signal) configuration into the instantaneous Kerr nonlinear medium are examined. Control beams are taken identical and applied to instantaneous Kerr nonlinear waveguide with contra propagating, power is monitored at the center of the waveguide.

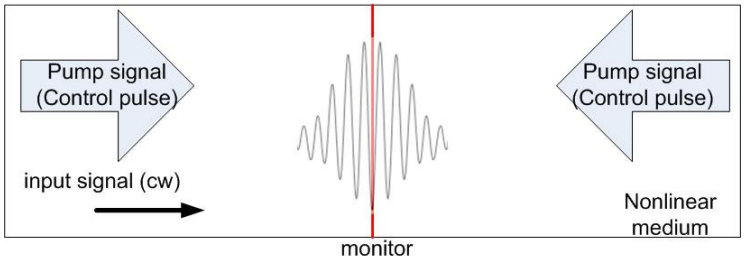

Figure 4.21. Monitoring the interference pump signal and the probe signal in instantaneous Kerr nonlinear medium

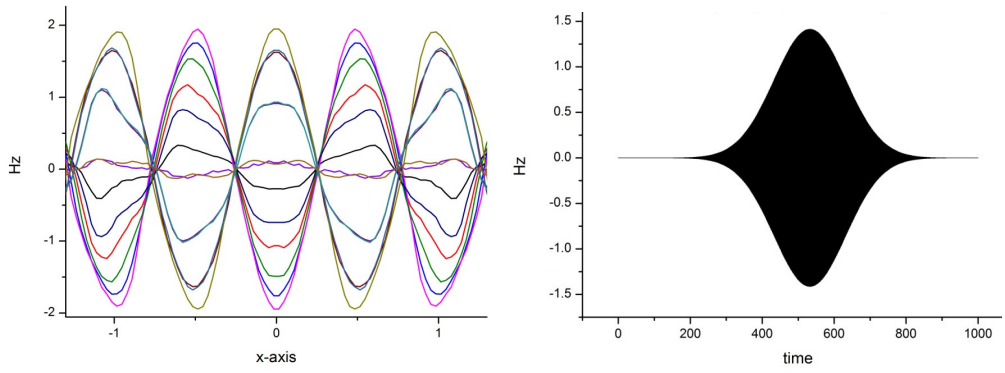

(a)

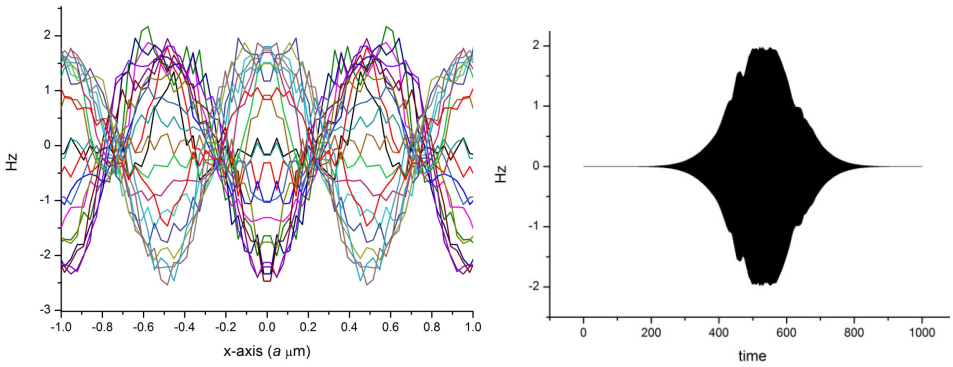

(b)

Figure 4.22. Anharmonic time variation of contra-propagation interference Hz field profile along the grating *x*-axis (a) without (b) with instantaneous Kerr nonlinearity

Bragg period is seen from interference patterns and fundamental Bragg frequency can be estimated from average index change before the simulation as the following. When two control beam with amplitude coefficient A=2 (a.u) is applied, average index change

is calculated as 0.12 for the Kerr coefficient (n_2) and average power are 0.2 (a.u) and 0.5 (a.u) respectively. Fundamental Bragg wavelength is calculated as 1.608 (f_B=0.6218 c/*a*). Pump (control) signal is taken Hz polarize (TM) gaussian pulse and defined as mode profile at center frequency 0.650019c/*a*. Probe (input) signal is taken Ez polarize (TE) continuous wave (cw). Bragg frequency is searched in the input frequency range between 0.56 c/*a*-0.68c/*a*. Input signal is also given as mode profile at each frequency. Transmitted probe (input) signal is affected from pump (control) signal pulse frequency width and response time on nonlinear medium and following results are observed. Since c = 1 in Meep units, *a* (or *a* / c) is our unit of time as well. For example, normalized frequency f corresponding to λ = 1.53μm is calculated as f=1/1.53 = 0.65 for *a* = 1μm. Simulation should be run 153 time units for 100 periods (100/f).

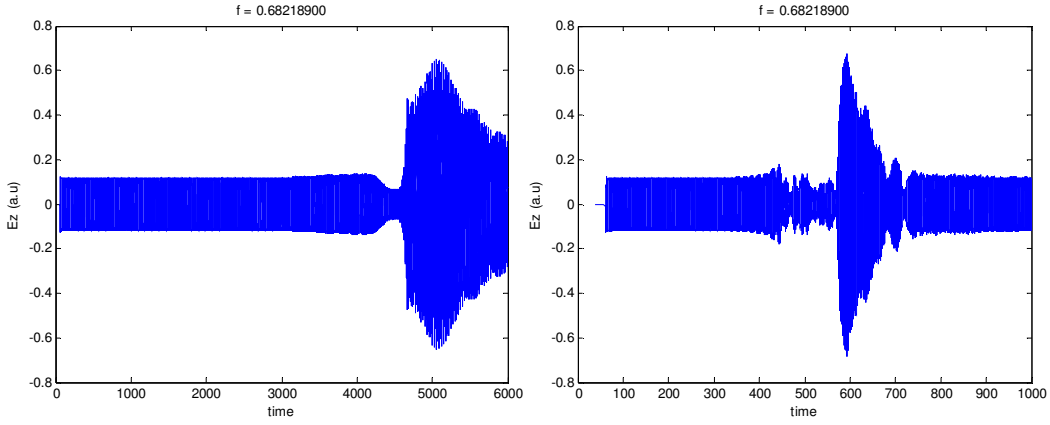

(a) (b)

Figure 4.23. TM mode (Ez) continuous wave probe (input) signal variation under the TE mode (Hz) pump (control) pulse signal with different frequency width a) df=0.001 b) df=0.01

4.4.1.1 Short pulse (df=0.01)

Input signal (Ez) propagation for applying a control (pump) pulse with the frequency width df=0.01 and amplitude A=2(a.u)

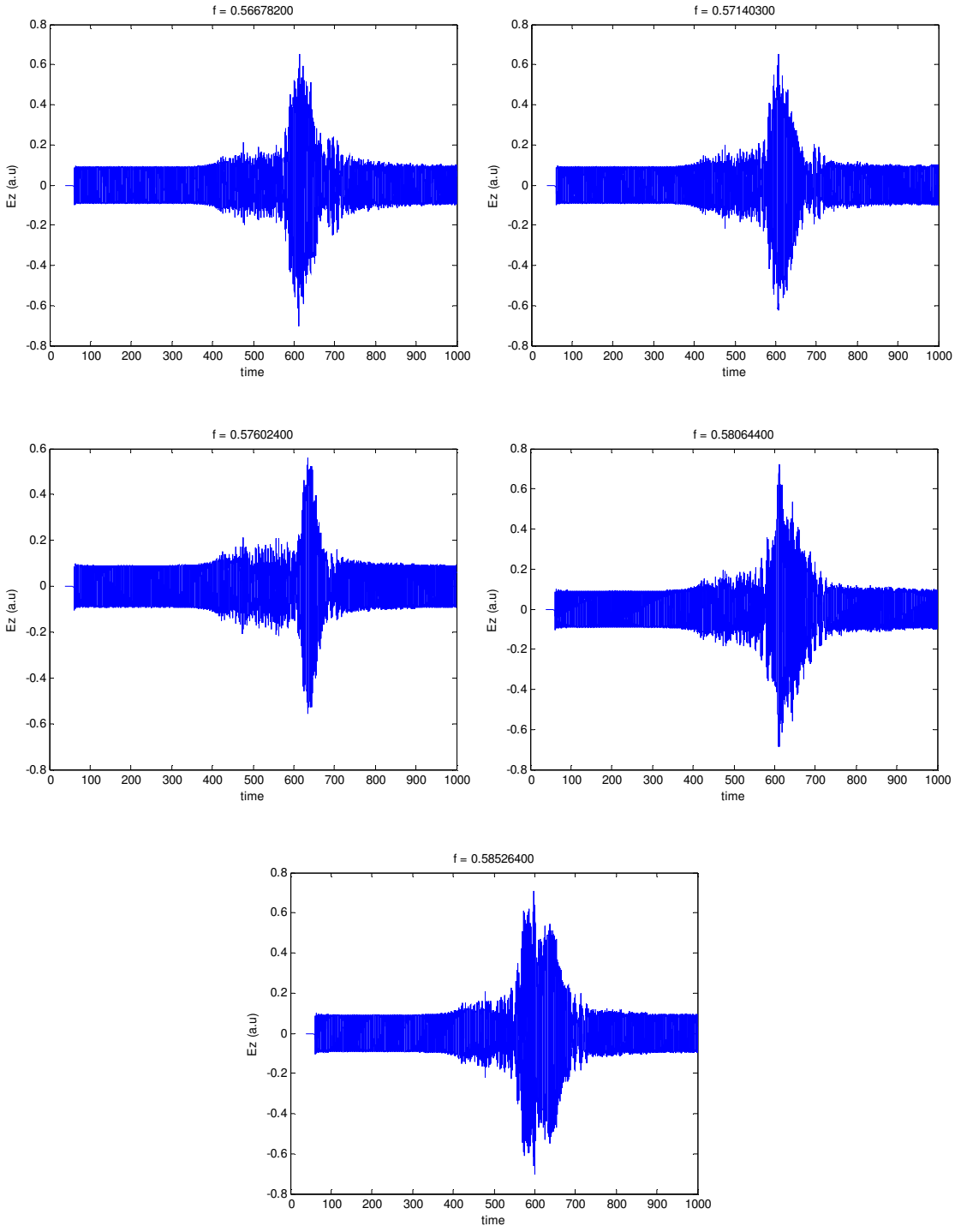

Figure 4.24. Time variation of input (Ez) signal under the contra-propagation interference pump pulse (Hz) along the grating *x*-axis

(cont. on next page)

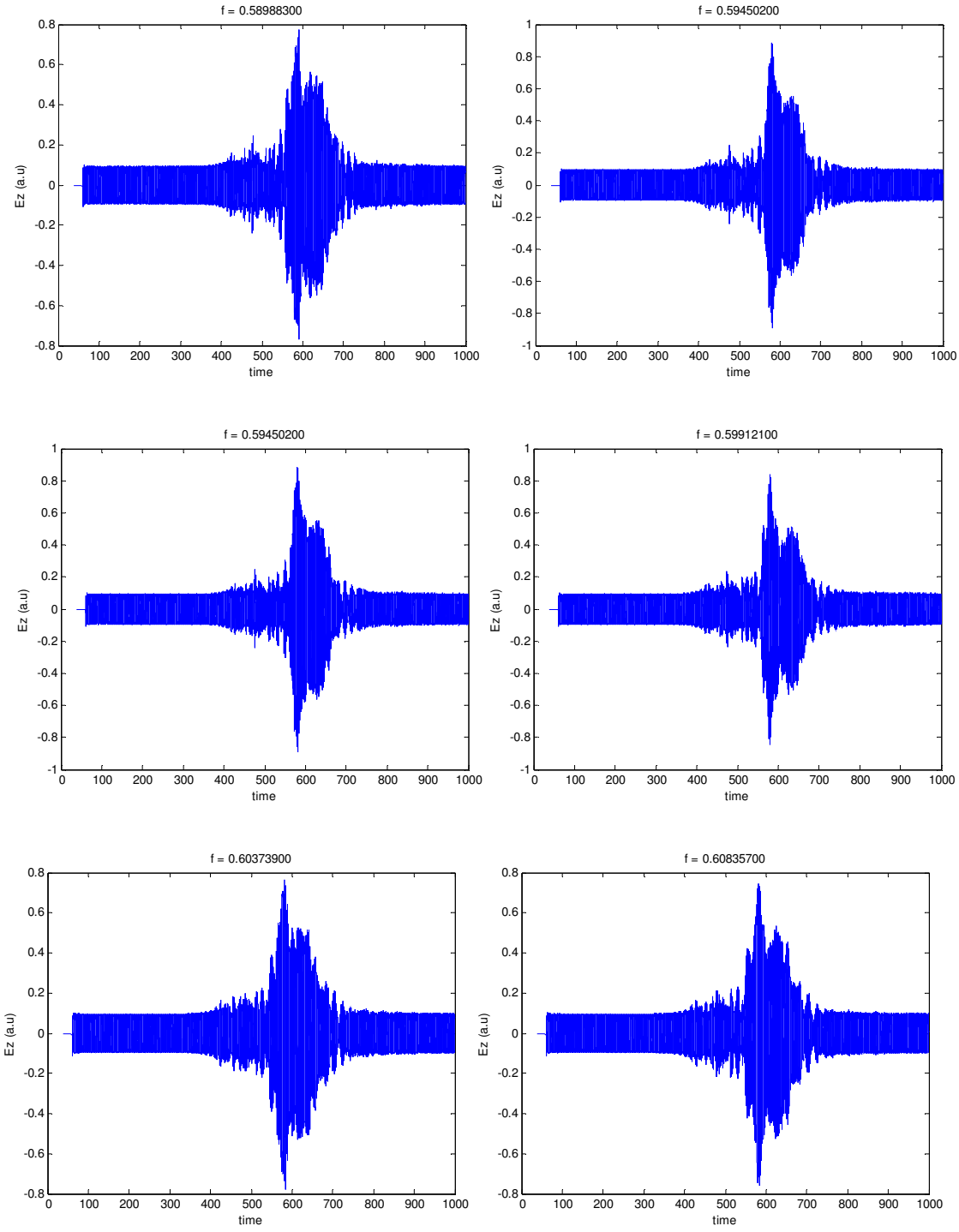

Figure 4.24 (cont.)

(cont. on next page)

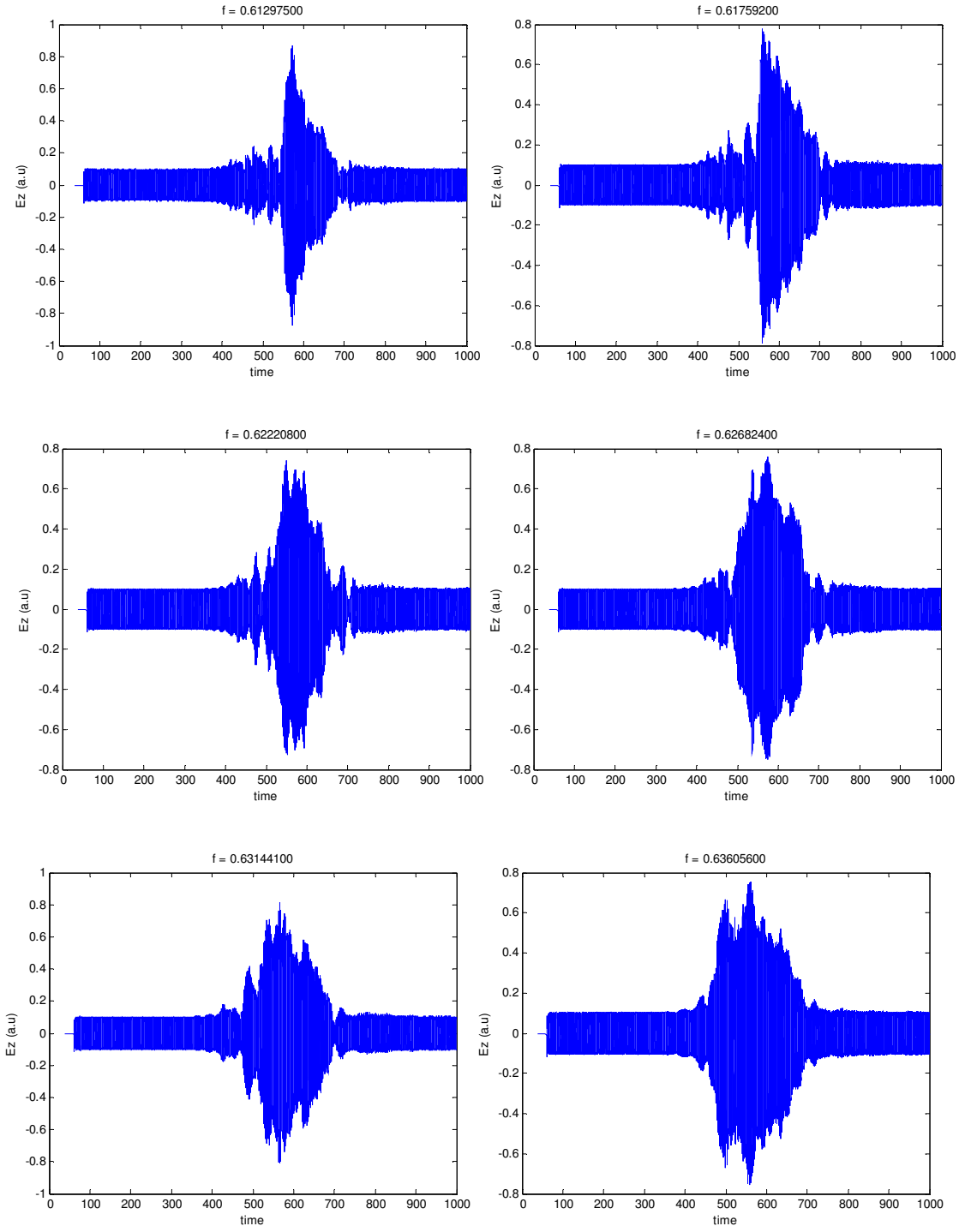

Figure 4.24 (cont.)

(cont. on next page)

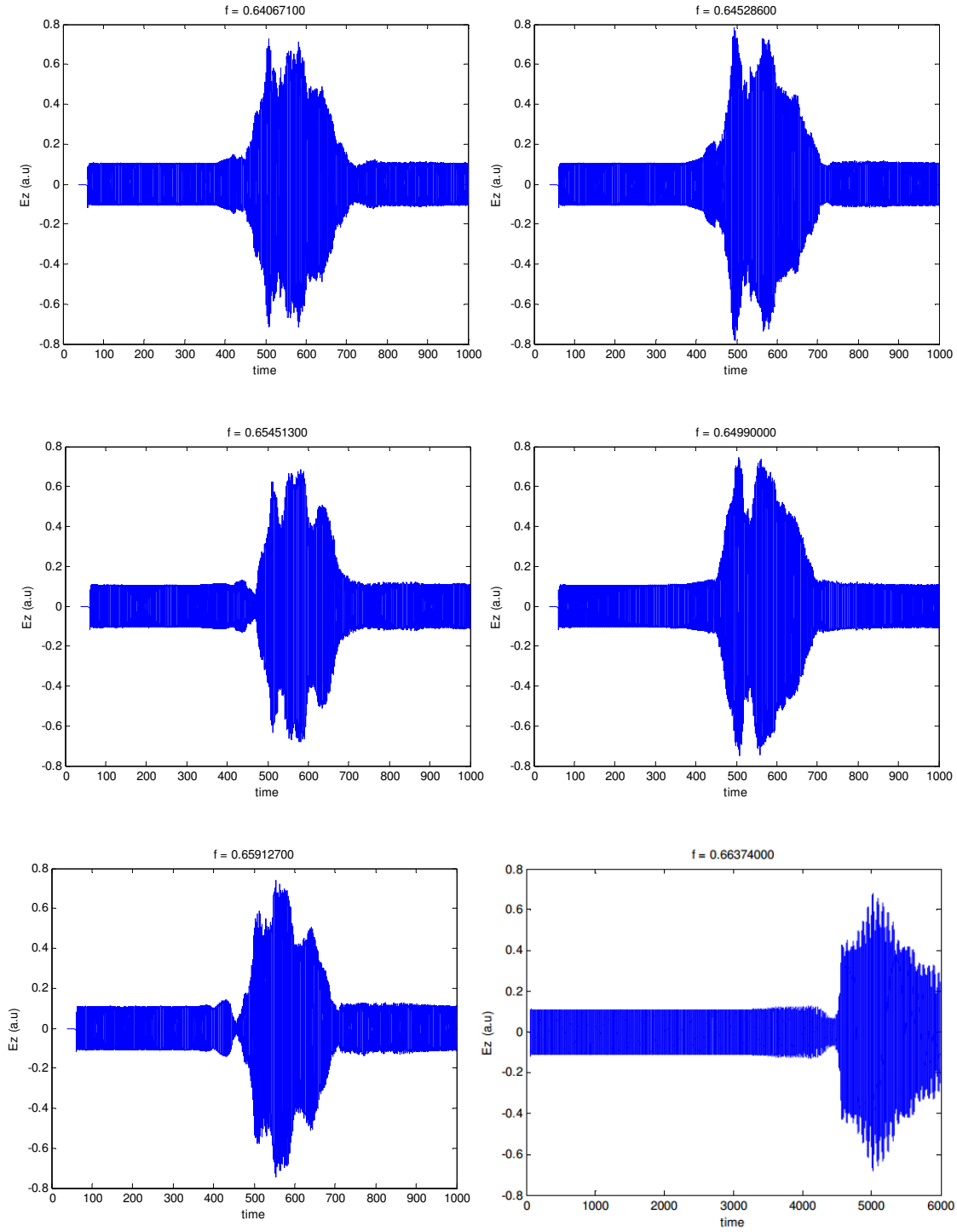

Figure 4.24 (cont.)

(cont. on next page)

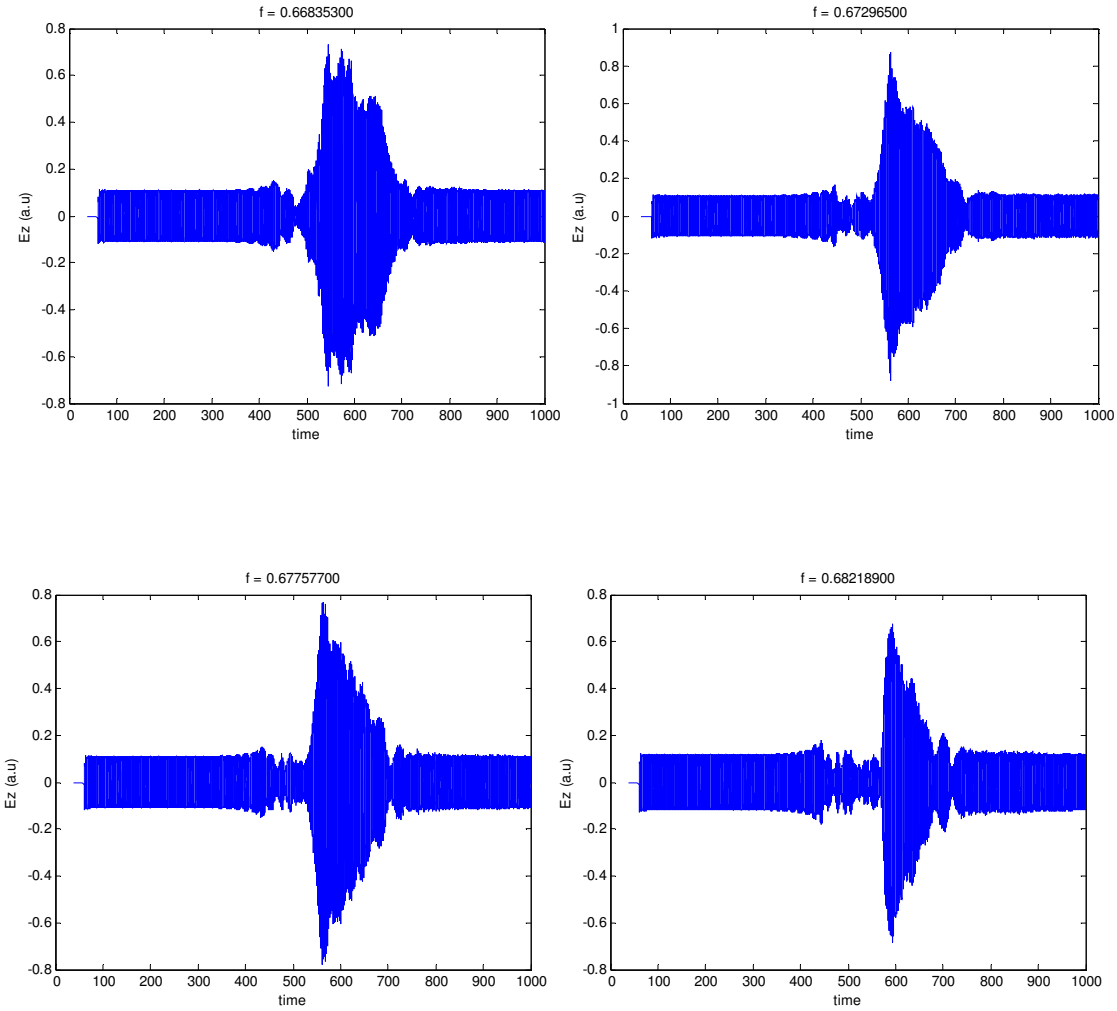

Figure 4.24 (end)

4.4.1.2 Long Pulse (df=0.001)

Input signal (Ez) propagation for applying a control (pump) pulse with the frequency width df=0.001 and amplitude A=1.5(a.u)

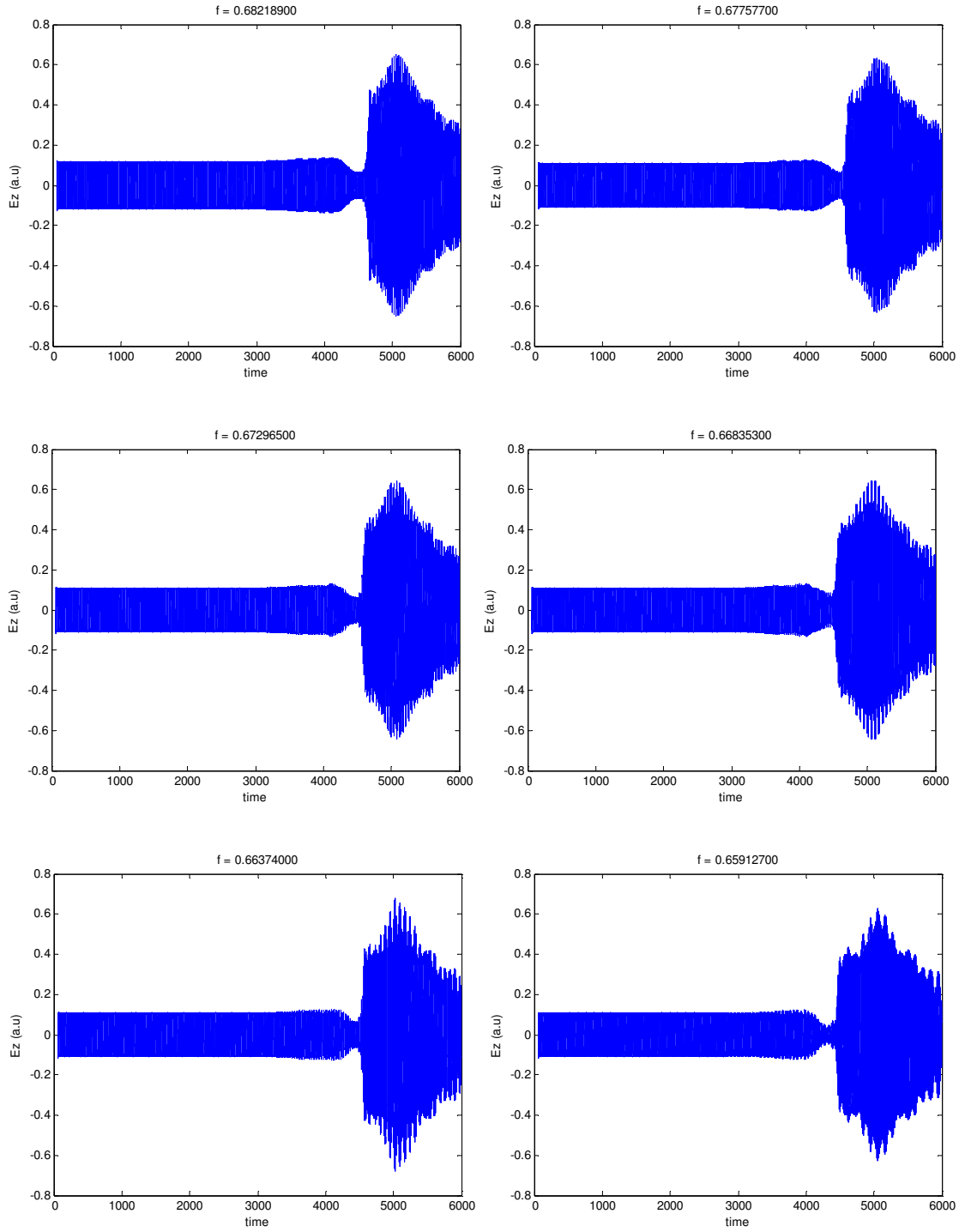

Figure 4.25. Time variation of input (Ez) signal under the contra-propagation interference pump pulse (Hz) along the grating *x*-axis

(cont. on next page)

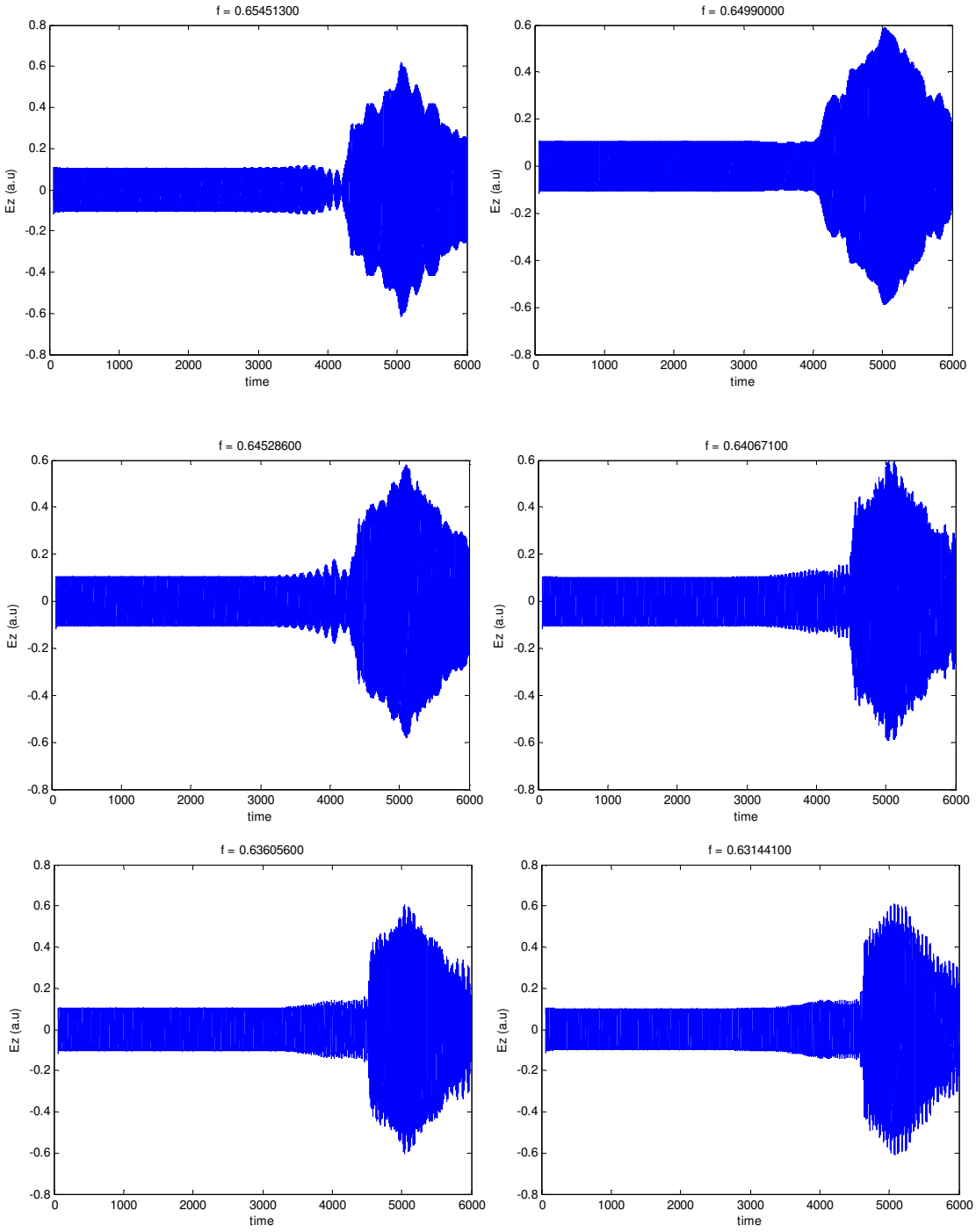

Figure 4.25. (end)

4.5 Discussion on Results

An instantaneous response results in the case that the transmitted probe pulse shape is proportional to the square of the pump shape, whereas a non-instantaneous response causes the transmitted probe temporal shape is proportional to the square of the dynamics of the Kerr effect. The induced transient interference has the same form as the pump pulse shape, when the relaxation time is very fast compared to the excitation duration. The index variation is determined by the dynamics of the optical Kerr effect in the medium as long as the pump pulse duration is much shorter than the relaxation process [21], [60]. Because the refractive index variation follows the pump pulse intensity shape in instantaneously case, transient grating structure is not constant. The different parts in time of signal pulse are faced to different index value. So Bragg frequency is continuously altered. Only a small part of the control signal is matched with the estimated Bragg frequency. Naturally, the stop level obtained from simulation result is very low. When the pump pulse reaches at waveguide, probe signal dramatically changes as shown in Figure 4.23. Attenuation occurs at different frequency for pump pulse frequency width. The attenuation period is too short and signal level is increases soon after. Reflectivity decreases but oscillates after the pump signal passes. [61]. While the probe signal is constant, permanent stable switching or unstable transient switching are observed with the pump signal altering. [61], [62]. If the nonlinearity is ignored and the pump is assumed constant in grating (CW), spectrum shifts compatible with the results of Chapter 4.3 [61].

CHAPTER 5

MICROCAVITY BASED PHOTONIC CRYSTAL FILTERS

Essential components of PhC which are channel drop filters and coupled cavity waveguides are exploit the coupling of defect modes. Effect on the defect modes shift is much more sensitive than the band edge shift by small change in refractive index. This sensitivity is useful for power reduction in all optical switching [63], [64]. Degeneracy is result of symmetry properties of modes in PhC where the modes see the same lattice when rotated [1]. Many studies are performed whether the modes are degenerate and classifying the degenerate modes [65]–[68]. The degeneracy of modes is broken with introducing a perturbation in the PhC cavity. Then the defect modes have different frequency and splitted. By mode splitting, more frequency band is allowed in the resonance structure, hence the capability of signal processing is increased [66].

In this part of study, dual-mode dual-band photonic crystal bandpass filter is proposed and its transmission characteristics are investigated for various configurations. PhC microcavity constructed by a point defect placed at the corner of the line defect waveguide is shown in Figure 5.3. Degenerate modes can be splitted by modifying the auxiliary perturbation rods. Exploiting degenerate mode splitting in PhC cavity, single band filter characteristics has been obtained by recent studies [17], [67]. Deviating from that studies, in the present work PhC compact bandpass filter exhibiting dual-mode dual-band characteristic is proposed.

5.1 Microcavity Structures

Light is confined temporally and spatially at resonance frequency in optical cavity structures which is named optical resonator. Optical resonator is essential functionality block for filtering, modulating, buffering, switching in the integrated optical circuits systems [8]. Quality factor (Q-factor) and mode volume are the

measurements of temporally decay time and spatially occupation of modes in resonator, respectively. While the Q-factor and transmission characteristics are important for narrow band filter in wavelength division multiplexing (WDM) applications, small mode volume is necessary for lasing applications. Additionally, powerful confinement of light enhances the nonlinear interaction [69].

Optical resonators are usually used with the waveguides, and the interaction between them is determined by the coupled mode theory (CMT). Optical resonators are classified into two groups with the attribution as standing wave (SW) and traveling wave (TW) resonator. Distributed feedback resonator and ring resonator are given as example for SW and TW resonator, respectively [1], [8]. Waveguide cavity interaction of the proposed structures in the previous chapter and this chapter can be taken as standing waves form.

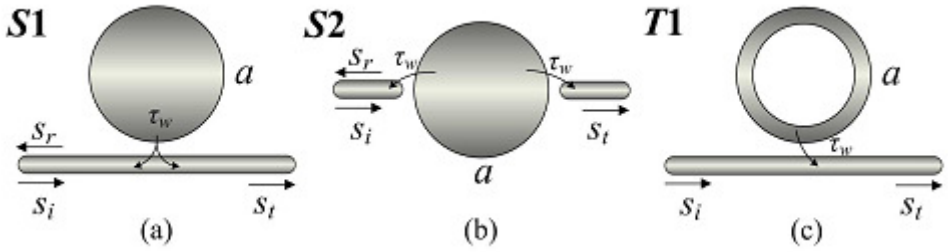

Figure 5.1. (a)-(b) SW resonators with side-coupling and shoulder coupling (c) TW resonator [8]

Constituting the optical resonator structures in PhC has two ways. One of them is line defect or point defect resonator by changing the rod properties such as size or dielectric constant. The other one is ring resonator that the some rods are modified as a ring shape [8]. The optical communication devices such as filter, add-drop multiplexer are performed with the SW or TW types of resonator which are placed between the two optical waveguides in PhC as shown in Figure 5.2. Light signal can be dropped or added between the waveguides through resonator structure. The PhC resonator structure can be used as data transfer junction of optical wavelength-division multiplexing (OWDM) systems [70].

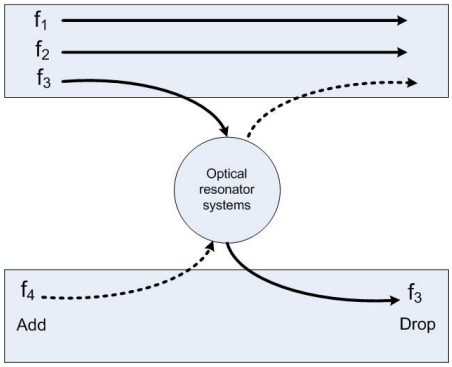

(a)

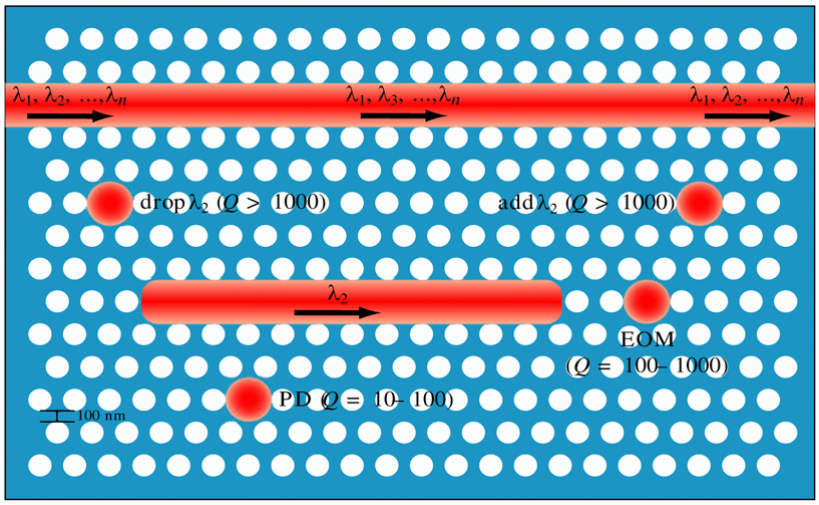

(b)

Figure 5.2. Possible implementation of resonator structure in PhC a) schematic model b) realistic model of OADM [70]

5.2 Proposed Photonic Crystal Microcavity Structure

In this part of thesis study, two-dimensional (2D) square lattice PhC structure with alumina rods in air substrate is considered. As simulation geometry depicted in Figure 5.3, there is a line defect PhC waveguide with a microcavity having radius rd that is placed at the bend. PhC dimensions are 25*a* x 25*a* along the x and y directions of 2D PhC. The lattice constant '*a*' is in unit of μm. If the normalized values are used, then all the values in the simulation are normalized with μm and frequency is also

normalized to a/λ. All other lengths are expressed in terms of 'a' that is set to 400 μm which is very convenient for fabrication corresponds the THz range [3], [71].

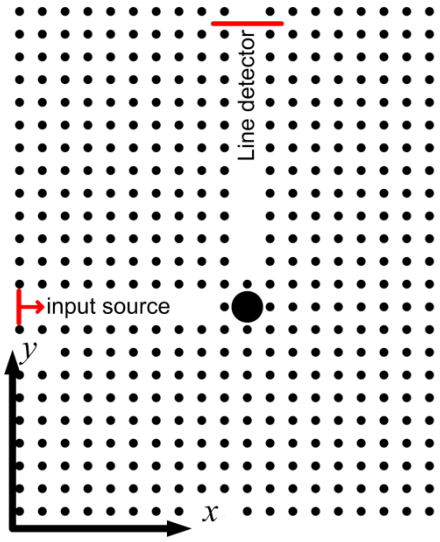

Figure 5.3. 2D PhC structure

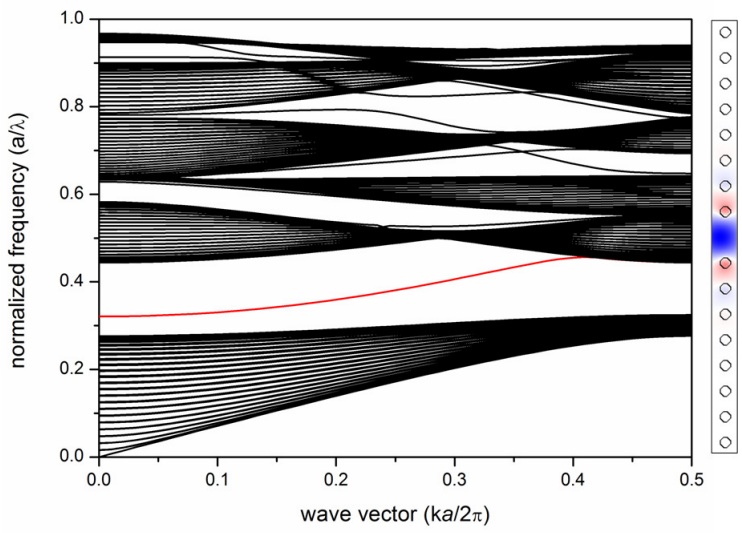

Figure 5.4. TE (TM, according to Meep) band structure of square PhC with a line defect waveguide and propagated mode profile

The radius of the rods is chosen 0.2a and the dielectric constant of alumina is 8.9 (ε). Propagating modes are obtained from the band diagram of line defect PhC as shown in Figure 5.4 with a red line. Fourier transformed propagated mode profile is computed

by MATLAB and applied to the input of waveguide as a plane wave source. Thus, single guided mode (eigenmode) excitation is guaranteed. The transmitted mode fields are detected with a line detector at the output. Throughout the simulations, the field is assumed as TE polarized (TM, according to Meep) where the electric field vector is perpendicular to the plane of PhC.

PhC microcavity resonator in this study has C4v symmetry where this structure does not change by 90º rotation. Hence, the cavity modes can be classified as doubly degenerate and non-degenerate in accordance with the symmetry properties. The modes are called non-degenerate if their shapes are invariant under the rotation operator. [72]. There are four modes revealed in the PhC microcavity. The two modes are doubly degenerate and the other two are non-degenerate if the radius of microcavity rod is about $0.7a$ [1], [73]. Doubly degenerate hexapole and dipole resonance modes at the frequency of the lower band (0.29 THz) and the upper band (0.324 THz) are shown in Figure 5.5 (a) and quality factor, Q of the microcavity is calculated as $0.3\text{x}10^6$ and $0.6\text{x}10^6$, respectively.

In order to excite the degenerate modes in each band simultaneously, a novel perturbation structure is needed and investigated in this study. There are three small perturbation rods at upper left corner of the microcavity. Their names are r_{pmid} and r_p (Figure 5.6). Apart from the other perturbation rods, the middle rod has different radius. The refractive index of all perturbation rods is the same as the PhC rods. Exact position of r_{pmid} and r_p are (0.625, 0.625), (-0.375, 0.75), (-0.75, 0.375) points with respect to the center of microcavity rod r_d, (0,0) in (x,y) plane. The degenerate modes appear by applying the perturbation rods configuration as seen in Figure 5.5(a-b).

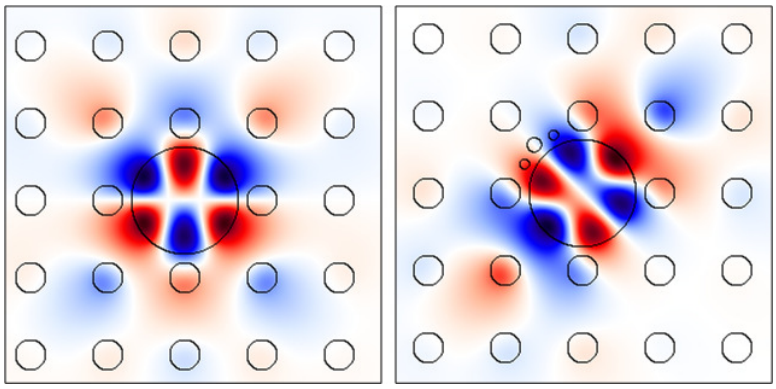

(a)

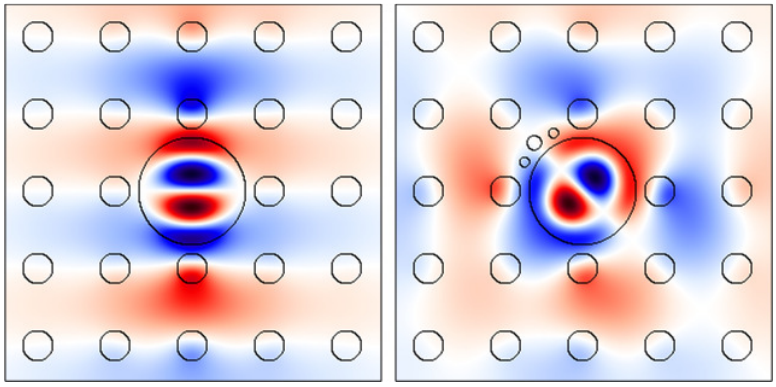

(b)

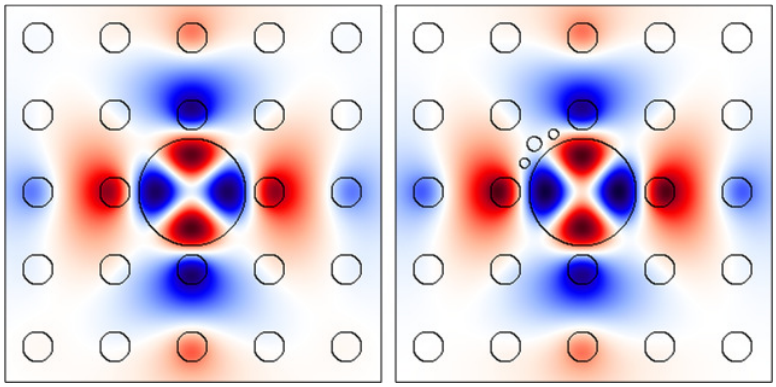

(c)

Figure 5.5. Doubly degenerate (left) and coupled (right) a) hexapole and b) dipole modes for 0.29 THz and 0.324 THz respectively. Non-degenerate (left) and coupled (right) c) quadrupole and d) monopole mode for 0.261 THz and 0.264 THz respectively.

(cont. on next page)

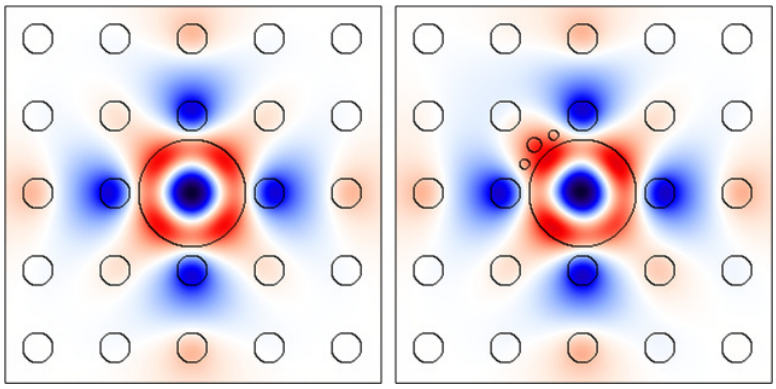

(d)

Figure 5.5. (end)

The quality factor of coupled hexapole and dipole modes can be calculated as $1.6\text{x}10^6$ for 0.29 THz and $0.15\text{x}10^6$ for 0.324 THz with perturbation $r_p=0.07a$, $r_{pmid}=0.1a$. Besides, field distributions of nondegenerate quadrupole and monopole modes persist with the perturbation in Figure 5.5(c-d).

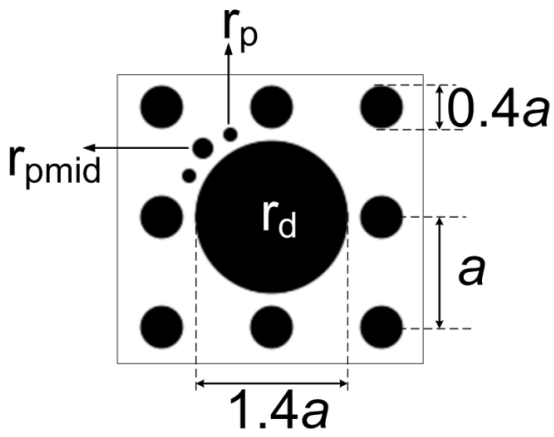

Figure 5.6. Dual-mode dual-band microcavity

5.3 Dual Mode Dual Band Filter Characteristics

The filter characteristics are obtained for various perturbation configurations as shown in the Figure 5.7 (a) to (g). There is no transmission in the line defect waveguide when using the microcavity without perturbation rods as depicted in Figure 5.7(a). According to Figure 5.7 (b), the transmission spectrum is dramatically changed by introducing a rod r_{pmid}=0.07*a* at the upper left corner of microcavity and between two PhC rods. The band at the frequency of 0.29 THz, which is called lower band, is transmitting, but the degenerate modes are splitted as two peaks. Meanwhile, the transmissivity of upper band, at the frequency of 0.324 is increased, but the reflection level is more than -5 dB. The transmission begins at the upper band with the larger value of r_{pmid} as 0.1*a*; however, the degenerate modes in the lower band are overcoupled which means the band is deformed. A degenerate mode in the upper band is not excited in this case as seen in Figure 5.7 (c). If only r_p perturbation is applied as in Figure 5.7 (d), the lower band is turned to transmit; however the upper band transmission remains at the level of -5dB. Similarly to Figure 5.7 (c), transmission of the upper band and mode splitting can be seen in Figure 5.7(e) by using the larger value of r_p=0.1. By proposing the novel perturbation structure as seen in Figure 5.7(f), dual-mode dual-band bandpass filter is obtained by splitting degenerate modes at the both bands. In the last configuration in Figure 5.7(f), the mode in the upper band is splitted by employing the perturbation of r_p=0.07*a* and r_{pmid}=0.1*a*. Degenerate modes in the lower band as well as the upper band are overcoupled with a further increase of r_{pmid} as presented in Figure 5.7(g). According to the simulation results, the isolation is higher than 10 dB and the insertion losses are 1.55 and 1.02 dB as shown in Figure 5.8. 3dB bandwidth is also 0.0011 THz and 0.0014 THz for the left and right modes at lower band, respectively. In contrast to the lower band, the upper band presents larger bandpass filter characteristics with the isolation is higher than 7 dB and the insertion losses is 0.41 dB and 3dB bandwidth is 0.0075 THz. The upper band exhibits better flat spectral characteristic than the lower band. Fractional bandwidth ($\Delta f/f$) is calculated as % 0.3 and % 0.4 for each mode of the lower band and % 2.3 for the upper band. Fractional bandwidth can be tuned by perturbation rods.

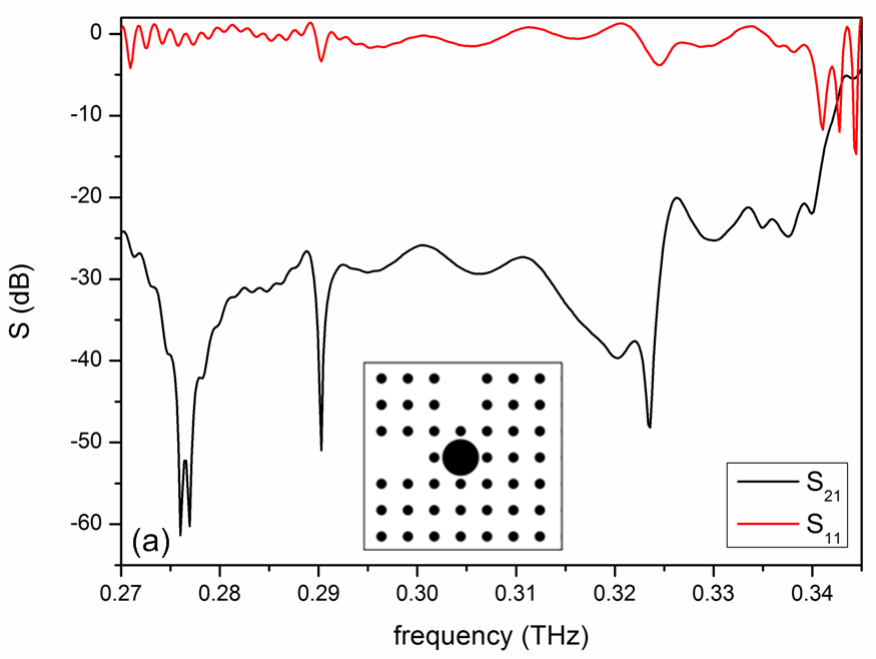

(a)

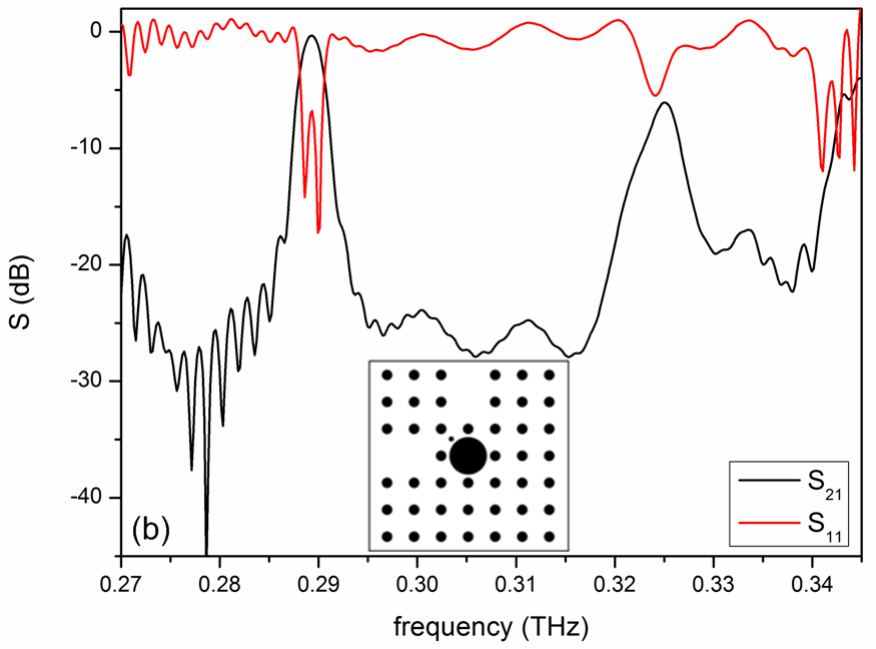

(b)

Figure 5.7. (a) Transmission and reflection spectrum of microcavity with r_p=0 and r_{pmid}=0 (b) r_p=0 and r_{pmid}=0.07a (c) r_p=0 and r_{pmid}=0.1a (d) r_p=0.07a and r_{pmid}=0 (e) r_p=0.1a and r_{pmid}=0 (f) r_p=0.07a and r_{pmid}=0.1a (g) r_p=0.07a and r_{pmid}=0.15a

(cont. on next page)

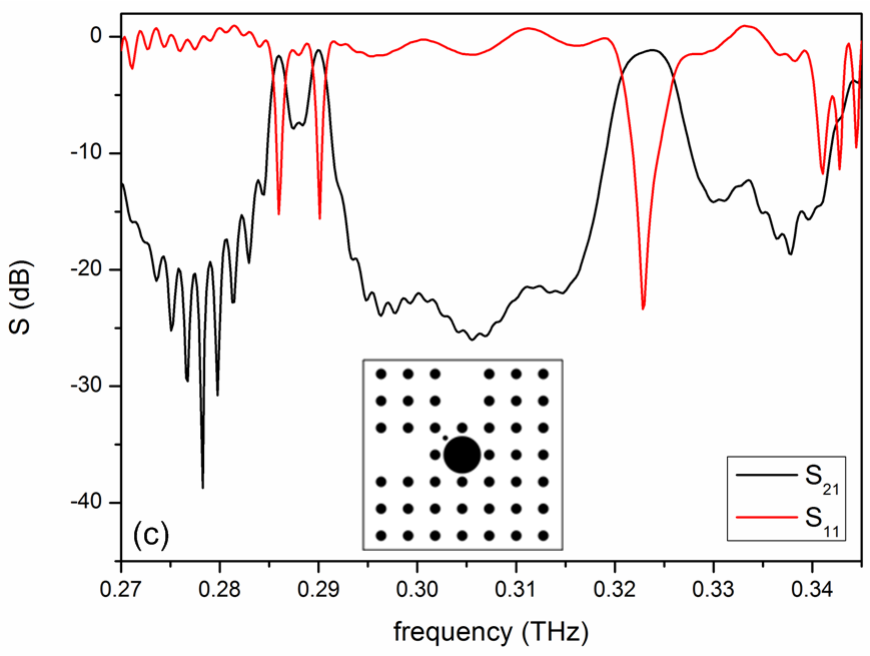

(c)

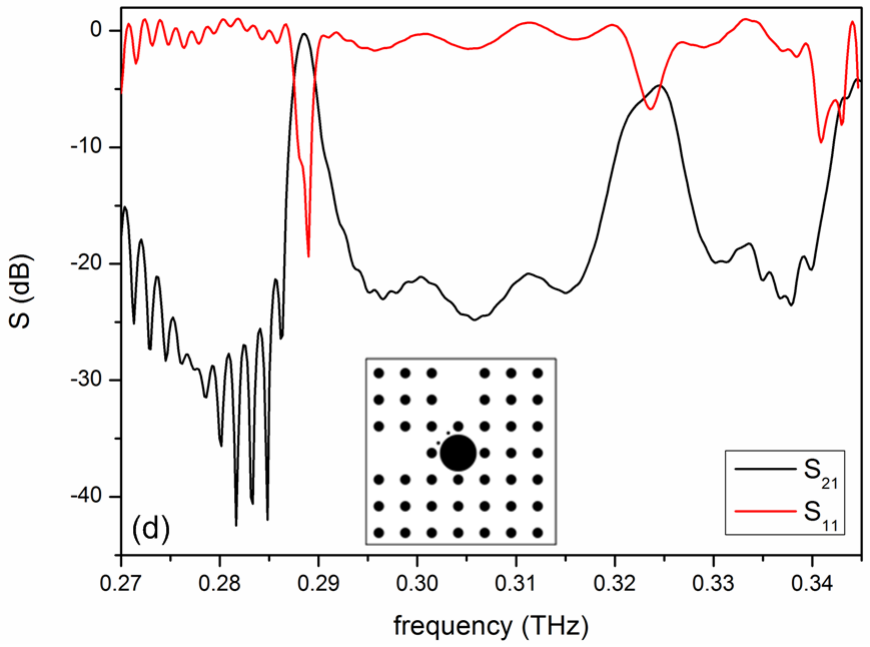

(d)

Figure 5.7. (cont.)

(cont. on next page)

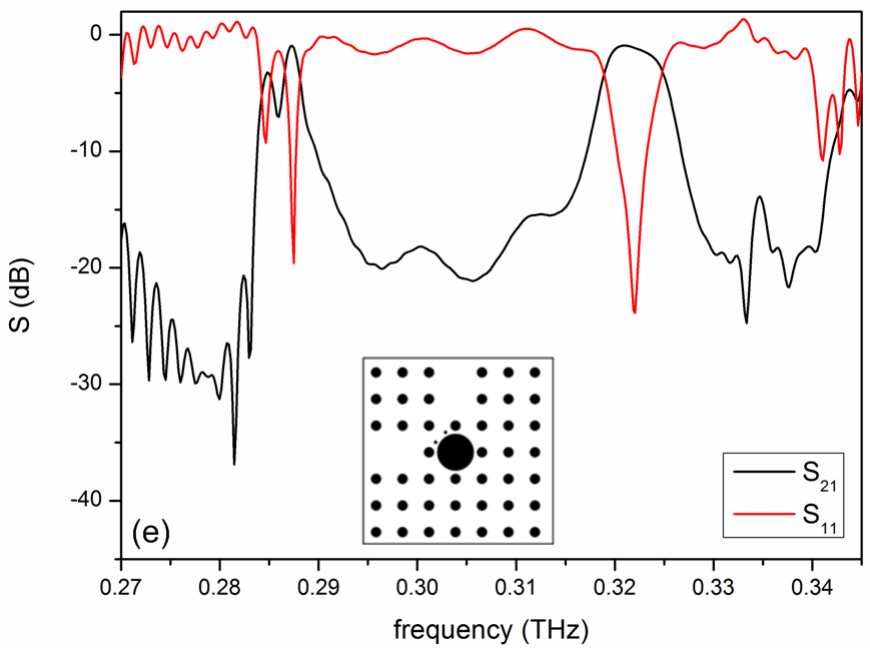

(e)

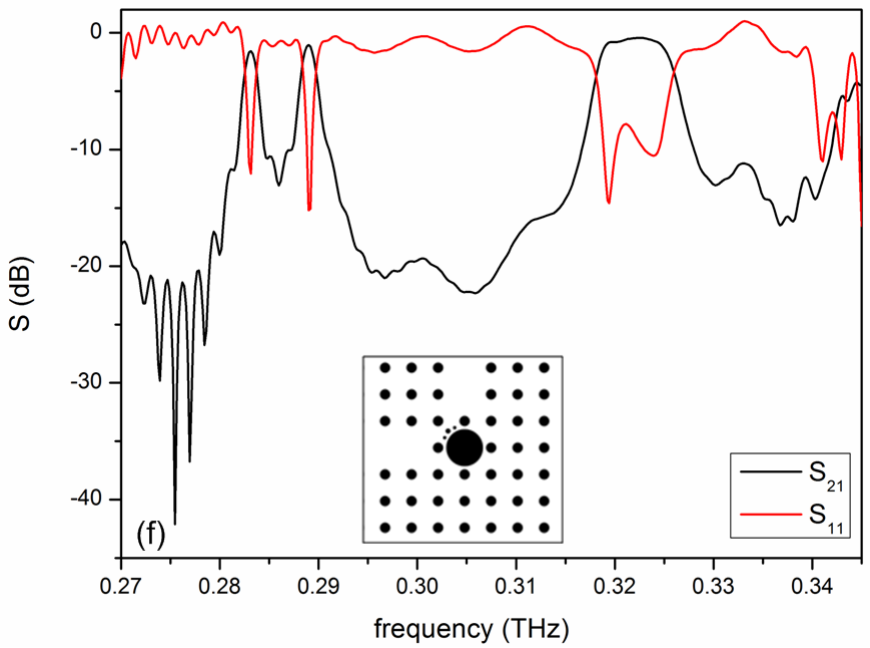

(f)

Figure 5.7. (cont.)

(cont. on next page)

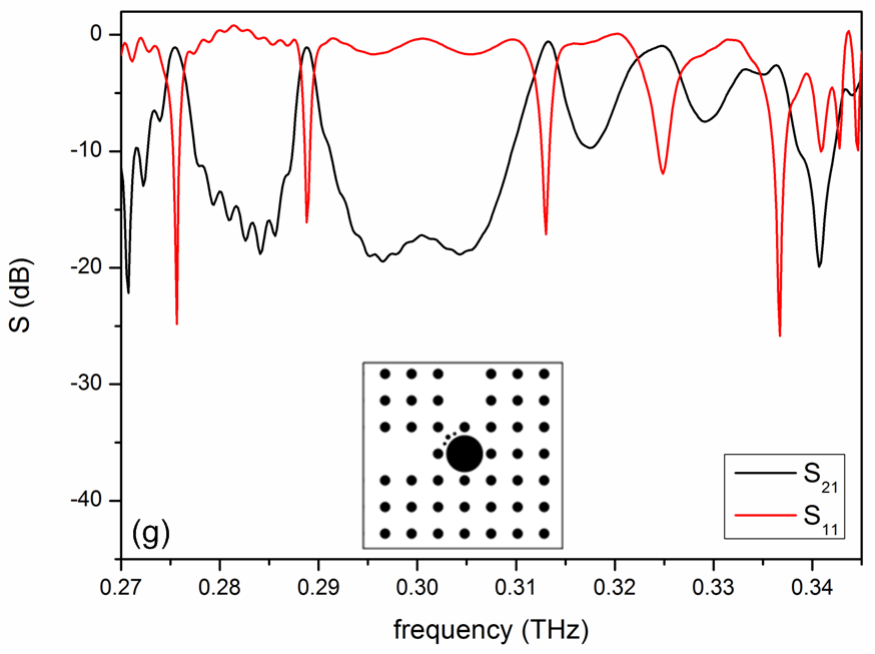

(g)

Figure 5.7. (end)

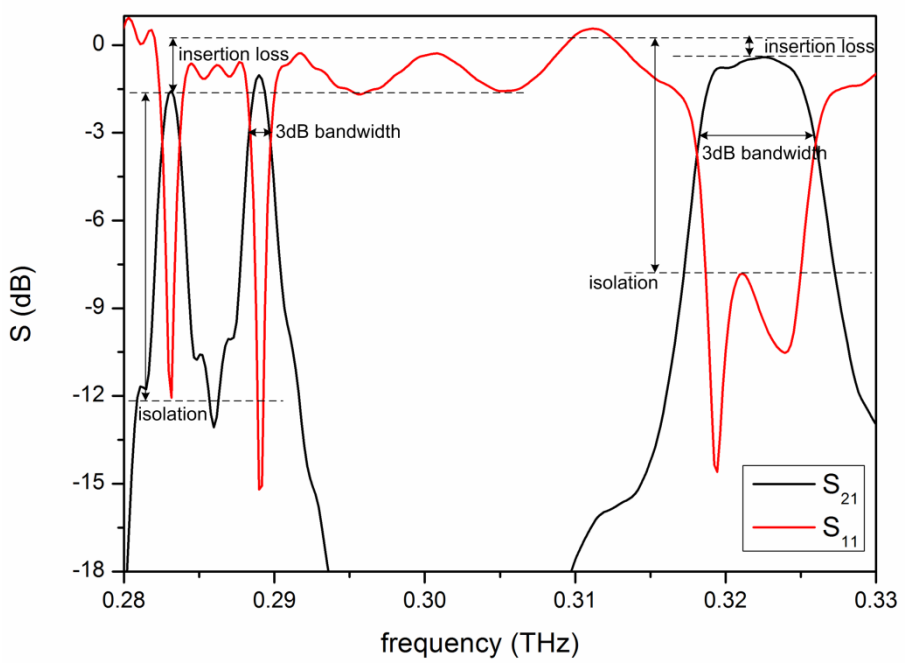

Figure 5.8. Transmission parameters of the lower and upper band with $r_p=0.07a$ and $r_{pmid}=0.1a$

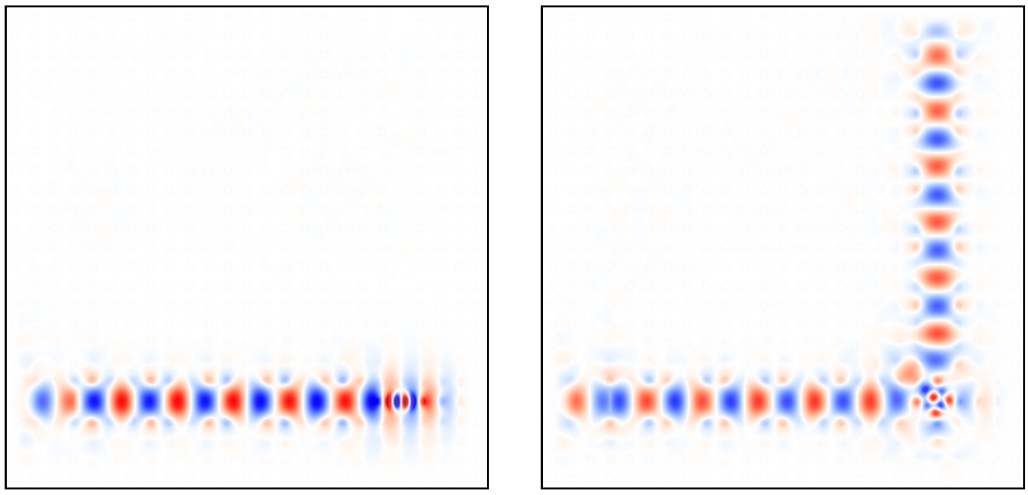

(a) (b)

Figure 5.9. Input signal propagation at the frequency of 0.322 THz (a) without and (b) with the perturbation (r_p=0.07*a* and r_{pmid}=0.1*a*)

5.4 Optimization of Dual Mode Dual Band Filter Parameters

Various forms of the PhC microcavity structures have been investigated by changing radius of the perturbation rods, rpmid 0.03*a* to 0.15*a* while the r_p is set to 0.05*a*. The lower band at frequency 0.29 THz is excited before the upper band at frequency 0.324 THz. The critical coupling value of r_{pmid} is 0.03*a* and 0.10*a* for the lower band and the upper bands, respectively. At the values 0.10*a* of the rpmid then the upper band is to split as shown in Figure 5.10(a). Adjusting the middle perturbation rods radius rpmid as 0.11*a*, both bands can be simultaneously excited. Spectral shift between the degenerate mode frequencies in each band is increased by r_{pmid}. Transmission coefficient (S_{21}) and bandwidth of the both bands are also increased by r_{pmid}. But for the larger values of r_{pmid}, the upper band is over coupled because of the decreasing S_{21} as seen in Figure 5.10(b). Besides, when the splitting of modes is increased by r_{pmid}, the bandwidth of modes is increased as depicted in Figure 5.10(c-d). Additionally, resonance mode frequency can be tuned with exploiting nonlinearity in PhC cavity. If refractive index of the microcavity rod is increased about %1, the band frequency shifts about 0.003 THz to lower frequency part of the spectrum. Apart from the index change of microcavity rods, the transmission spectrum is not affected by the index variation of

perturbation rods. The modes can be easily tuned by perturbation rod structure and/or nonlinear index variation of microcavity rod.

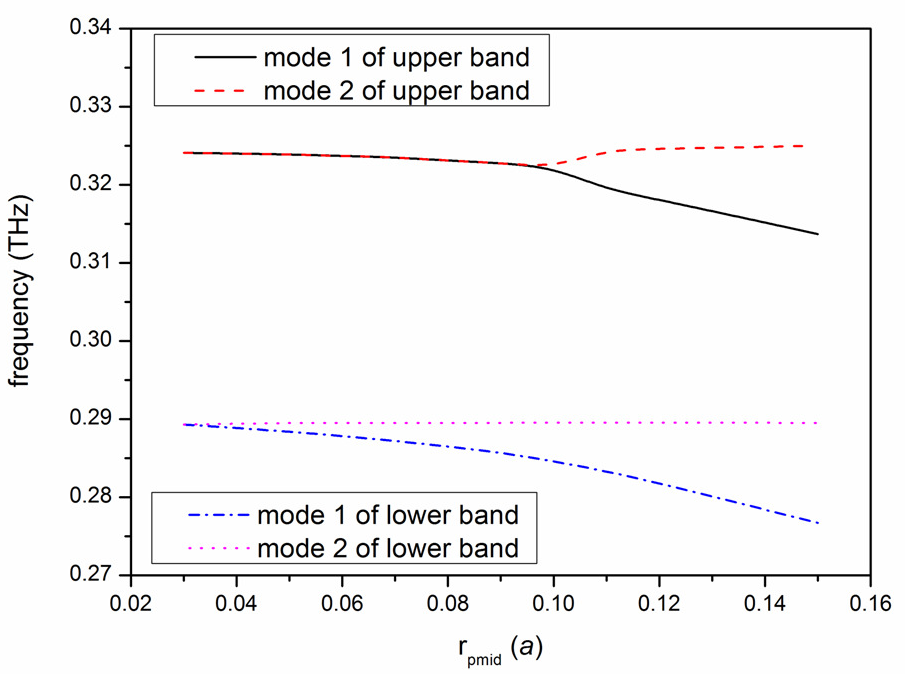

(a)

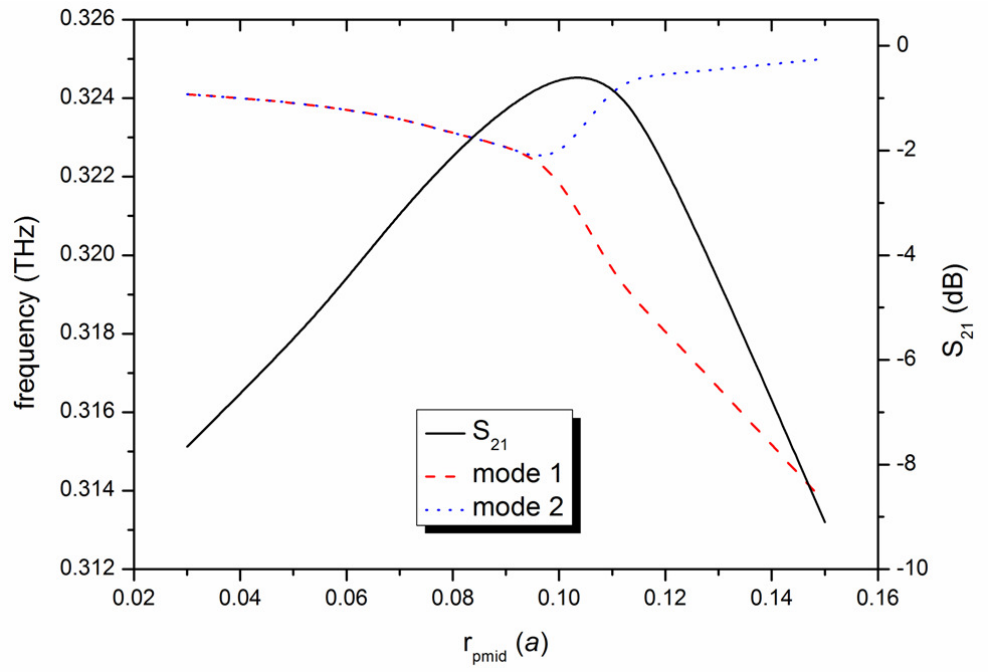

(b)

Figure 5.10. Band splitting properties for rpmid variation (r_p is set to 0.05a)

(cont. on next page)

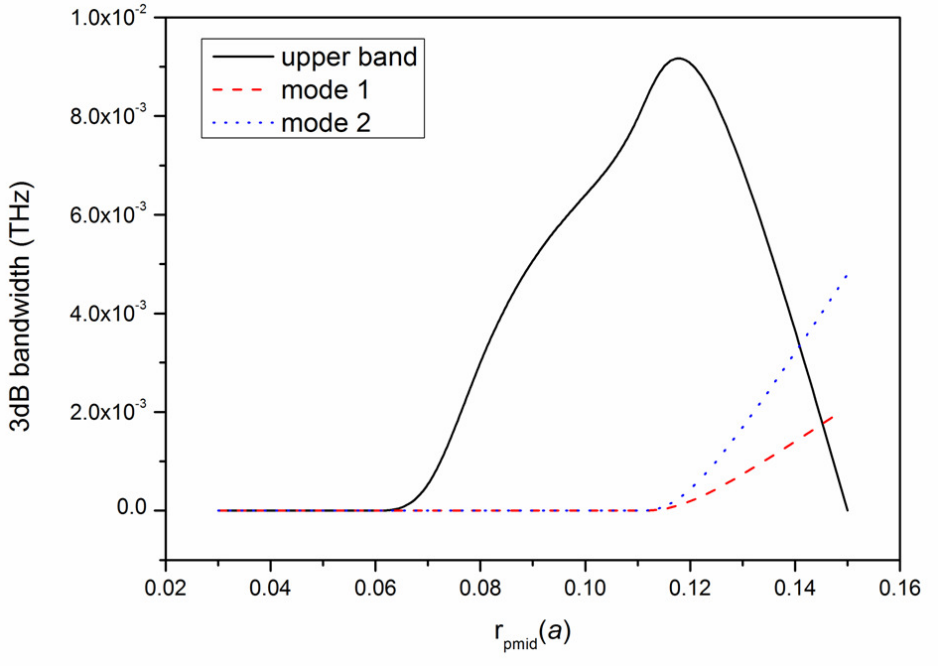

(c)

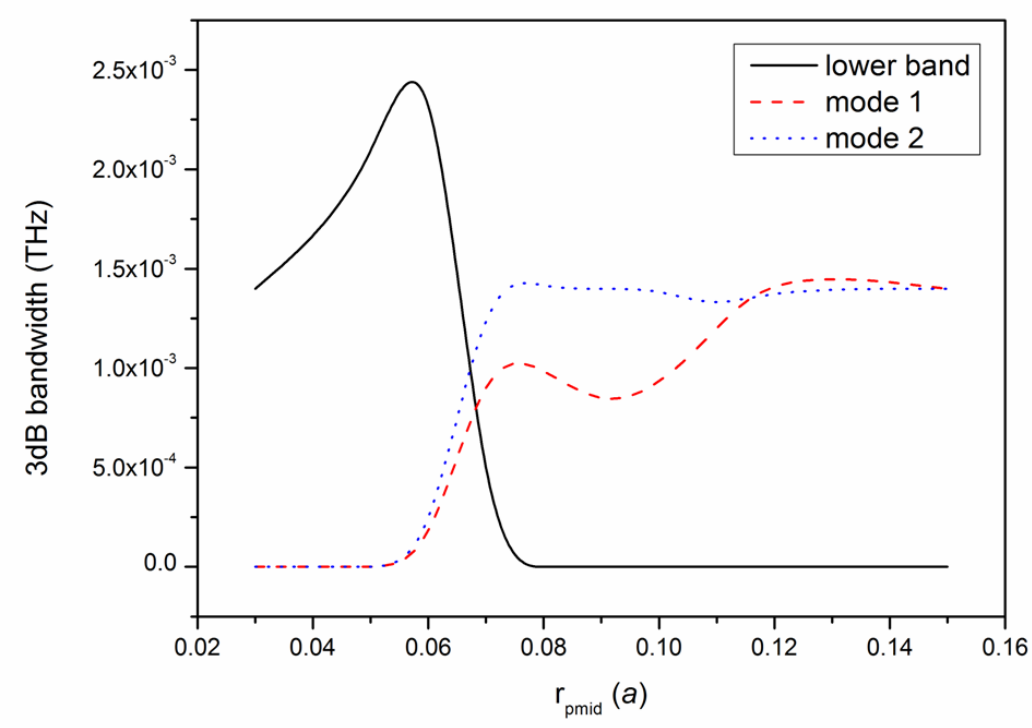

(d)

Figure 5.10. (end)

5.5 Discussion on Results

In this part of thesis, we have proposed PhC microcavity structures having perturbation rods that show dual-mode, dual-band filter characteristics with narrow bands, high isolation, low insertion loss and high quality. The degenerate modes at each band can be activated concurrently with the perturbation rods with r_p=0.05 and r_{pmid}=0.11. The upper band presents flat spectral characteristics as bandwidth is 0.0076 THz with fractional bandwidth % 2.3 at 0.322 THz. The lower band becomes overcoupled with the larger value of r_{pmid}. However, it can be used as a narrow band filter with the bandwidth of 0.0012 THz and 0.0014 THz and fractional bandwidth of % 0.4 for each mode of 0.283 THz and 0.289 THz, respectively. Although the transmission spectrum is dramatically affected by changing the perturbation rod diameter, changing the refractive index of the perturbation rods does not produce same effects. Additionally, the band frequency is shifted about 0.003 THz to lower frequency part of the spectrum by the refractive index of the microcavity rod is increased about %1. This study may contribute to the development of functional devices for wireless communication application at THz range.

CHAPTER 6

CONCLUSION

The reconfigurable and dynamically tunable wavelength selective component, which is the main subject of this thesis, can be constructed with a interference grating or microcavity with perturbation rods in PhC. Hereby, two dimensional plane waves with Gaussian form of amplitude variation are applied to PhC as a control beam and the grating is composed in the Kerr type nonlinear bus waveguide at the region of coupling. Transmission characteristics of the nonlinear grating waveguide have been analyzed by simulating the model by using the FDTD method. The results for transmission characteristics have been presented for optimization parameters of Kerr nonlinear coefficients and beam incidence angles. Also, the characteristics are extended for two wavelengths for spectral performance evaluation. According to the simulation results, transmission characteristics are tuned by interference beam parameters.

Due to very fast response requirement of optical communications, the most suitable approach to control bandgap and then realization of fast optical devices is to exploit nonlinearity in PhCs. However, it has been confirmed from the simulation result that instantaneous nonlinearity is not suitable for transient grating. Because of the refractive index variation follows the control pulse intensity shape in instantaneously case, different parts of signal are faced to different index value. Therefore, transient grating structure is not constant. Noninstantaneous response nonlinearity (Raman) not included in the study.

As an example of another filter devices, microcavity based PhC dual-mode dual-band filter is designed and its transmission characteristics are investigated for various configurations. Exploiting degenerate mode splitting in microcavity, PhC compact bandpass filter exhibiting dual-mode dual-band characteristic with narrow bands, high isolation, low insertion loss, and high quality are proposed.

The results have confirmed that these structures are also used for switching operation. When the drop wavelength is applied, that is reflected back from the reconfigurable wavelength selective component and this mode is coupled out with the wavelength selective filter placed at the input. This can be an effective method for controlling optical signals in the photonic crystal for all optical switching/routing applications as a part of add/drop multiplexing.

Integration of the PhC devices is another research area that needs to be deeply investigated. That configurations in general, called PhC Circuits (PCCs), may also include functions more than just bending or coupling, but rather dynamically controlling and modulating the light signal in order to switching and/or routing among the layers or the light paths. This approach brings very fast dynamical tunability and compatibility into the nonlinear photonic crystal circuits.

REFERENCES

[1] R. D. M. J.D. Joannopoulos , S.G Johnson, J.N Winn, *Photonic Crystals: Molding the Flow of Light*, 2nd ed. New Jersey: Princeton University Press, 2008.

[2] A. F. Matthews, "Experimental demonstration of self-collimation beaming and splitting in photonic crystals at microwave frequencies," *Opt. Commun.*, vol. 282, no. 9, pp. 1789–1792, May 2009.

[3] S. Kirihara, "Fabrication of Photonic Crystal Cavities for Terahertz Wave Resonations,Nanofabrication," in *Fabrication of Photonic Crystal Cavities for Terahertz Wave Resonations, Nanofabrication*, 2011.

[4] K. Raman, *Fiber Bragg Gratings*, 2nd ed. Academic Press, 2009.

[5] A. Mekis, J. C. Chen, I. Kurland, S. Fan, P. R. Villeneuve, and J. D. Joannopoulos, "High Transmission through Sharp Bends in Photonic Crystal Waveguides," *Phys. Rev. Lett.*, vol. 77, no. 18, pp. 3787–3790, Oct. 1996.

[6] T. Liu, "Photonic crystal based optical devices," 2005.

[7] S. Mingaleev and Y. Kivshar, "Nonlinear Photonic Crystals Toward All-Optical Technologies," *Opt. Photonics News*, vol. 13, no. 7, p. 48, Jul. 2002.

[8] Q. Li, T. Wang, Y. Su, M. Yan, and M. Qiu, "Coupled mode theory analysis of mode-splitting in coupled cavity system.," *Opt. Express*, vol. 18, no. 8, pp. 8367–82, Apr. 2010.

[9] S. Fan, P. Villeneuve, J. Joannopoulos, and H. Haus, "Channel drop filters in photonic crystals," *Opt. Express*, vol. 3, no. 1, p. 4, Jul. 1998.

[10] S. M. Hendrickson, A. C. Foster, R. M. Camacho, and B. D. Clader, "Integrated nonlinear photonics: emerging applications and ongoing challenges [Invited]," *J. Opt. Soc. Am. B*, vol. 31, no. 12, p. 3193, Nov. 2014.

[11] L. Ye, Z. Fei, Z. Dao-Zhong, and L. Zhi-Yuan, "Energy Squeeze of Ultrashort Light Pulse by Kerr Nonlinear Photonic Crystals," *Chinese Physics Letters*, vol. 26, no. 1. p. 014208, 2009.

[12] Z.-Y. Li and Z.-M. Meng, "Polystyrene Kerr nonlinear photonic crystals for building ultrafast optical switching and logic devices," *J. Mater. Chem. C*, vol. 2, no. 5, pp. 783–800, Jan. 2014.

[13] J. J. J. Bonnefois, G. Guida, and a. Priou, "Nonlinear response of a 2D photonic crystal made of Kerr effect nonlinear parallel rods of large diameter," *J. Mod. Opt.*, vol. 56, no. 5, pp. 646–652, 2009.

[14] R. W. Boyd, *Nonlinear Optics*. Academic Press, 2008.

[15] Y. Liu, F. Qin, Z.-Y. Wei, Q.-B. Meng, D.-Z. Zhang, and Z.-Y. Li, "10 fs ultrafast all-optical switching in polystyrene nonlinear photonic crystals," *Appl. Phys. Lett.*, vol. 95, no. 13, p. 131116, 2009.

[16] R. Katouf, T. Komikado, M. Itoh, T. Yatagai, and S. Umegaki, "Ultra-fast optical switches using 1D polymeric photonic crystals," pp. 4–7, 2005.

[17] C. Chun-ping, T. Anada, S. Greedy, T. M. Benson, and P. Sewell, "A Novel Photonic Crystal Band-Pass Filter Using Degenerate Modes of a Point-Defect Microcavity for Terahertz Communication," *Microw. Opt. Technol. Lett.*, vol. 56, no. 4, pp. 792–797, 2014.

[18] A. F. Oskooi, D. Roundy, M. Ibanescu, P. Bermel, J. D. Joannopoulos, and S. G. Johnson, "Meep: A flexible free-software package for electromagnetic simulations by the FDTD method," *Comput. Phys. Commun.*, vol. 181, no. 3, pp. 687–702, 2010.

[19] W. E. Born M., *Principles of Optics*. Cambridge University Press, 1999.

[20] B. E. A. Saleh, *Fundamentals of Photonics*, 2nd ed. Wiley, 2007.

[21] Jean-Claude Diels, *Ultrashort Laser Pulse Phenomena*, 2nd ed. Academic Press, 2006.

[22] T. Allen, *Computational Electrodynamics: The Finite-Difference Time-Domain Method*, Third Edit. Artech House, 2005.

[23] Hellworth, "Third-order optical susceptibility of liquids and solids," *J. Prog. Quantum Electron.*

[24] I. S. Maksymov, L. F. Marsal, and J. Pallares, "An FDTD analysis of nonlinear photonic crystal waveguides," *Opt. Quantum Electron.*, vol. 38, no. 1–3, pp. 149–160, 2006.

[25] C. M. Reinke, A. Jafarpour, B. Momeni, M. Soltani, S. Khorasani, A. Adibi, Y. Xu, and R. K. Lee, "Nonlinear Finite-Difference Time-Domain Method for the Simulation of Anisotropic, \chi(2), and \chi(3) Optical Effects," *J. Light. Technol.*, vol. 24, no. 1, p. 624–, 2006.

[26] T. Kamalakis and T. Sphicopoulos, "A new formulation of coupled propagation equations in periodic nanophotonic waveguides for the treatment of Kerr-induced nonlinearities," *IEEE J. Quantum Electron.*, vol. 43, no. 10, pp. 923–933, 2007.

[27] M. Plihal and A. Maradudin, "Photonic band structure of two-dimensional systems: The triangular lattice," *Physical Review B*, vol. 44, no. 16. pp. 8565–8571, 1991.

[28] K. M. Ho, C. T. Chan, and C. M. Soukoulis, “Existence of a photonic gap in periodic dielectric structures,” *Phys. Rev. Lett.*, vol. 65, no. 25, pp. 3152–3155, 1990.

[29] J. B. Pendry and A. MacKinnon, “Calculation of photon dispersion relations,” *Phys. Rev. Lett.*, vol. 69, no. 19, pp. 2772–2775, 1992.

[30] K. C., *Kittel C., Introduction to Solid State Physics*. Wiley, 1995.

[31] K. Sakoda, *Optical Properties of Photonic Crystals*. Springer, 2001.

[32] K. S. Yee, “Numerical Solution of Initial Boundary Value Problems Involving Maxwell’s Equations in Isotropic Media,” *IEEE Transscations Antennas Propag.*, 1966.

[33] J. B. Schneider, *Understanding the Finite-Difference Time-Domain Method*. Washington State University, 2015.

[34] A. Taflove and M. E. E. Brodwin, “Numerical Solution of Steady-State Electromagnetic Scattering Problems Using the Time-Dependent Maxwell’s Equations,” *Microw. Theory Tech. IEEE Trans.*, vol. 23, no. 8, pp. 623–630, 1974.

[35] J.-P. Berenger, “A perfectly matched layer for the absorption of electromagnetic waves,” *J. Comput. Phys.*, vol. 114, no. 2, pp. 185–200, Oct. 1994.

[36] X. Zeng and K. Liang, “Analytic solutions for spectral properties of superstructure, Gaussian-apodized and phase shift gratings with short- or long-period,” *Optics Express*, vol. 19, no. 23. p. 22797, 2011.

[37] G. A. Miller, C. G. Askins, and E. J. Friebele, “Modified F-matrix calculation of bragg grating spectra and its use with a novel nonlinear index growth law,” *J. Light. Technol.*, vol. 24, no. 6, pp. 2416–2426, 2006.

[38] Z. H. Wang, G. D. Peng, and P. L. Chu, “Improved Rouard’s method for fiber and waveguide gratings,” *Opt. Commun.*, vol. 177, no. 1, pp. 245–250, 2000.

[39] N.-H. Sun, J.-J. Liau, Y.-W. Kiang, S.-C. Lin, R.-Y. Ro, and J.-S. Chiang, “Numerical Analysis of Apodized FBGs using Coupled Model Theory,” *Prog. Electromagn. Res.*, vol. 99, pp. 289–306, 2009.

[40] Y. Q. and Y. Sheng, *Fiber Bragg Grating Modeling*. Center for Optics, Photonics and Laser Laval University, 2008.

[41] T. Erdogan, “Fiber grating spectra,” *J. Light. Technol.*, vol. 15, no. 8, pp. 1277–1294, 1997.

[42] M. Sayin, M. S. Özyazici, and N. Dogru, "Theoretical model of the mode-locked hybrid soliton pulse source," *Optical Engineering*, vol. 46, no. 6. p. 064201, 2007.

[43] Z.-Y. Li, "Principles of the plane-wave transfer-matrix method for photonic crystals," *Sci. Technol. Adv. Mater.*, vol. 6, no. 7, pp. 837–841, Oct. 2005.

[44] J. de Boor, N. Geyer, U. Gösele, and V. Schmidt, "Three-beam interference lithography: upgrading a Lloyd's interferometer for single-exposure hexagonal patterning.," *Opt. Lett.*, vol. 34, no. 12, pp. 1783–1785, 2009.

[45] M. E. Walsh, "On the design of lithographic interferometers and their application," Massachusetts Institute of Technology, 2004.

[46] J. H. Moon, J. Ford, and S. Yang, "Fabricating three-dimensional polymeric photonic structures by multi-beam interference lithography," *Polym. Adv. Technol.*, vol. 17, no. 2, pp. 83–93, Feb. 2006.

[47] L. Yuan, G. P. Wang, and X. Huang, "Arrangements of four beams for any Bravais lattice.," *Opt. Lett.*, vol. 28, no. 19, pp. 1769–1771, 2003.

[48] L. Z. Cai, X. L. Yang, Q. Liu, and Y. R. Wang, "What kind of Bravais lattices can be made by the interference of four umbrellalike beams?," *Opt. Commun.*, vol. 224, no. 4–6, pp. 243–246, 2003.

[49] L. Z. Cai, X. L. Yang, and Q. Liu, "General representation of interference contrast formed by arbitrarily polarized waves and its application in wave design for holographic fabrication of photonic crystals," *Opt. Laser Technol.*, vol. 36, no. 6, pp. 453–457, 2004.

[50] J. L. Stay and T. K. Gaylord, "Contrast in four-beam-interference lithography.," *Opt. Lett.*, vol. 33, no. 13, pp. 1434–1436, 2008.

[51] E. Li, K. Tieu, and M. Mackenzie, "Interference Patterns of Two Focused Gaussian Beams in an LDA Measuring Volume," *Optics and Lasers in Engineering*, vol. 27, no. 4. pp. 395–407, 1997.

[52] O. Akin and M. S. Dinleyici, "An All-Optical Switching Based on Resonance Breaking With a Transient Grating," *J. Light. Technol.*, vol. 28, no. 23, pp. 3470–3477, Dec. 2010.

[53] X. Zhang, C. Wang, Y. Zeng, and J. Zhang, "Nonlinear Refraction and Photo induced Birefringence in the Methyl-Red-Doped Polymer Thin Film," *Journal of Nonlinear Optical Physics & Materials*, vol. 19, no. 03. pp. 437–444, 2010.

[54] T. He, Y. Cheng, Y. Du, and Y. Mo, "Z-scan determination of third-order nonlinear optical nonlinearity of three azobenzenes doped polymer films," *Opt. Commun.*, vol. 275, no. 1, pp. 240–244, 2007.

[55] D. W. Eichler, Hans Joachim, Günter, Peter, Pohl, *Laser-Induced Dynamic Gratings*. Springer Series in Optical Sciences, 1986.

[56] R. Paschotta, *Encyclopedia of Laser Physics and Technology*. Wliey-VCH, 2008.

[57] H. G. Winful, J. H. Marburger, and E. Garmire, "Theory of bistability in nonlinear distributed feedback structures," *Appl. Phys. Lett.*, vol. 35, no. 5, p. 379, Aug. 1979.

[58] C. M. de Sterke, "Optical push broom," *Opt. Lett.*, vol. 17, no. 13, p. 914, Jul. 1992.

[59] N. Primerov, "Generation and application of dynamic gratings in optical fibers using stimulated Brillouin scattering To my parents and Denise Bayard," 2013.

[60] G. L. Saux, F. Salin, P. Georges, G. Roger, and A. Brun, "Single shot measurement of the optical Kerr effect kinetics.," *Appl. Opt.*, vol. 27, no. 4, pp. 777–9, Feb. 1988.

[61] N. G. . Broderick, "Bistable switching in nonlinear Bragg gratings," *Opt. Commun.*, vol. 148, no. 1–3, pp. 90–94, Mar. 1998.

[62] K. Ogusu, "Stability of nonlinear Bragg gratings with a finite material response time," *J. Opt. Soc. Am. B*, vol. 17, no. 11, p. 1894, Nov. 2000.

[63] E. Ozbay, M. Bayindir, I. Bulu, and E. Cubukcu, "Investigation of localized coupled-cavity modes in two-dimensional photonic bandgap structures," *IEEE J. Quantum Electron.*, vol. 38, no. 7, pp. 837–843, Jul. 2002.

[64] S. Mahmoodian, R. McPhedran, C. de Sterke, K. Dossou, C. Poulton, and L. Botten, "Single and coupled degenerate defect modes in two-dimensional photonic crystal band gaps," *Phys. Rev. A*, vol. 79, no. 1, p. 013814, Jan. 2009.

[65] S. Mahmoodian, R. C. McPhedran, C. M. De Sterke, K. B. Dossou, C. G. Poulton, and L. C. Botten, "Single and coupled degenerate defect modes in two-dimensional photonic crystal band gaps," *Phys. Rev. A - At. Mol. Opt. Phys.*, vol. 79, no. 1, 2009.

[66] Z. Zhang, M. Dainese, L. Wosinski, and M. Qiu, "Resonance-splitting and enhanced notch depth in SOI ring resonators with mutual mode coupling," *Opt. Express*, vol. 16, no. 7, p. 4621, Mar. 2008.

[67] A. Daraei and F. Khozeymeh, "Investigation on Mode Splitting and Degeneracy in the L3 Photonic Crystal Nanocavity via Unsymmetrical Displacement of," *Int. J. Eng. Sci.*, vol. 2, no. 2, pp. 146–150, 2013.

[68] K. Sakoda and H. Shiroma, "Numerical method for localized defect modes in photonic lattices," *Phys. Rev. B*, vol. 56, no. 8, pp. 4830–4835, Aug. 1997.

[69] "Nanophotonics and Integrated Optics Photonic Crystal Cavities," *whitepaper, CST Comput. Simul. Technol.*

[70] R. G. Beausoleil, P. J. Kuekes, G. S. Snider, and R. S. Williams, "Nanoelectronic and Nanophotonic Interconnect," *Proc. IEEE*, vol. 96, no. 2, pp. 230–247, Feb. 2008.

[71] M. J. Fitch and R. Osiander, "Terahertz Waves for Communications and Sensing," *Johns Hopkins Apl Tech. Dig.*, vol. 25, no. 4, 2004.

[72] S. Kim and Y. Lee, "Symmetry Relations of Two-Dimensional Photonic Crystal Cavity Modes," *IEEE Int. J. Quantum Electron.*, vol. 39, no. 9, pp. 1081–1085, 2003.

[73] P. R. Villeneuve, S. Fan, and J. D. Joannopoulos, "Microcavities in photonic crystals: Mode symmetry, tunability, and coupling efficiency," *Phys. Rev. B*, vol. 54, no. 11, pp. 7837–7842, Sep. 1996.

VITA

Personal Information
Özgür Önder KARAKILINÇ
Pamukkale University, Electrical-Electronics Eng. Dept.,
20070 Denizli- TURKEY
e-mail: okarakilinc@pau.edu.tr

Education

2007-2015	: PhD.-Izmir Institute of High Technology-Izmir
2002-2005	: Ms -Pamukkale University -Denizli
1994-1999	: Bs. - Yıldız Technical University-Istanbul
1991-1994	: Çal High School -Denizli

Employement

2007-present	: Specialist, Pamukkale University Electrical-Electronics Eng.Dept.
2002-2007	: Research Assistant, Pamukkale University Electrical-Electronics Eng.Dept.
1999-2001	: Cellular Field Engineer, Motorola Telecom., Istanbul

A- Publications from the thesis
Papers in refereed journals (SCI, SCI Expanded indexed)

Karakilinc O.O., Dinleyici M.S., "Design of Dual-Mode Dual-Band Photonic Crystal Bandpass Filters for Terahertz Communication Applications", Microwave and Optical Technology Letters, vol.57, no 8, pp. 1806-1810, 2015.

Karakilinc O.O., Dinleyici M.S.,"Interference Grating Structures in Photonic Crystal Circuits",Optical and Quantum Electronics, vol.42, pp.645-656., 2011.

Papers in peer-reviewed conference proceedings (SCI, SCI Expanded indexed)

Karakılınç Özgür Önder, Dinleyici M. Salih, "$\chi(3)$ Tip Malzeme Kullanan Doğrusal Olmayan Fotonik Kristal Optik Anahtarlama Üzerine Bir Çalışma", IEEE 17. Sinyal İşleme ve İletişim Uygulamaları Kurultayı, Antalya, 2009.

Papers in peer-reviewed conference proceedings
Karakilinc O. Onder., Dinleyici M. Salih., "Novel Transient Grating Structures in Photonic Crystal Circuits", 15th International Conference, ELECTRONICS 2011, Lithuania, 2011.

Reviewers for
Optics Express
Optics Letters
Applied Optics
Memberships OSA, SPIE